Physicochemical foundations of glass

Walter Schirmacher

https://www.staff.uni-mainz.de/schirmac/jena.html

Contents

1 Introduction

Glasses [1] are by definition non-crystalline, i.e. amorphous materials. In contrast to crystals, in which the molecules are arranged regularly, the molecular positions are random, like a snapshot

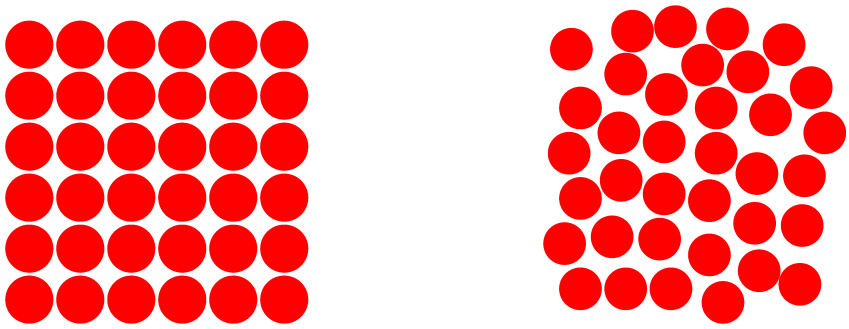

Figure 1: Molecular arrangements of a crystal (left) and a glass (right)

of a liquid. Pure elementary materials cannot be frozen from the liquid state [2] to form a glass. This is, because nothing hinders a one-component liquid, if cooled down, to form a crystal. The molecule immediately find a suitable crystal-lattice position. This may be not the case in a more-component liquid. In more-component liquids, it might not be easy for the molecules to find appropriate regular positions. Their time to do so is restricted by the cooling rate imposed by the experimentalist. If the cooling rate is rapid enough, crystallization may be avoided, and a glass may be formed from the undercooled liquid.

1.1 Glass between physics and chemistry

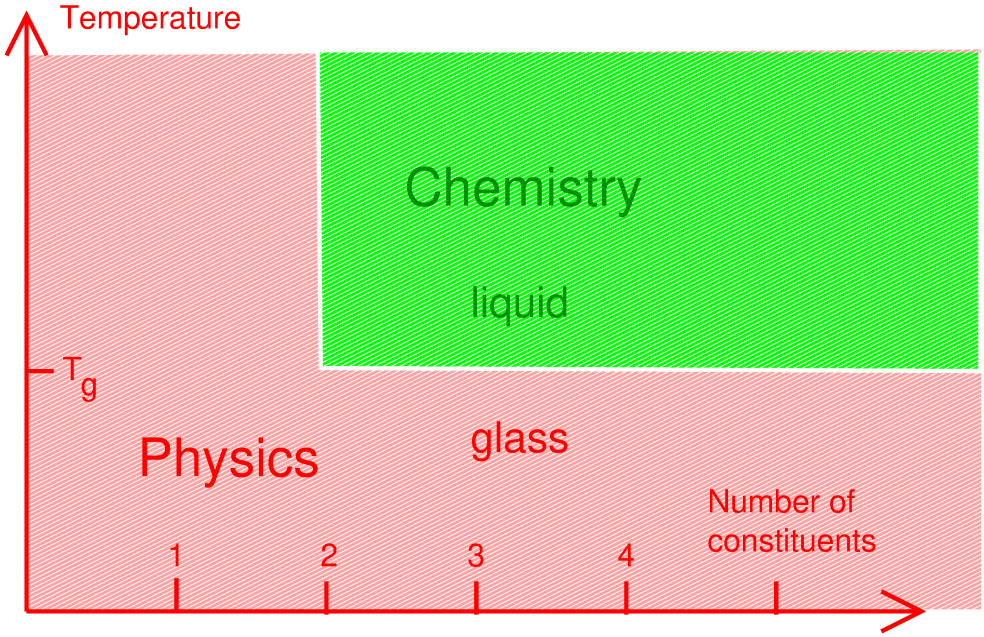

Figure 2: Glass betweeen physics and chemistry

Glass-forming liquids are therefore composed of a number of constituient materials. This embeds glass science into chemistry, because in more-component liquids all kinds of chemical-bond equilibria may be present, as pointed out by John Enderby (1982) [3] in his review article, entitled "Liquid state physics – or is it chemistry?". Such chemical bonds can – depending on the specific materials – be of covalent, ionic or of metallic type. In the present lecture course we shall encounter all three types.

On the other hand, once in the frozen glassy state no more chemical reactions can happen, and the remaining dynamical processes are of physical nature: relaxations, in which molecules may re-arrange their positions, and vibrations, in which the centers of mass remain the same. This is, why in Fig. 2 we shaded the low-temperature regime below the glass freezing temperature T_g in red, attributing the regime to physics. Scientists, who perform computer simulations in order to understand the glassy freezing process, have invented model materials, which ony interact by pairwise forces. These model liquids are prevented from crystallization by varying the ranges of the forces in a statistical way [4]. In this – effectively – one-component "material" no chemistry happens. The physics of the freezing of such model liquids into a glassy state is of interest and is subject to a very large amount of scientific literature [5].

1.2 Glass in everyday life

Figure 3: Examples of use of glas.

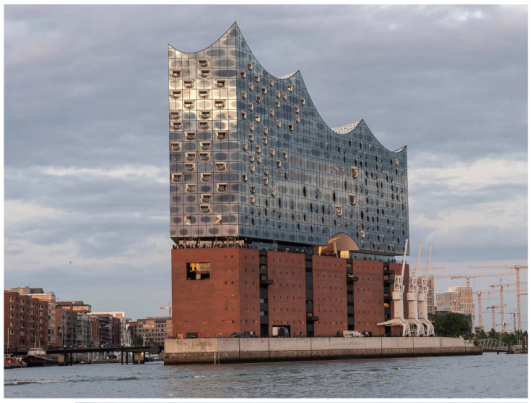

Figure 4: Examples of glas in arcitecture: The Elbphilharmonie Hamburg, the Louis-Vitton Foundation in Paris, The main station in Berlin and the European Central Bank in Frankfurt

Glass can be said to dominate our everyday life. Not only cellphone covers, drinking glasses, house- and car windows are made of glass, but un-numerous other items from chemical test-tubes and pH meters to optical lenses and prisms (Fig. 3). Glass has as well advanced from window material to substantial building material in architecture (Fig. 4). If one includes plastics to the consideration, (which make sense, because polymer materials are, like glass, non-crystalline,) one may follow D. L. Morse of Corning Inc. [6] in calling the present, modern age the glass age.
Glass (in the conventional sense) is a non-crystalline solid material, made predominately of silicates. Glassy rock material is only very rare in the earth crust, but our ancestors in the stone age were already attracted by the properties of obsidian and flint (Feuerstein) for making weapons and fire [7, 8]. Later, in the near orient it became possible (650 b. C.) to produce glass from melting a mixture of sand, chalk, soda and ashes and to obtain vessels by blowing (200 b. C.). In the following 2000 years glass became, step by step, the versatile material of today.
While glass and plastic dominate the technical world, the theoretical understanding of the glassy state is still unsatisfactory. While the material properties of crystalline materials may be readily understood in terms of the well-established group theory of crystalline lattices, and their melting in terms of the theory of first-order phase transitions, the structural and dynamical properties of glasses are far from completely understood. However, the Understanding the physics (and chemistry) of glassy materials has made large progresses in the last decades.

1.3 Overview

In the present set of lectures we give first an introduction to the phenomenology of glass materials. Then we describe the various approaches for treating the transition from a liquid to a glass. Emphasis will be on the mode-coupling theory in terms of spatial and temporal correlation functions. The (possible) relation to thermodynamics will be treated in a more qualitative way. In a third part we discuss the electrical transport properties of glasses. This issue will be used to introduce dynamic susceptibilities and their usefulness for AC conduction. These quantities are just the Fourier-Laplace transforms of the mentioned correlation functions.
The fourth part of this lecture will be devoted to the vibrational properties of glasses by means of a generalization of elasticity theory, allowing for disorder-induced spatial fluctuations of elastic moduli. We shall uncover a deep mathematical analogy between AC conduction and vibrational spectra in disordered materials by using the dynamical susceptibilities.

2 Types of glasses

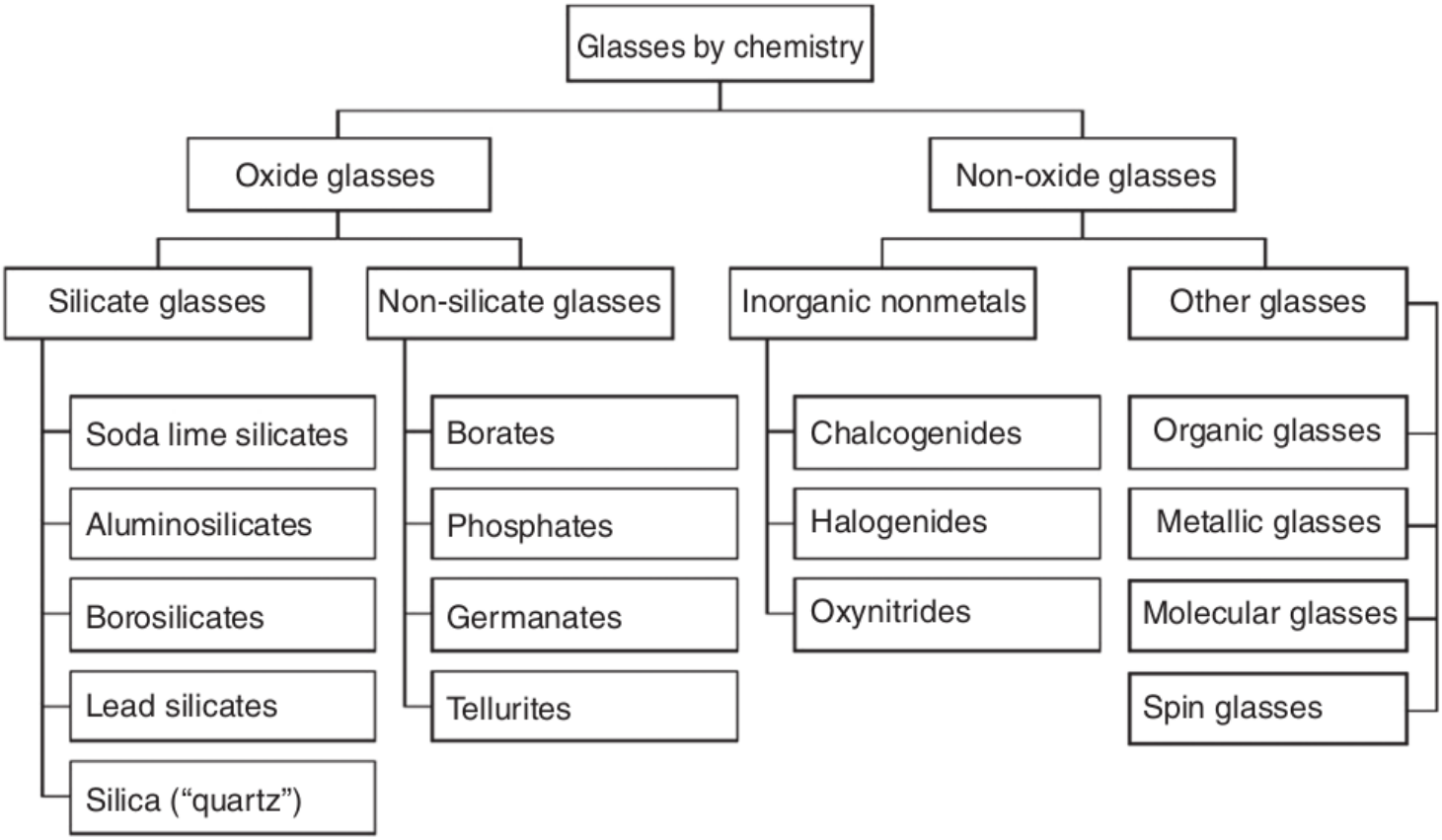

Figure 5: Glasses of different chemical composition; from [9]

2.1 Silicates

The basic ingredient for making every-day glass is sand, which consists predominantly of quartz, which is the crystalline version of SiO_2.

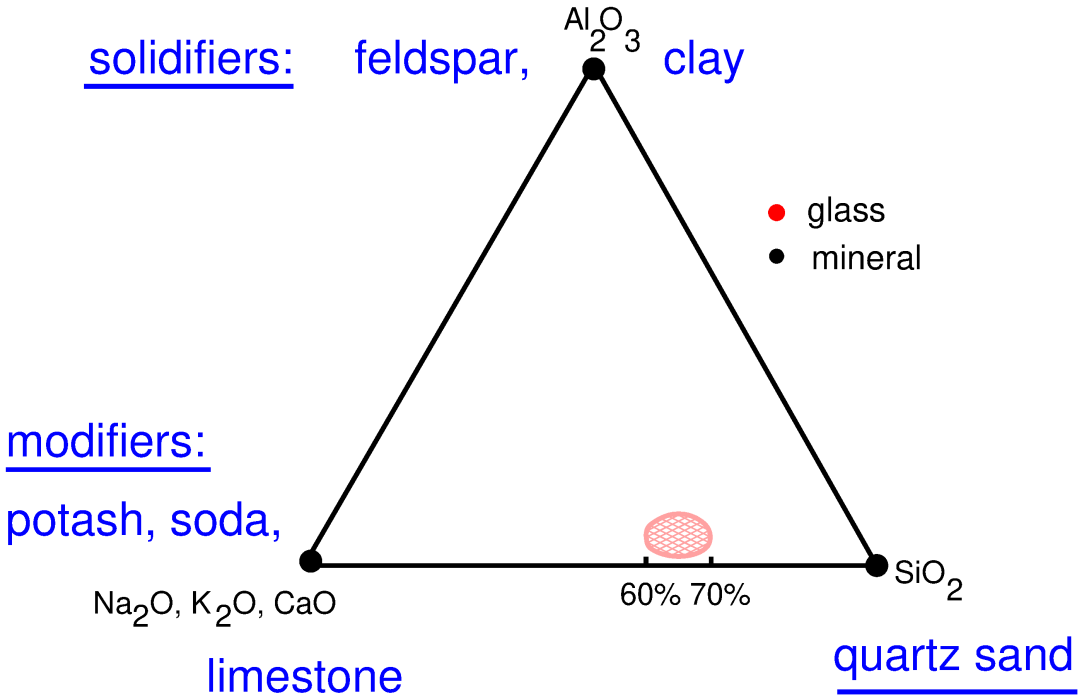

Figure 6: Composition diagram of soda-lime glass.

In order to reduce the melting temperature of SiO_2, which is around $T_m \sim$ 2000 K to around 1400 K, Kations K^+ (potash K_2O and Na^+ (soda Na_2 O) are added, the so-called network modifiers. In order to make the material more stable, lime (CaO) and alumina (feldspar, clay, Al_2O_3 are further added. Such soda-lime glass comprises the majority of every-day silicate glass.

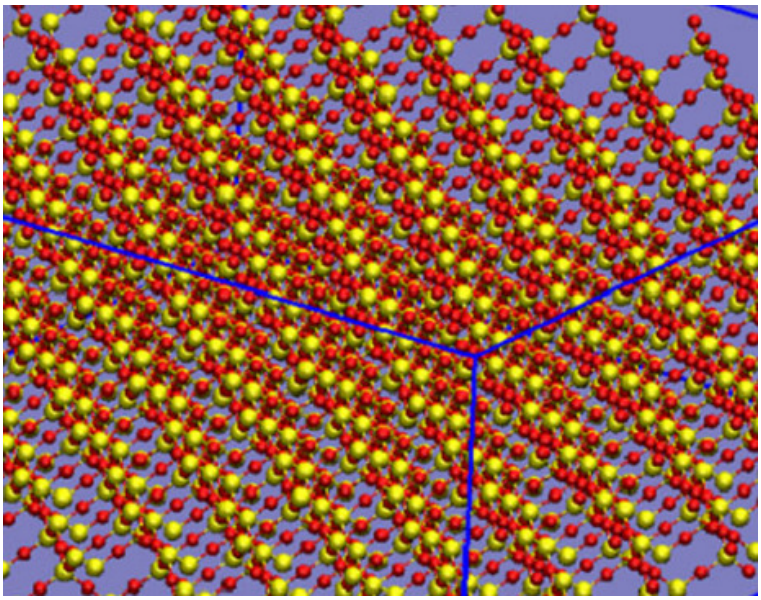

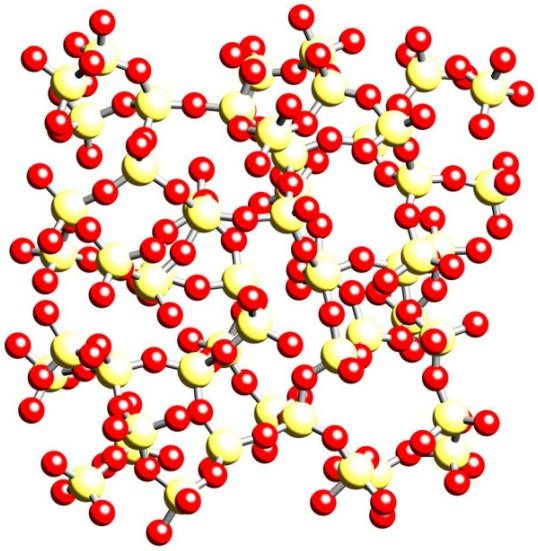

Figure 7: Structure models of crystalline and amorphous SiO_2.

2.2 Fragile glasses

There are a large number of glass-forming materials, which do not form a covalent network in the glassy state. They have been termed "fragile" by C. Austen Angell (see picture), who contributed many scientific ideas to glass science. These materials include

C. Austen Angell 1933 - 2021

boron oxide	B_2O_3
arsen selenide	As_2Se_3
propanol	$CH_3(CH_2)^2OH$
glycerol	$(CH_2OH)^2CHOH$
zinc chloride	$ZnCl_2$
toluene	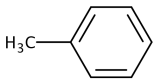
propylene carbonate	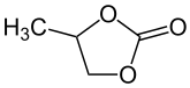
o-terphenyl	
molten salts like Potassium-Calcium Nitrate	$3KNO_3$-$2Ca(NO_3)_2$

These materials not only become glasses when cooled without forming a covalent network. The viscosity of these materials increases much more rapidly with decreasing temperature than that of silicate glasses. We will discuss these phenomena in detail in chapters 4 and 5.

2.3 Polymers

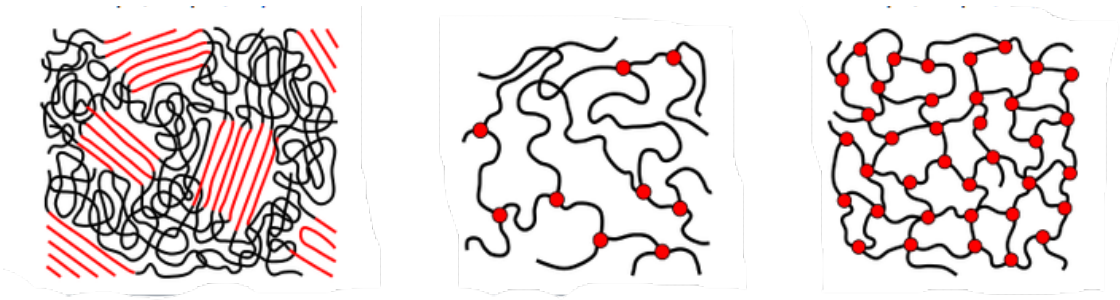

Figure 8: Structure of different types of polymeric materials. Left: Thermoplastic consisting of un-crosslinked polymers; middle: elastomers like rubber; right: thermoset (Duroplast). (from Wikipedia).

Polymer materials (Plastics) are nowadays ubiquitous. They are essentially of amorphous structure, although there exist crystalline patches, in which the "spaghettis" just line up. In fact, we are facing a severe polution of our environment, especially sea water, with remnants of plastics. Polymeric materials can be just macro-molecules or cross-linked macromolecules (thermoplastics). The former comprise the common plastic materials. Crosslinked plastics are more elastic like rubber, and heavily crosslinked materials (thermoset) withstand heat.

2.4 Organic Semiconductors

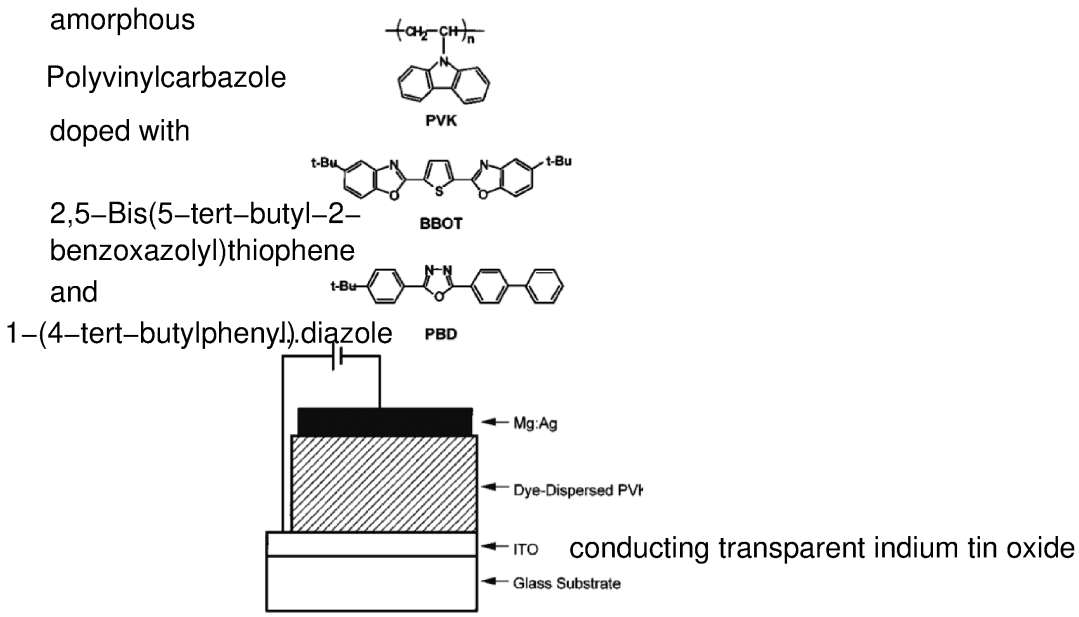

Device structure and materials used in the first polymer-based white OLED reported by Kido, Shionoya, and Nagai (1995). BBOT and PBD are electron-transporting materials that are added to the hole-transporting PVK matrix to improve carrier balance. From Kido, Shionoya, and Nagai, 1995.

Figure 9: Structure of an organic light-emitting diod (OLED) with constituing materials; from [10].

Organic semiconductors have revolutionized everyday-lighting, as the organic light-emitting diods, LED have replaced the filament bulb, as they consume apreciably less energy. The luminecent material, PET is an aromatic poly material, which structurally disordered like plastics.

2.5 Metallic Glasses

Metallic Glass	R_c (K s^{-1})
$Au_{55}Cu_{25}Si_{20}$	3.4×10^4
$Fe_{48}Cr_{15}Mo_{14}Y_2C_{15}B_6$	140–190
$Co_{75}Si_{15}B_{10}$	3.8×10^8
$Fe_{79}Si_{10}B_{11}$	3.7×10^8
$Ni_{75}Si_8B_{17}$	2.4×10^8
$Pd_{77.5}Cu_6Si_{16.5}$	1.5×10^8
$Pd_{40}Ni_{40}P_{20}$	1.4×10^7
$Zr_{41.2}Ti_{13.8}Cu_{12.5}Ni_{10.0}Be_{22.5}$	≤ 10
$Al_{51}Ge_{35}Ni_{14}$	10^4
$Fe_{76}Si_9B_{10}P_5$	≤ 550
$Pd_{40}Cu_{30}Ni_{10}P_{20}$	2.08×10^{-5}
$Au_{49}Ag_{5.5}Pd_{2.3}Cu_{26.9}Si_{16.3}$	600
$Zr_{52.5}Ti_5Al_{10}Ni_{14.6}Cu_{17.9}$	10^3–10^5
$Fe_{67}Mo_{4.5}Cr_{2.3}Al_2Si_3C_7P_{8.7}B_{5.5}$	9.3×10^4
$Al_{86}Ni_6Y_{4.5}Co_2La_{1.5}$	3.01×10^3

Figure 10: List of metallic glasses together with the necessary cooling rate for producing them; from [11]

For a long time metallic glasses could only be prepared by very rapid quenching from the metallic melt. Cooling rate as high as 10^8 K/s could be achieved by directing a jet of liquid metal onto a spinning wheel (melt spinning). Another method was placing a drop of liquid metal on an anvil and strike at it with a hammer (splat cooling). The glass-forming liquids were mainly binary and ternary alloys. By these methods only very thin samples ("lametta") could be produced. Later it was found that by mixing more and more constituent metals much lower cooling rates could be achieved. This enabled to prepare bulk metallic glasses. These materials are very strong and elastic.

2.6 Spin Glasses

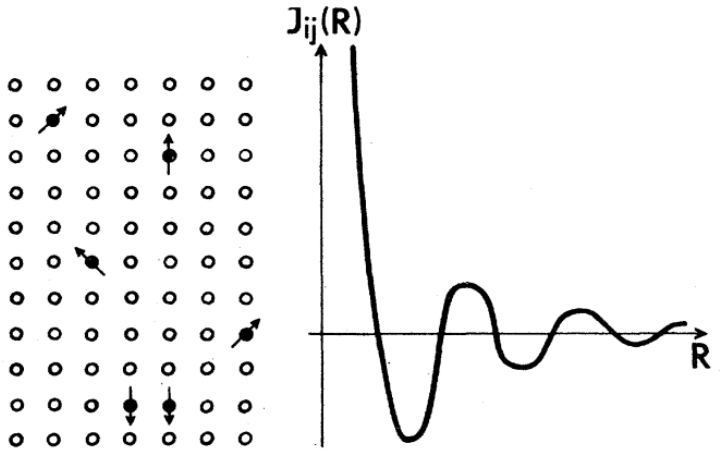

Schematic sketch of magnetic moments randomly diluted in a metallic matrix, and the resulting RKKY exchange integral plotted as a function of distance.

Figere 11: Ruderman-Kittel-Kasuya-Yosida (RKKY) interaction between Mn spins in a crystalline Cu host; from [12]

Spin glasses are dilute magnetic alloys in which the magnetic moments interact with a potential, which may take both signs (Ruderman-Kittel-Kasuya-Yosida ,RKKY, interaction). This interaction is mediated by the electron gas of the metallic non-magnetic host material. The oscillatory behavior of the RKKY interaction stems from the sharp kink in the occupation number (Fermi function) of the electron gas.

Giorgio Parisi, Nobel prize 2021

The question, whether there is a thermodynamic spin-glass transition has generated a plethora of theoretical investigations. Sherrington and Kirkpatrick came up with a model of spins, in which every spin interacts with every other spin, and the interaction strength is just ± 1. Giorgio Parisi applied the so-called Replica method to obtain a rigorous thermodynamic description of this model, including a thermodynamic glass transition.

Finally he obtained a Nobel price for his related work, which is much more general, as it may describe complex systems like neuronal networks or finance markets. The replica spin-glass theory had its way into the attempts for describing the freezing of glass materials, but the outcome is still rather

controversal. We shall discuss these issues in chapter 5.

3 Structure and thermodynamic relations

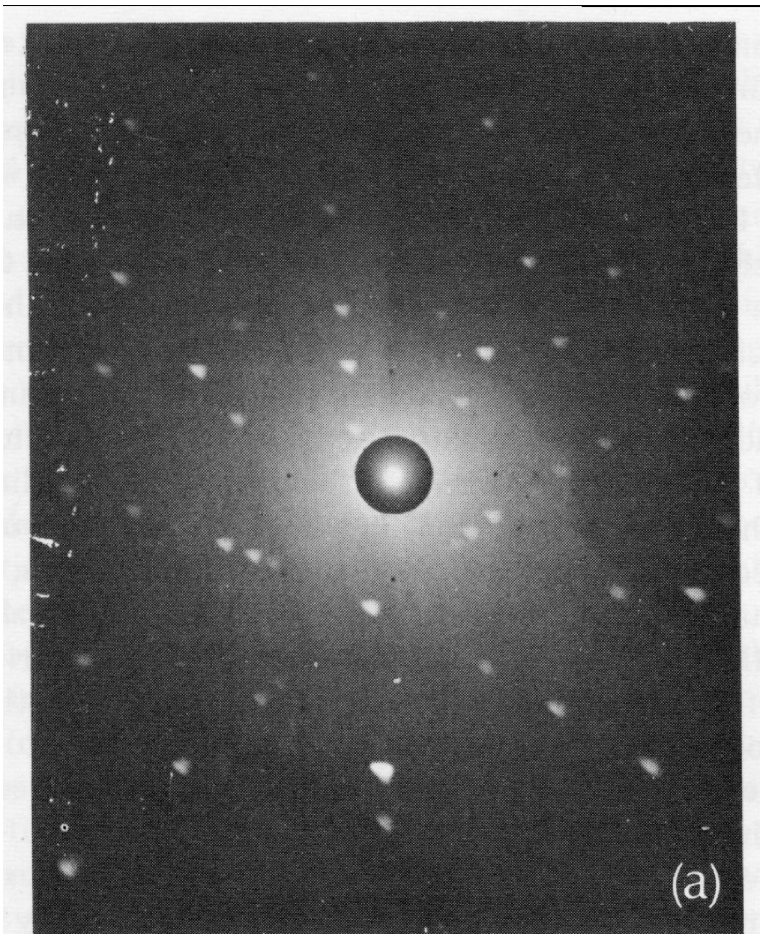

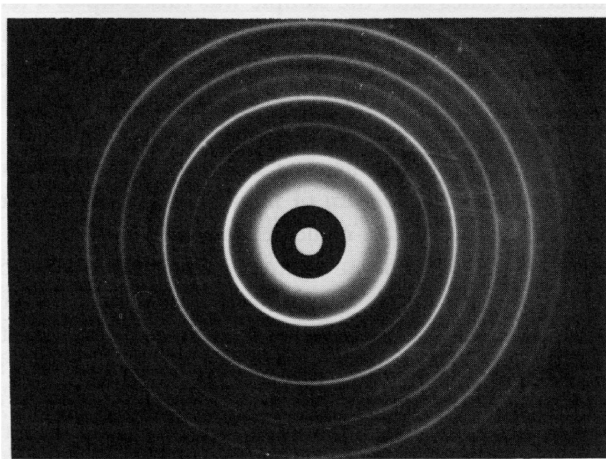

Figure 12: X-ray pictures of crystalline and glassy material.

3.1 Spatial and time Fourier transforms

3.1.1 The Fourier transforms

In our treatment we shall frequently use Fourier transforms both with respect to space and time[1] A Fourier transform of a function $f(t)$ is given by

$$f(\omega) = \int_{-\infty}^{\infty} \mathrm{d}t e^{i\omega t} f(t) \tag{3.1}$$

$f(\omega)$ is also called the power spectrum of the function $f(t)$.
A spatially farying function $f(\mathbf{r})$ can be Fourier transformed as

$$f(\mathbf{q}) = \int_{-\infty}^{\infty} \mathrm{d}^3\mathbf{r} e^{i\mathbf{qr}} f(\mathbf{r}) \tag{3.2}$$

with

$$\int_{-\infty}^{\infty} \mathrm{d}^3\mathbf{r} \doteq \int_{-\infty}^{\infty} \mathrm{d}x \int_{-\infty}^{\infty} \mathrm{d}y \int_{-\infty}^{\infty} \mathrm{d}z \tag{3.3}$$

[1] All the following improper integrals are understood to apply to functions, which vanish rapidly enough at infinity in order to guarantee convergence.

3.1.2 The back transforms

$$f(t) = \frac{1}{2\pi}\int_{-\infty}^{\infty} \mathrm{d}\omega e^{-i\omega t} f(\omega) \tag{3.4}$$

$$f(\mathbf{r}) = \left(\frac{1}{2\pi}\right)^3 \int_{-\infty}^{\infty} \mathrm{d}^3\mathbf{q} e^{-i\mathbf{q}\mathbf{r}} f(\mathbf{q}) \tag{3.5}$$

with

$$\int_{-\infty}^{\infty} \mathrm{d}^3\mathbf{q} \doteq \int_{-\infty}^{\infty} \mathrm{d}q_x \int_{-\infty}^{\infty} \mathrm{d}q_y \int_{-\infty}^{\infty} \mathrm{d}q_z \tag{3.6}$$

3.1.3 Fourier transform of a delta function

$$f_\delta(\omega) = \int_{-\infty}^{\infty} \mathrm{d}t e^{i\omega t}\delta(t-t_0) = e^{i\omega t_0} \tag{3.7}$$

from which follows the back transform

$$\delta(t-t_0) = \frac{1}{2\pi}\int_{-\infty}^{\infty} \mathrm{d}\omega e^{-i\omega[t-t_0]} \tag{3.8}$$

In particular, setting $t_0 = 0$:

$$\delta(t) = \frac{1}{2\pi}\int_{-\infty}^{\infty} \mathrm{d}\omega e^{-i\omega t} 1 \tag{3.9}$$

i.e. the Fourier transform of a delta pulse is a constant as a function of frequency. This is called a white-noise spectrum. The reverse is also valid: The Fourier transform of a constant in time is a delta function in frequency space. All this applies as well to spatial Fourier transforms.

3.1.4 Spatial Fourier transform of a function depending on the modulus r

If a spatial function depends only on the modulus of $\mathbf{r}$, $r = |\mathbf{r}|$ we may change to spherical coordinates and perform the angular integration straight away:

$$\begin{aligned}
f(\mathbf{q}) &= \underbrace{\int_0^{\infty} r^2 \mathrm{d}r \int_0^{\pi} \sin\theta \mathrm{d}\theta \int_0^{2\pi} \mathrm{d}\phi}_{\int_{-\infty}^{\infty} \mathrm{d}^3\mathbf{r}} e^{iqr\underbrace{\cos\theta}_{\zeta}} f(r) && (3.10)\\
&= 2\pi \int_0^{\infty} r^2 \mathrm{d}r \int_{-1}^{1} \mathrm{d}\zeta e^{iqr\zeta} && (3.11)\\
&= 4\pi \int_0^{\infty} r^2 \mathrm{d}r \frac{\sin(qr)}{qr} f(r) && (3.12)\\
&= \frac{1}{q} 4\pi \int_0^{\infty} r \mathrm{d}r \sin(qr) f(r) = f(q) && (3.13)
\end{aligned}$$

3.1.5 Convolution theorem

A convolution (Faltung) is defined by

$$h(t) = [f \circ g](t) = \int_{-\infty}^{\infty} \mathrm{d}\tilde{t} f(\tilde{t}) g(t - \tilde{t}) \tag{3.14}$$

Its Fourier transform is given by

$$\begin{aligned} h(\omega) &= \int_{-\infty}^{\infty} \mathrm{d}t e^{i\omega t} \int_{-\infty}^{\infty} \mathrm{d}\tilde{t} f(\tilde{t}) g(\underbrace{t - \tilde{t}}_{\tau}) && (3.15) \\ &= \int_{-\infty}^{\infty} \mathrm{d}\tau e^{i\omega\tau} g(\tau) \int_{-\infty}^{\infty} \mathrm{d}\tilde{t} e^{i\omega\tilde{t}} f(\tilde{t}) \stackrel{!}{=} f(\omega) g(\omega) && (3.16) \end{aligned}$$

As a Corrollar follows $f \circ g = g \circ f$. The 3-dimensional spatial version is

$$h(\mathbf{r}) = [f \circ g](\mathbf{r}) \int_{-\infty}^{\infty} \mathrm{d}^3\tilde{\mathbf{r}} f(\tilde{\mathbf{r}}) g(\mathbf{r} - \tilde{\mathbf{r}}) \tag{3.17}$$

$$h(\mathbf{q}) = f(\mathbf{q}) g(\mathbf{q}) \tag{3.18}$$

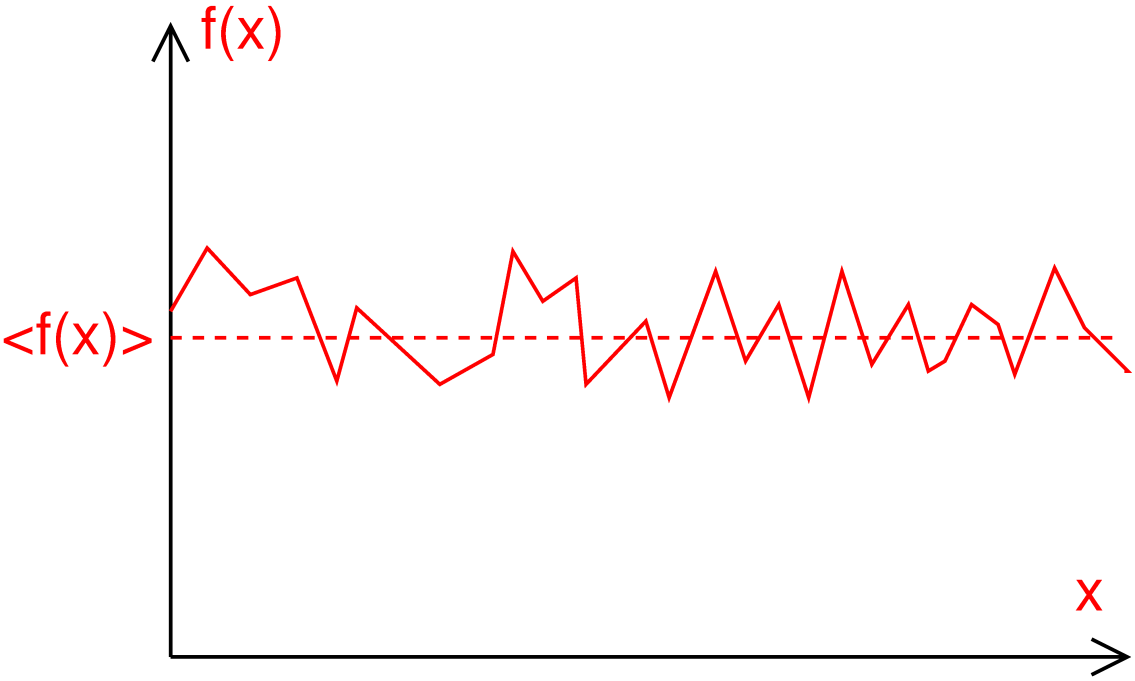

Figure 13: Fluctuating function $f(x)$ and its mean value $\langle f(x)\rangle$.

3.1.6 Fluctuations and Correlation functions

The complexity of the physical world leads to all kind of random motions and random structures. The temperature in some geographic place does not only oscillate due to the day-night cycle but exhibit also random fluctuations. If one looks at the surface of an object with a microscope, it exhibit spatial fluctuations. The fluctuations are defined as the deviation from a mean or average value

$$\Delta f(x) = f(x) - \langle f(x)\rangle \tag{3.19}$$

with the x average[2]

$$\langle f(x)\rangle \equiv \langle f\rangle = \frac{1}{L}\int\limits_L dx f(x)\,, \tag{3.20}$$

where L is the measured interval, which may be pushed towards ∞, if L is large compared with the typical fluctuation intervals.

In Fig. 13 we show a fluctuating function $f(x)$ together with its average.

If x is the time, one speaks of fluctuations in time and a time average, if x is one of the Cartesian coordinates, one speaks of a spatial fluctuations and a spatial average.
A correlation function describes how nearby parts of $\Delta f(x)$ are similar to each other:

$$C_{ff} = \Big\langle \Delta f(x_0)\Delta f(x+x_0)\Big\rangle = \frac{1}{L}\int_L dx_0 \Delta f(x_0)\Delta f(x+x_0) \tag{3.21}$$

One can also correlate two functions $f(x)$ and $g(x)$

$$C_{fg} = \langle \Delta f(x_0)\Delta g(x+x_0)\rangle = \frac{1}{L}\int_L dx_0 \Delta f(x_0)\Delta g(x+x_0)\,. \tag{3.22}$$

[2]In the mathematical literature the average (or mean) is called expectation value.

In the first case one speaks of an auto-correlation, in the second case a cross-correlation

- Important remark:

A correlation of two fluctuating functions does not imply a causal relation. (If in a local geographic region a correlation of the population of storchs and the birth rate exists, this does not mean that the little kids are brought by the storchs.)

3.1.7 Annealed and quenched disorder

In thermal equilibrium the timely and spatial fluctuations are characterized by the Boltzmann distribution of the possible arrangements of the canonical coordinates and momenta. This type of disorder is called annealed disorder. A system in thermal equilibrium, like a liquid or a gas, has the

ergodic property:

- The ensemble average performed with a Boltzmann weight is equal to a time average.

A glass is a disordered system, which is not in thermal equilibium, and has not the ergodic property. The disorder is a frozen configurational one, and one speaks of quenched disorder. In computer simulations one can prepare a lot of quenched samples and then perform a sample average, which may for a large amount of samples be equal to an ensemble average (over all possible configurations). However, if a single sample is very large and is sufficiently large-scale homogeneous, it may have the

self-averaging property:

- The ensemble average performed over different samples is equal to a spatial average.

In the following we assume that we are allowed to perform an average of a spatially fluctuating quantity $A(\mathbf{r})$ as

$$\langle A(\mathbf{r})\rangle = \frac{1}{V}\int\limits_V \mathrm{d}^3\mathbf{r}A(\mathbf{r}) \tag{3.23}$$

Here V is the sample volume. Theoreticians very often take the thermodynamic limit:

$$\lim_{\substack{N\to\infty\\ V\to\infty}} \langle A(\mathbf{r})\rangle = \frac{1}{V}\int\limits_V \mathrm{d}^3\mathbf{r}A(\mathbf{r})\Big|_{\rho_0=N/V=\mathrm{const.}} \tag{3.24}$$

This is certainly justified, of one is interested in samples with $N = 10^{23}$ molecules.

3.1.8 Density-autocorrelation function

We define a local density as

$$\rho(\mathbf{r}) = \sum_{\alpha=1}^{N} \delta(\mathbf{r} - \mathbf{r}_\alpha) \tag{3.25}$$

If $\rho(\mathbf{r})$ is integrated over a certain volume the integral gives just the number of the particles inside of this volume, which shows that this definition is correct. The spatial average gives the mean density

$$\langle \rho \rangle = \frac{1}{V} \int_V \mathrm{d}^3\mathbf{r} \rho(\mathbf{r}) = \frac{1}{V} \int_V \mathrm{d}^3\mathbf{r} \sum_{\alpha=1}^{N} \delta(\mathbf{r} - \mathbf{r}_\alpha) = \frac{N}{V} \equiv \rho_0 \tag{3.26}$$

A density fluctiation is therefore defined as

$$\Delta\rho(\mathbf{r}) = \rho(\mathbf{r}) - \rho_0 \tag{3.27}$$

The density-density correlation function is

$$C_{\rho\rho} \lim_{V\to\infty} \frac{1}{V} \int_V \mathrm{d}^3\mathbf{r} \Big\langle \Delta\rho(\mathbf{r} + \mathbf{r}_0) \Delta\rho(\mathbf{r}_0) \Big\rangle \tag{3.28}$$

To evaluate this quantity we need to take care of several subtleties. First we apply the general identity

$$\Big\langle \Delta A(\mathbf{r} + \mathbf{r}_0) \Delta A(\mathbf{r}_0) \Big\rangle = \Big\langle A(\mathbf{r} + \mathbf{r}_0) A(\mathbf{r}_0) \Big\rangle - \langle A \rangle^2 \tag{3.29}$$

to the density-density correlation function

$$\Big\langle \big[\rho(\mathbf{r} + \mathbf{r}_0) - \rho_0\big] \big[\rho(\mathbf{r}_0) - \rho_0\big] \Big\rangle = \Big[\Big\langle \rho(\mathbf{r} + \mathbf{r}_0) \rho(\mathbf{r}_0) \Big\rangle - \rho_0^2 \Big] \tag{3.30}$$

Then we split the double sum into the $\alpha = \beta$ term and the $\alpha \neq \beta$ terms:

$$\begin{aligned} \Big\langle \rho(\mathbf{r} + \mathbf{r}_0) \rho(\mathbf{r}_0) \Big\rangle &= \Big\langle \sum_{\alpha\beta} \delta(\mathbf{r} + \mathbf{r}_0 - \mathbf{r}_\alpha) \delta(\mathbf{r}_0 - \mathbf{r}_\beta) \Big\rangle \\ &= \Big\langle \sum_{\alpha} \delta(\mathbf{r} + \mathbf{r}_0 - \mathbf{r}_\alpha) \delta(\mathbf{r}_0 - \mathbf{r}_\alpha) \Big\rangle + \Big\langle \sum_{\alpha\neq\beta} \delta(\mathbf{r} + \mathbf{r}_0 - \mathbf{r}_\alpha) \delta(\mathbf{r}_0 - \mathbf{r}_\beta) \Big\rangle \end{aligned} \tag{3.31}$$

The first term just gives

$$\frac{1}{V} \sum_\alpha \int \mathrm{d}^3\mathbf{r}_0 \Big(\delta(\mathbf{r}_0 - \mathbf{r}_\alpha) \Big) \delta(\mathbf{r} + \mathbf{r}_0 - \mathbf{r}_\alpha) = \frac{N}{V} \delta(\mathbf{r}) \tag{3.32}$$

The second term is the so-called two-partical density distribution function

$$\rho^{(2)}(r) = \Big\langle \sum_{\alpha\neq\beta} \delta(\mathbf{r} + \mathbf{r}_0 - \mathbf{r}_\alpha) \delta(\mathbf{r}_0 - \mathbf{r}_\beta) \Big\rangle \equiv \rho_0^2 g(r)\,, \tag{3.33}$$

$g(r)$ is the radial pair distribution function, which has the following properties:

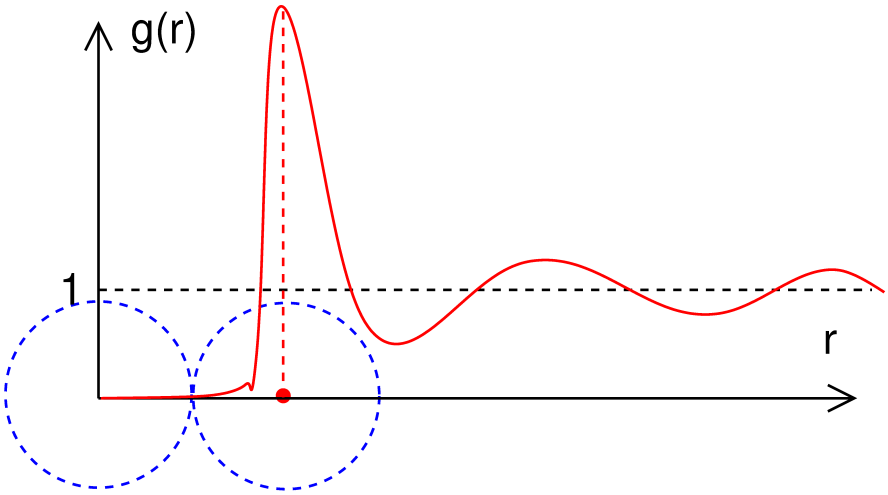

Figure 14: Radial distribution function $g(r)$ of a liquid or glass. The peak of $g(r)$ gives the nearest-neighor distance between two molecules or atoms.

- $$P(r) = 4\pi\rho_0 r^2 g(r) dr$$

  gives the average number of particles inside the interval $[r, r+dr]$, where r is the distance from a given particle placed at $r = 0$.

- $$Z(R) = 4\pi\rho_0 \int_0^R \mathrm{d}r r^2 g(r)$$

  gives the average number of particles inside a sphere of radius R around a particle placed at the center of the sphere. If R is taken as the first minimum in $g(r)$, Z is the number of nearest neighbours or coordination number.

We can now collect the three terms contributing to the density-density correlation function:

$$C_{\rho\rho}(r) = \rho_0 \delta(\mathbf{r}) + \rho_0^2 g(r) - \rho_0^2 \tag{3.34}$$

The Fourier transform is then

$$C_{\rho\rho}(q) = \rho_0 S(q) \tag{3.35}$$

with the structure factor

$$\begin{aligned} S(q) &= 1 + \rho_0 \int \mathrm{d}^3\mathbf{r}\, e^{i\mathbf{qr}} \left[g(r) - 1\right] \\ &= 1 + 4\pi\rho_0 \int_0^\infty \mathrm{d}r r^2 \frac{\sin(qr)}{qr} \left[g(r) - 1\right] \\ &= \frac{1}{N} \sum_{\alpha\beta} e^{i\mathbf{q}[\mathbf{r}_\alpha - \mathbf{r}_\beta]} \cancel{- \rho_0 \delta(\mathbf{q})} \end{aligned} \tag{3.36}$$

Note that the sum now includes the $\alpha = \beta$ term. The $\delta(\mathbf{q})$ term is usually discarded.

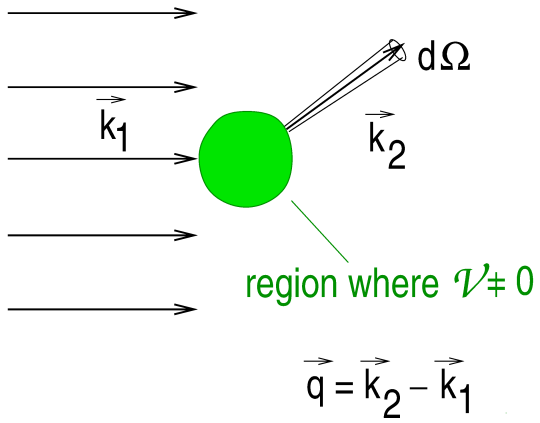

Figure 15: Geometry for a scattering experiment with incoming plane wave and outgoing spherical wave

3.1.9 Scattering theory

We want to describe the (elastic) scattering of X-rays or neutrons from a simple glass sample. We study an ingoing plane wave (1st term) and an outgoing scattered spherical wave (2nd term), as depicted in Fig. 15, of the following asymptotic form

$$\psi(\mathbf{r}) \overset{|\mathbf{r}|\to\infty}{=} e^{i\mathbf{k}_1\cdot\mathbf{r}} + f(\theta)\frac{1}{r}e^{ik_2 r} \tag{3.37}$$

The scattering cross-section into the solid angle element $\mathrm{d}\Omega$ in the direction of $\mathbf{k}_2$ is then given by the modulus-square of the scattering amplitude

$$\frac{\mathrm{d}\sigma}{\mathrm{d}\Omega} = |f(\theta)|^2 \tag{3.38}$$

If the scattering potential (the potential between the scattered rays and the sample) can be decomposed as

$$\mathcal{V}(\mathbf{r}) = \sum_{\alpha=1}^{N} v(\mathbf{r}-\mathbf{r}_\alpha) \tag{3.39}$$

Its Fourier transform is

$$\begin{aligned}
\mathcal{V}(\mathbf{q}) &= \int \mathrm{d}^3\mathbf{r} e^{i\mathbf{q}\mathbf{r}} \sum_{\alpha=1}^{N} v(\underbrace{\mathbf{r}-\mathbf{r}_\alpha}_{\tilde{\mathbf{r}}_\alpha}) \qquad \mathbf{r} = \tilde{\mathbf{r}}_\alpha + \mathbf{r}_\alpha \\
&= \sum_{\alpha=1}^{N} e^{i\mathbf{q}\mathbf{r}_\alpha} \int \mathrm{d}^3\tilde{\mathbf{r}}_\alpha e^{i\mathbf{q}\tilde{\mathbf{r}}_\alpha} v(\tilde{\mathbf{r}}_\alpha) \\
&= \sum_{\alpha=1}^{N} e^{i\mathbf{q}\mathbf{r}_\alpha} v(\mathbf{q})
\end{aligned} \tag{3.40}$$

the scattering amplitude is given in lowest approximation

$$f(\theta) = -\frac{m}{2\pi\hbar^2}\langle\mathbf{k}_2|\mathcal{V}|\mathbf{k}_1\rangle \tag{3.41}$$

The wavefunction of a plane-wave X-ray or neutron is given by

$$\langle\mathbf{r}|\mathbf{k}\rangle = \frac{1}{V^{1/2}}\, e^{i\mathbf{k}\mathbf{r}} \tag{3.42}$$

Therefore we get for the matrix element of the potential

$$\langle \mathbf{k}_2|\mathcal{V}|\mathbf{k}_1\rangle = \int \mathrm{d}^3\mathbf{r}\mathcal{V}(\mathbf{r})\frac{1}{V}e^{i\mathbf{r}\underbrace{(\mathbf{k}_2-\mathbf{k}_1)}_{\mathbf{q}}} = \frac{1}{V}\sum_{\alpha=1}^{N} e^{i\mathbf{q}\mathbf{r}_\alpha}v(\mathbf{q}) \tag{3.43}$$

$$f(\theta) = -\frac{m}{2\pi\hbar^2 V}\mathcal{V}(\mathbf{q}) = -\frac{m}{2\pi\hbar^2 V}\sum_{\alpha=1}^{N} e^{i\mathbf{q}\cdot\mathbf{r}_\alpha}v(\mathbf{q}) \equiv \sum_{\alpha=1}^{N} e^{i\mathbf{q}\cdot\mathbf{r}_\alpha}f(\mathbf{q})\,, \tag{3.44}$$

If the scattered radiation does not exchange any energy with the specimen, one speaks of elastic scattering. In this case

$$|\mathbf{k}_1| = |\mathbf{k}_2| = k = \frac{2\pi}{\lambda}\,, \tag{3.45}$$

where λ is the wavelength of the scattered radiation.
The elastic scattering cross-section depends only on the modulus $q = |\mathbf{q}|$ of the exchanged momentum, and we have

$$q = |\mathbf{k}_1 - \mathbf{k}_2| = \sqrt{k^2 + k^2 - 2k^2\cos(\theta)} = k\sqrt{2[1-\cos(\theta)]} = \frac{4\pi}{\lambda}\sin\left(\frac{\theta}{2}\right)\,, \tag{3.46}$$

where θ is the angle between $\mathbf{k}_1$ and $\mathbf{k}_2$. The last equality in Eq. (3.46) follows from the identity

$$\cos(\theta) = \cos^2\left(\frac{\theta}{2}\right) - \sin^2\left(\frac{\theta}{2}\right) = 1 - 2\sin^2\left(\frac{\theta}{2}\right) \tag{3.47}$$

In the case of neutrons, which scatter from the nuclei, whose potential $v(\mathbf{r})$ is extremely short-ranged, $f(q)$ does not depend on q (in the range of interest $q < 20$ Å^{-1}) and is called scattering length and is denoted by the letter b.
Inserting (3.41) into (3.38) and averaging over an ensemble of different configurations we obtain

$$\frac{\mathrm{d}\sigma}{\mathrm{d}\Omega} = |f(q)|^2\left\langle \sum_{\alpha,\beta=1}^{N} e^{i\mathbf{q}\cdot[\mathbf{r}_\alpha-\mathbf{r}_\beta]}\right\rangle \equiv \underbrace{|f(q)|^2}_{\text{form factor}}\; N\; \underbrace{S(q)}_{\text{structure factor}}\,, \tag{3.48}$$

We show again the relation of the structure factor with the pair distribution function $g(r)$

$$S(q) = \frac{1}{N}\left\langle \sum_{\alpha,\beta=1}^{N} e^{i\mathbf{q}\cdot[\mathbf{r}_\alpha-\mathbf{r}_\beta]}\right\rangle = 1 + \frac{4\pi\rho_0}{q}\int_0^\infty \mathrm{d}r\,\sin(qr)\,r\Big(g(r)-1\Big) \tag{3.49}$$

In experimental evaluations of $S(q)$ often the function

$$T(r) = rg(r) \tag{3.50}$$

is plotted, instead of $g(r)$. In Fig. 16 we show the example of the structure factor for glassy SiO_2, as measured by [13] by means of neutron diffraction, together with $T(r)$. The X-ray treat the Si and O atoms as almost indistinguishable, so that the peaks in $T(r)$ can be associated with $O-O$, $Si-O$, and $Si-Si$ distances.

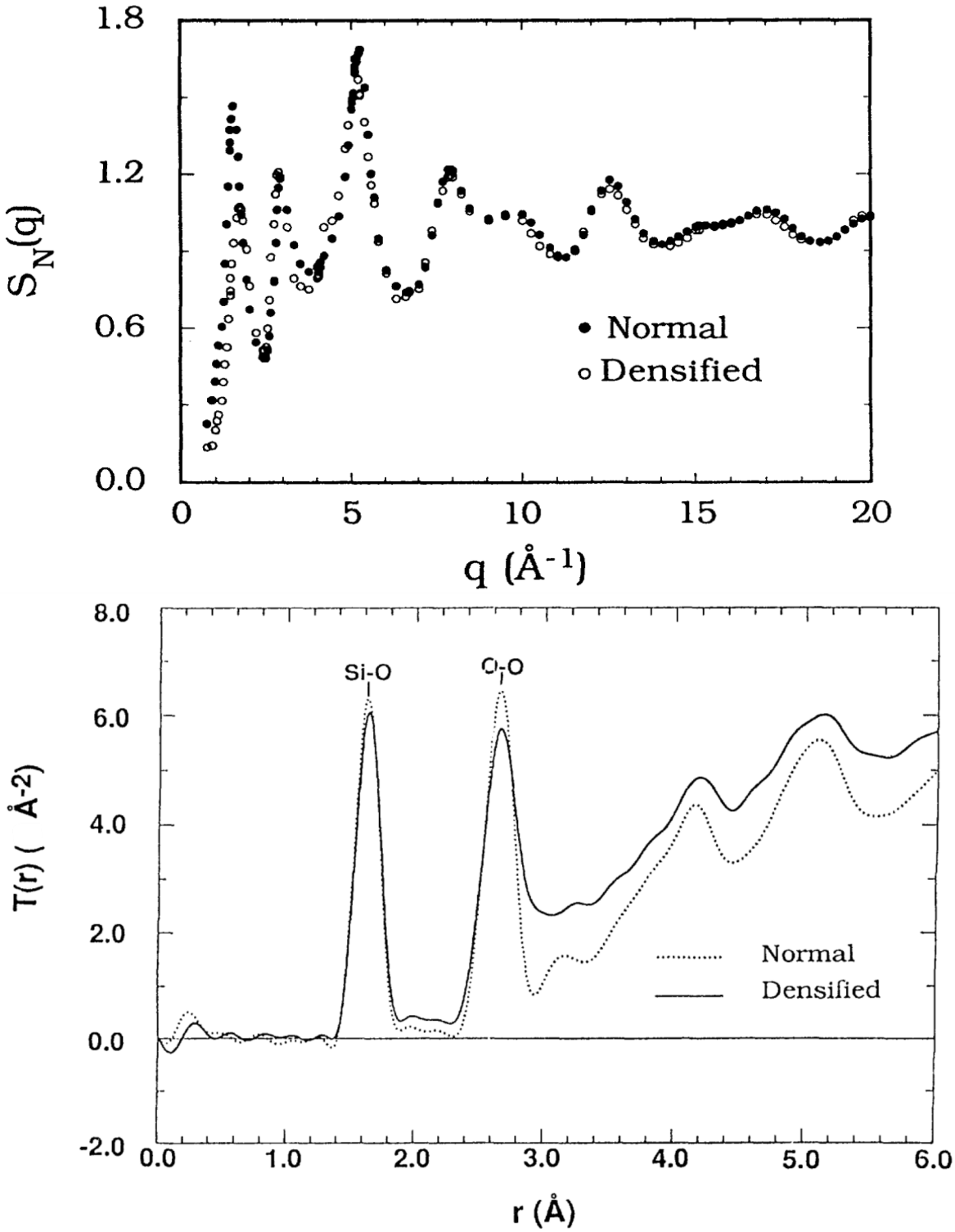

Figure 16: Top panel: Structure factor of normal and pressure-densified glassy SiO_2, measured by neutron diffraction [13].
Bottom panel: Corresponding modified pair distribution function $T(r) = 4\pi r \rho_0 g(r)$

3.1.10 Thermodynamic relations for $g(r)$

We are now assuming that the liquid under consideration can be described by a Hamiltonian with a pairwise interaction potential

$$\mathcal{H} = \sum_{\alpha=1}^{N} \frac{1}{2} m \dot{\mathbf{r}}_\alpha^2 + \frac{1}{2} \sum_{\alpha \neq \beta} \phi(|\mathbf{r}_\alpha - \mathbf{r}_\beta|) \,. \tag{3.51}$$

$\phi(|\mathbf{r}_\alpha - \mathbf{r}_\beta|)$ is the interaction potential between the atoms or molecules, not to be confused with the interaction $v(\mathbf{r} - \mathbf{r}_\alpha)$ between the scattering waves and the atoms.

There are the following thermodynamic relationships, called equations of state:

Energy

$$\frac{U}{N} = 2\pi\rho_0 \int_0^\infty \mathrm{d}r \; r^2 \phi(r) g(r) \tag{3.52}$$

Pressure

$$\frac{PV}{N k_B T} = \frac{P}{\rho_0 k_B T} = 1 - \frac{2\pi\rho_0}{3 k_B T} \int_0^\infty \mathrm{d}r \; r^3 \phi'(r) g(r) \tag{3.53}$$

Compressibility

$$S(q{=}0) = \rho_0 k_B T \kappa_T = 1 + 4\pi\rho_0 \int_0^\infty \mathrm{d}r \; r^2 [g(r) - 1] \tag{3.54}$$

with the isothermal compressibility

$$\kappa_T = -\frac{1}{V} \left(\frac{\partial V}{\partial P} \right)_T \tag{3.55}$$

Figure 17: Shape of the main British island as example of a fractal.

3.2 Fractal Geometry, Percolation and Gelation

3.2.1 Fractals

In his book "The fractal geometry of nature" [14], which appeared in 1977, the French mathematician Benoit Mandelbrot coined the word *fractal* for geometrical objects, which do not have an inherent length scale, i.e. they are *self similar*. They just look the same at very different length scales. Such object are trees, sponges, termination deltas of rivers, tidal streaming traces, clouds, mountains – and coast lines. Although Mandelbrot made fractals a fashionable subject in physics, self-similar objects have been studied much earlier, e.g some 150 years ago by people like David Hilbert, Giuseppe Peano or Georg Cantor.

Let us start with coast lines. How long is the coast line of England/Scotland? You may measure it with conventional geodesic wooden sticks to come up with a number of about ten thousand km. (The figure given by www.coastalguide.org is 13560 km.) However, if you make your measuring device smaller, so that you can follow all small wrinkles you might be able to double the number: The length of the coast line depends on the scale of the measuring device, or, in other words, if you want to draw the coast line its length depends on the thickness or the sharpness of the pencil. In fact a coastline is a typical fractal object: It has similar wrinkles at different length scales.

In discussing the length of the coast line we found that there is some difficulty to indentify it as a one-dimensional object, as it has a typical property of an object with dimensionality greater than one: It length depends on something else: For an area this is the width, for the coast line it is the thickness of the pencil. In fact fractals turn out *not to have an integer dimensionality.*

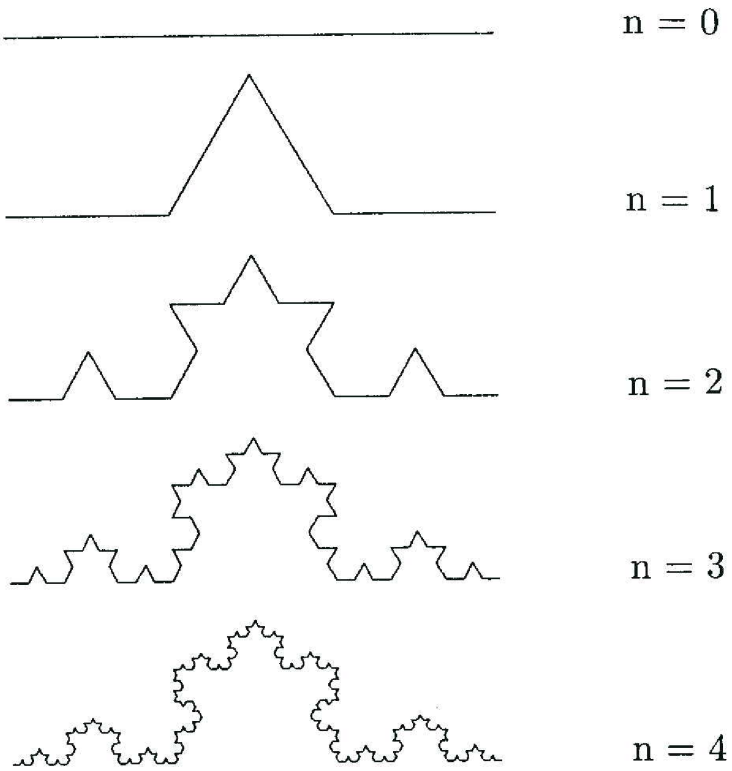

Figure 18: 4 iterations of the Koch curve

Its dimensionality is a *non-integer* number d_f, which is called *fractal dimension.* Let us resume, how in "normal" geometry the dimension is defined: If we multiply the linear size L of a d-dimensional object by a factor b the mass of the object changes by a factor b^d:

$$M(bL) = b^d M(L) \tag{3.56}$$

Let us discuss a regular geometric coast line, which is the *Koch curve* depicted in Fig. 18. A straight line is divided into 3 and the inner part is replaced by the upper part of an equilateral triangle. This procedure is repeated for all 4 new sides. As the Koch curve is iteratively constructed from lines, i.e. one-dimensional objects its "mass" is just its length. This length steadily increases as the iteration is continued, just as in the coastline example. For the Koch curve we can deduce the value of the fractal dimension: Every time the length is increased by a factor of 3 its length increases by a factor of 4. If we call the length of the Koch curve also M we have

$$M(3L) = 4M(L) \tag{3.57}$$

We want to define the fractal dimension just as in (3.56)

$$M(bL) = b^{d_f} M(L) \tag{3.58}$$

comparing (3.57) with (3.58) we obtain

$$d_f = \ln 4/\ln 3 = 1.26185954\cdots \tag{3.59}$$

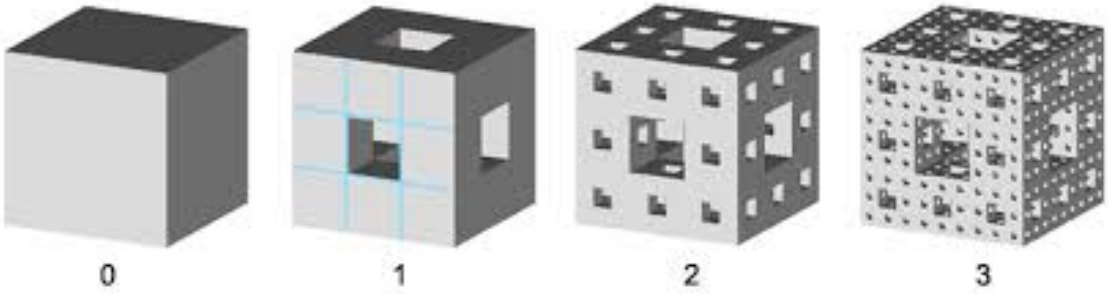

Figure 19: 3 iterations of the Sierpinsi sponge

Figure 20: real sponge

A similar procedure can also repeated with a square or a cube. For the latter (*"Sierpinski sponge"*)

$$M(3L) = 20M(L) \quad \Leftrightarrow \quad d_f = \ln 20/\ln 3 = 2.72683311\cdots \tag{3.60}$$

Note that this number is now between 2 and 3.
One even can generate fractals with dimensions *below* 1. These are point-like objects, called *dusts* by Mandelbrot. The *Cantor set* is iterated by taking just the middle third out of the unity interval, and then this procedure is repeated for every remaining interval. For the remaining dust we have the scaling relation

$$M(3L) = 2M(L) \quad \Leftrightarrow \quad d_f = \ln 2/\ln 3 = 0.630929768\cdots \tag{3.61}$$

One can show that from a topological point of view the Cantor set has the Lebesgue measure 0, but its elements are *not* countable, i.e. it can not be mapped onto the set of integers.
In cases, in which the scaling law is not obvious one can calculate d_f *empirically* by the so-called *box counting algorithm*. For this we need to define

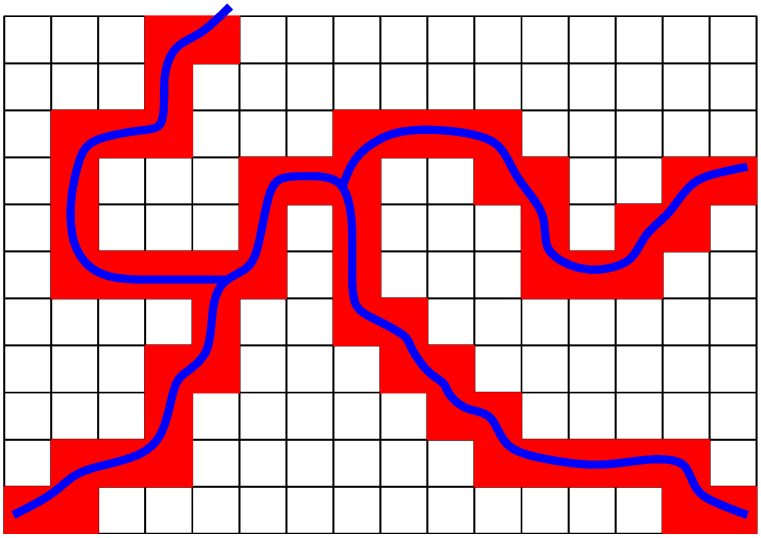

Figure 21: Box-counting determination of the fractal dimension

the *imbedding dimension*, which is just called d The imbedding dimension is the dimension of the space, in which the defining algorithm of the fractal is formulated. So for the Cantor set $d = 1$, for the Koch curve and the Sierpinski gasket $d = 2$, and for the Sierpinski sponge $d = 3$. For the fractal, for which one wants to determine d_f one sets up a mesh of boxes inside a big hypercube of length L, which are hypercubes of "mass" $(\epsilon L)^d$, where $\epsilon = L/N$ and N is the number of boxes along one edge of the big box.
The box-counting dimension is then defined as

$$d_f = \lim_{\epsilon \to 0} \frac{\ln[M(\epsilon L)/M(L)]}{\ln \epsilon} \tag{3.62}$$

One can show that the *static structure factor* of a fractal object has a small-q dependence according to

$$S(q) \propto q^{-d_f} \tag{3.63}$$

This means that we can measure the fractal dimension of a real fractal can be measured by X-ray or neutron diffraction.

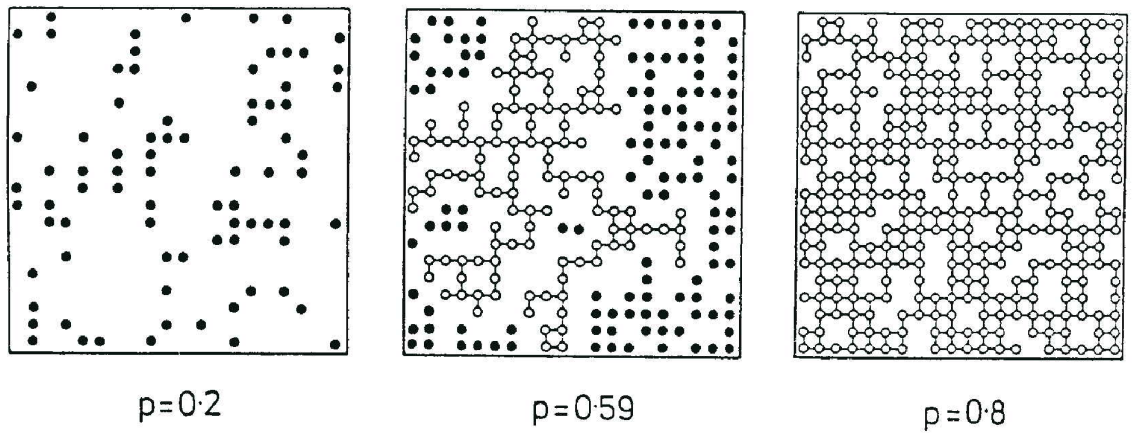

Figure 22: Percolation patterns for 3 different concentrations p. For $p = 0.59$ and $p = 0.8$ percolation clusters (marked by unfilled circles) exist. $p = 0.59$ is the critical concentration for the two-dimensional square-lattice site-percolation problem.

3.2.2 Percolation

An important concept, which generates random structures, which are of fractal character is percolation. At the same time percolation it is a "toy model" for a thermodynamic phase transition. It has two versions, namely the site percolation model and the bond percolation model. In the site percolation model the sites of a d-dimensional lattice is occupied randomly by metal atoms according to the concentration p. If two neighboring sites are occupied they are called connected. Connected sites form a cluster. If a cluster extends through the system of linear extension L it is called percolation cluster. The critical concentration p_c for the phase transition between the isolated state and the connected state is defined as follows:

- p_c is the smallest concentration for which a percolation cluster exists in the limit $L \to \infty$.

In the bond percolation model bonds are randomly distributed on the elementary nearest-neighbour bonds of the lattice.
As can be seen from the table the percolation concentrations p_c depend not only on dimensionality but on the type of lattice and whether we have site percolation.

Right at $p = p_c$ the percolation cluster forms a fractal.

- The fractal dimension is universal as it depends only on the embedding dimension:
  $d_f = 1.9 \ (d = 2), \quad d_f = 2.55 \ (d = 3).$

As in thermodynamic phase transitions one can define an order parameter $P(p)$. The order parameter is finite in the ordered (e.g. ferromagnetic) phase and zero in the disordered phase. The order parameter for the percolation problem which is the probability of a site to belong to the percolation cluster. Obviously $P(p) = 0$ for $p < p_c$, because for $p < p_c$ no percolstion cluster

$d = 2$	site	bond
square l.	0.59	$\frac{1}{2}$
triangular l.	$\frac{1}{2}$	0.35
honeycomb l.	0.7	0.65

$d = 3$	site	bond
simple c.	0.31	0.25
f.c.c	0.20	0.12
b.c.c	0.25	0.18
simple c.	0.31	0.25
diamond	0.43	0.39

Lattice	β	ν
quadratic	$\frac{5}{36}$	$\frac{4}{3}$
simple c.	0.417	0.875

Table 1: Left and center: Critical concentrations p_c for several lattices.
Right: Critical exponents β and ν corresponding to the order parameter $P(p)$ and correlation length $\xi(p)$.

exists. For $p \geq p_c$ we have

$$P(p) \propto (p - p_c)^{\beta} \tag{3.64}$$

for p near p_c.
For $p \approx 1$ the percolation cluster is obviously not a fractal, as there are only a few vacancies which do not involve a scaling law. As in the theory of phase transitions one can define a correlation length $\xi(p)$, which has the property that for length scales $L < \xi$ the percolation cluster looks like a fractal, i.e. $M(L) \propto L^{d_f}$, whereas for $L > \xi$ $M(L) \propto L^d$ holds. Near p_c we have the critical law

$$\xi(p) \propto (p - p_c)^{-\nu} \tag{3.65}$$

3.2.3 Modified silicate networks and silica glass under pressure

As mentioned in the beginning, ordinary soda-lime glasses are "doped" with kations Na^+ and K^+, which act as network modifyers. These kations turn out not to be randomly distributed in the silicate matrix, but, instead coalesce and form modifier channels. Beyond a critical concentration the channels percolate through the silicate network, so they constitute a percolation scenario. Because the kations migrate within the channels if an electrical field is applied, the percolation transition can be measured as a insulator-conductor transition.
Glasses formed with silver kations Ag^+ exhibit extraordinary high ionic conductivity, which make these materials canditates for batteries.

In a recent edition of Nature an article on the simulation of SiO_2 glass appeared with the title:
Percolation transitions in compressed SiO2 glasses.
The authors evaluated the coordination of Si atoms with O atoms at different pressure. The O- coordination number with respect to Si atoms continuously incleases as to be expected. The authors evaluated separately the networks with neighbouring SiO_n coordinations with the same coordination number n and found that for some n these networks exhibited a percolation transition. Evaluation of the structure factor right at the percolation pressures showed the fractal structure with fractal dimension $d_f = 2.5$.

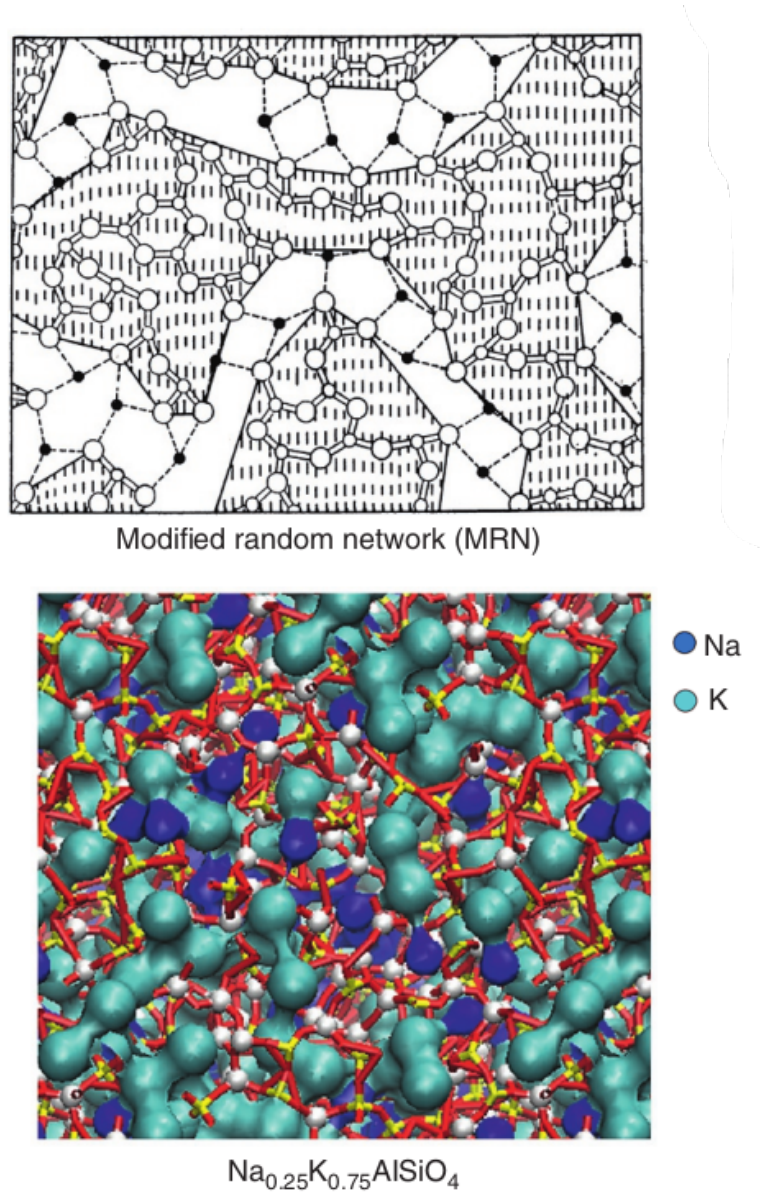

Figure 23: Percolation of network modifiers Na^+ and K^+ in Soda-lime glass (from G. N. Greaves [1])

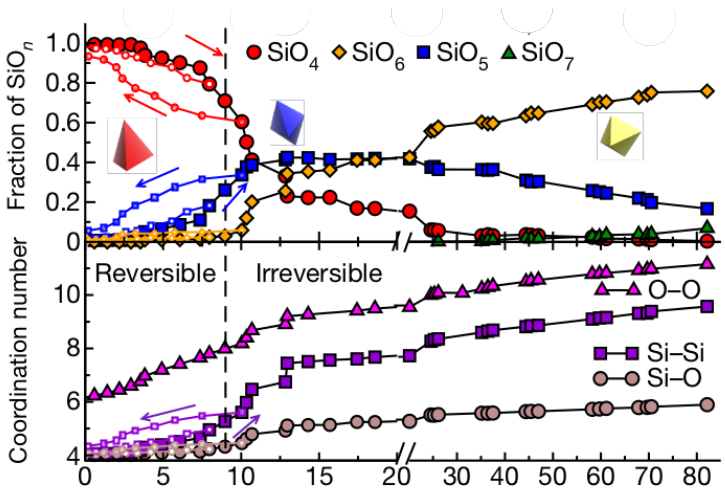

Figure 24: Coordination numbers as a function of pressure (from A. Hasmy [15])

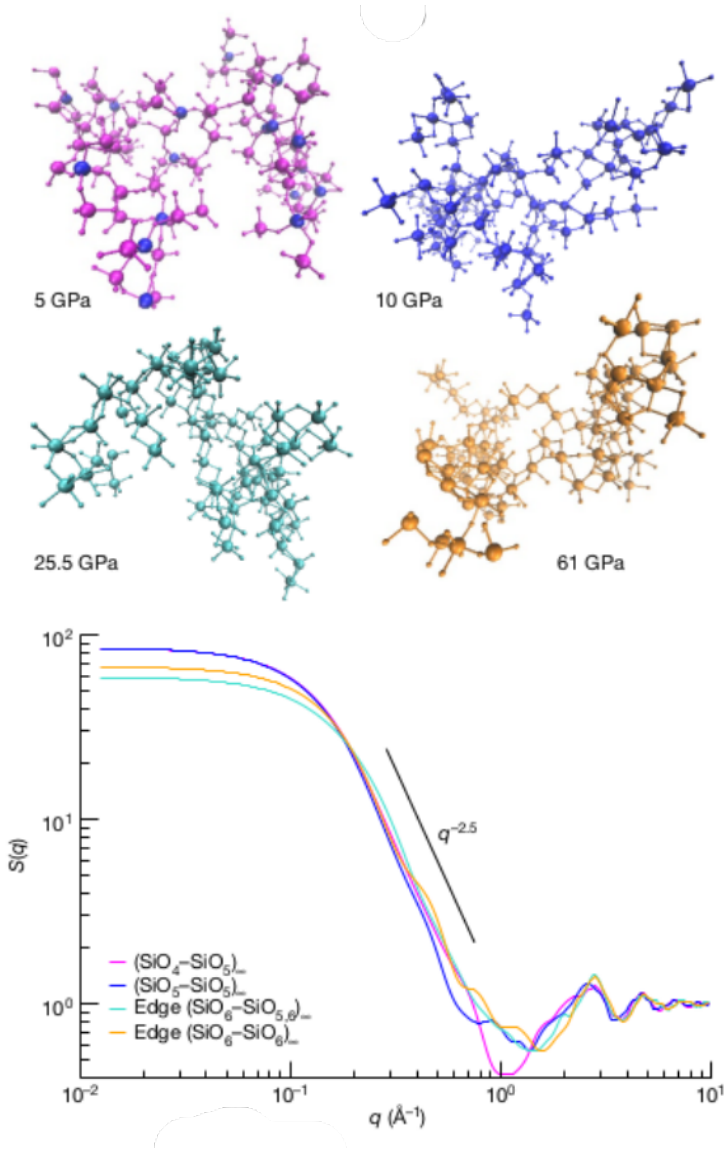

Figure 25: Percolation of SiO_n clusters. Top: Coordination numbers vs. pressure; middle: percolation clusters of SiO_n neighbouring polyhedra; structure factors of SiO_n percolation clusters. (from A. Hasmy [15])

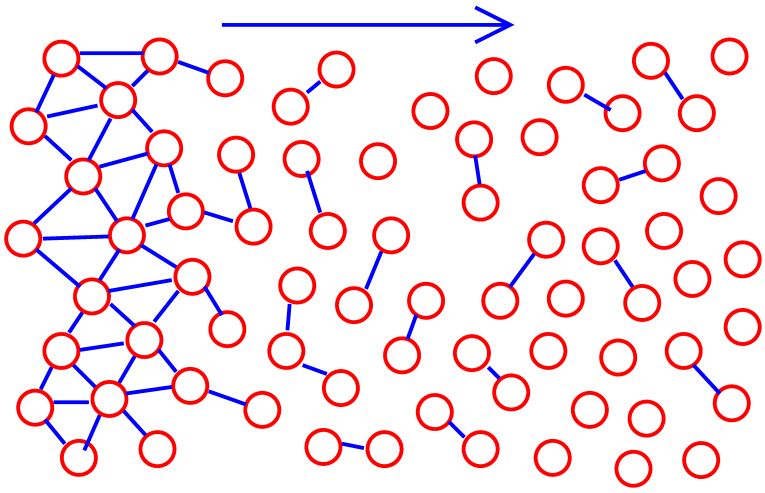

Figure 26: Schematic sketch of a gelation process

3.2.4 Gelation

Instead of quenching of a liquid one can form a disordered molecular-bonded network by a gelation process. This is a chemical reaction, which happens by vulcalization of rubber and in glue. We schematically show the gelation process in Fig. 26.

For modeling a gelation process, one can take a d-dimensional lattice with coordination number Z, which may be a hypercubic lattice just $Z = 2d$ and consider the case that only a fraction of p nearest-neighbor bonds are completed. This just defines a bond percolation model as discussed in the last section.

If p is very small, only isolated clusters appear. A system of network-forming polymer units, in which only a small fraction has formed clusters of finite size is called a sol. Beyond a critical concentration p_c the network extends through the entire system and a gel is formed. The percolation transition in the gelation process is called sol-gel transition and is – as the percolation transition – a second-order phase transition, although the control parameter is not the temperature but the bond concentration. However, if one considers a bond-breaking mechanism, which is thermally activated

$$q = 1 - p \propto e^{-E_A/k_B T} \tag{3.66}$$

one has transformed the p controlled phase transition to an ordinary T controlled transition, in which the sol phase is the high-temperature phase. In other important gelation processes (e.g. rubber vulcanisation, egg boiling, baking) the bond forming is thermally activated, which leads to gelation at high temperatures.

The first mean-field-type ideas in discussing this transition have been formulated by Flory (1941) [17] and Stockmayer (1944) [18], who considered a network without closed loops. Such a network is called a Bethe lattice (or Cayley tree, see the Figure) with branching order (or functionality) Z:

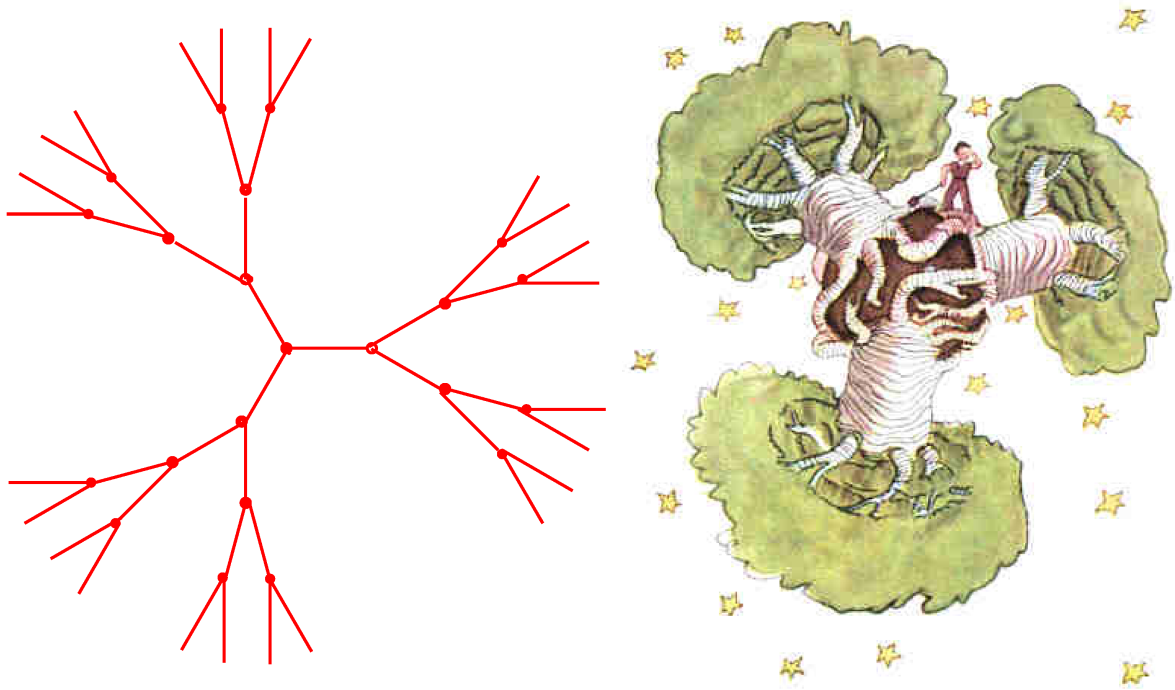

Figure 27: Left: Bethe lattice or Cayley tree with $Z = 3$ and $n = 4$. Right: Cayley tree (consisting of 3 baobabs) as drawn by Antoine de St. Exupéry [16].

Construction of a Bethe lattice (Cayley tree)

One starts with a point from which Z (here: $Z = 3$) branches start. These branches lead at every vertex to $Z - 1 = 2$ further outgoing branches:

Generation	additional	vertices
n	ΔN	
1	3	Z
2	6	$Z(Z-1)$
3	12	$Z(Z-1)^2$
...	...	...
n	$3 \cdot 2^{n-1}$	$Z(Z-1)^{n-1}$

The number of nodes N increases with the number n of generations as

$$\Delta N(n) = N(n) - N(n-1) = Z(Z-1)^{n-1} \tag{3.67}$$

One can now consider the case in which the bonds are formed with probability p. In this case ΔN is given by

$$\Delta N(p, n) = pZ[p(Z-1)]^{n-1} \tag{3.68}$$

If $p < p_c = 1/(Z-1)$ the series $N(n)$ can be summed, i.e. on the average one obtains only a finite Cayley tree of size

$$\langle N \rangle = 1 + \frac{pZ}{1 - p(Z-1)} = \frac{1+p}{1-p(Z-1)} = p_c \frac{1+p}{p_c - p}\,. \tag{3.69}$$

For $p \to p_c$ $\langle N \rangle$ diverges, which is then identified with the gelation threshold.

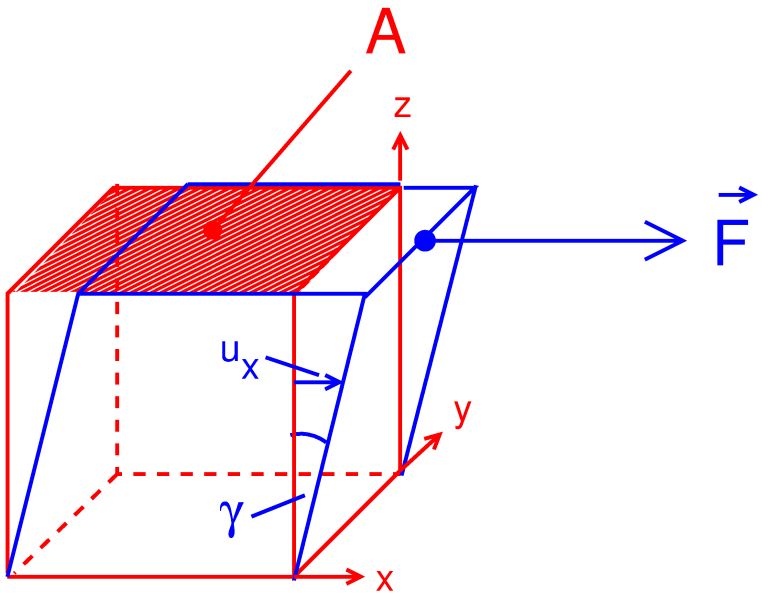

Figure 28: Shear geometry (see text)

4 Viscosity and glass transition

4.1 Maxwell Viscoelasticity

A stress exerted onto a solid body in the way indicated in Fig. 28 is a shear stress and is given by

$$\sigma_{xz} = |\mathbf{F}|/A \tag{4.1}$$

The indices x, z mean that $\mathbf{F}$ acts in x direction and that the area A is oriented in the z direction.

General definition:
If i and j denote one of the Cartesian coordinates x, y, z, then σ_{ij} denotes the Force per volume with a force in i direction and the orientation of the area in j direction. A physical quantity with two indices i, j is called a tensor[3]. σ_{ij} is the stress tensor.

The fundamental law for the elasticity of a solid in the presence of stresses is Hooke's law, which for such a geometry is

$$\sigma_{xz} = G\,\epsilon_{xz} = G\,\frac{\partial u_x}{\partial z} = G\sin\gamma \approx G\gamma \tag{4.2}$$

Here u_x is the elongation of the body in x direction and

$$\epsilon_{xz} = \frac{\partial u_x}{\partial z} = \sin\gamma \tag{4.3}$$

is the shear strain, which is the xz component of the strain tensor. The latter is generally defined as

$$\epsilon_{ij} = \frac{1}{2}\left(\frac{\partial u_i}{\partial j} + \frac{\partial u_j}{\partial i}\right) \tag{4.4}$$

[3] An additioal requirement for a quantity with two indices to be called a tensor is that the columns of the matrix of the tensor must transform like a vector when translated and/or rotated.

A similar law like Hooke's law applies if a shear stress is exerted to a liquid:

$$\sigma_{xz} = \eta\, v_{xz} = \eta\, \frac{\partial v_x}{\partial z} = \frac{d}{dt}\epsilon_{xz} = \eta\, \dot{\epsilon}_{xz} \tag{4.5}$$

Here v_x is the x component of the flow velocity of the liquid and η is the viscosity. $\frac{\partial v_x}{\partial z} = \dot{\epsilon}_{xz}$ is called the strain rate.

A glass-forming supercooled liquid has in most cases the property of visco-elasticity, which means that it

- for small time scales acts like a solid;
- for large time scales acts like a liquid.

James C. Maxwell introduced visco-elasticity of liquids in a famous article in the Philosophical Transaction of the Royal Society 1867 [19]. Let us follow verbatim his article
(we only change his notations for the stress, strain, etc. to ours):

> " A distortion of strain of some kind, which we may call ϵ, is produced in the body by displacement. A state of stress or elastic force, which we may call σ, is thus excited. The relation between the stress and the strain may be written $\sigma = G\epsilon$, where G is the coefficient of elasticity for that particular kind of strain. In a solid body free from viscosity, σ will remain $= G\epsilon$ and
>
> $$\frac{d\sigma}{dt} = G\frac{d\epsilon}{dt}\,. \tag{4.6}$$
>
> If, however, the body is viscous, σ will not remain constant, but will tend to disappear at a rate depending on the value of σ, and the nature of the body. If we suppose this rate proportional to σ, the equation may be written
>
> $$\boxed{\frac{d\sigma}{dt} = G\frac{d\epsilon}{dt} - \frac{\sigma}{\tau}\,, \qquad (4.7)}$$
>
> which will indicate the actual phenomena in an empirical manner. For if ϵ be constant,
>
> $$\sigma = G\,\epsilon\, e^{-\frac{t}{\tau}}\,, \tag{4.8}$$
>
> showing that σ gradually disappears, so that if the body is left to itself it gradually loses any stress, and the pressures are finally distributed as in a fluid at rest.
> If $\frac{d\epsilon}{dt} = \dot{\epsilon}$ is constant, that is, if there is a steady motion of the body which continually increases the displacement,
>
> $$\sigma = G\tau\dot{\epsilon} + Ce^{-\frac{t}{\tau}}\,, \tag{4.9}$$
>
> showing that σ tends to a constant value.. "

How did Maxwell did obtain this result?

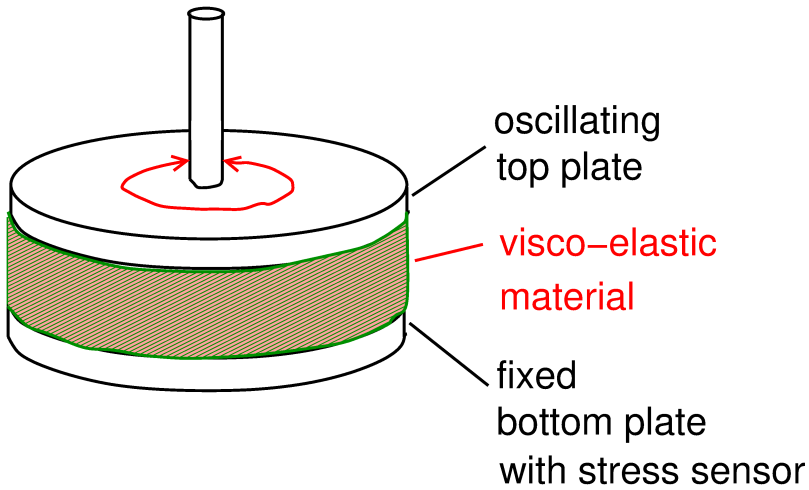

Figure 29: Sketch of a torsional-oscillating-plate rheometer

He solved the differential equation (4.7) (with constant $\dot{\epsilon}$)

$$\begin{aligned}
\frac{d\sigma}{dt} &= G\dot{\epsilon} - \frac{1}{\tau}\sigma \qquad \Rightarrow \qquad dt = \frac{d\sigma}{G\dot{\epsilon} - \frac{1}{\tau}\sigma} \\
t &= \int_{\sigma(0)}^{\sigma(t)} \frac{d\sigma}{G\dot{\epsilon} - \frac{1}{\tau}\sigma} = -\tau \ln[G\dot{\epsilon} - \frac{1}{\tau}\sigma]\Big|_{\sigma(0)}^{\sigma(t)} = -\tau \ln\left[\frac{G\dot{\epsilon} - \frac{1}{\tau}\sigma(t)}{G\dot{\epsilon} - \frac{1}{\tau}\sigma(0)}\right] \\
\Rightarrow & \\
& e^{-\frac{t}{\tau}}\left[\frac{1}{\tau}\sigma(0) - G\dot{\epsilon}\right] = \frac{1}{\tau}\sigma(t) - G\dot{\epsilon}
\end{aligned}$$

$\Rightarrow$

$$\boxed{\sigma(t) = \underbrace{\tau G}_{\eta}\,\dot{\epsilon} + \underbrace{\left[\sigma(0) - \tau G\dot{\epsilon}\right]}_{C} e^{-\frac{t}{\tau}}}$$

We note *en passant* Maxwell's famous expression for the relaxation time

$$\boxed{\tau = \frac{\eta}{G}}$$

In order to explore the different time scales, let us now look at the case of a oscillating strain

$$\epsilon(t) = \epsilon_0 \cos(\omega t) = \mathrm{Re}\{\widehat{\epsilon}(t)\} \tag{4.10}$$

with

$$\widehat{\epsilon}(t) = \epsilon_0\, e^{i\omega t} \tag{4.11}$$

which can be realized with a torsionally-oscillating plate rheometer, see Fig. 29.

We solve the inhomogeneous differential equation (4.7)

$$\frac{d\sigma}{dt} = G\frac{d\widehat{\epsilon}}{dt} - \frac{1}{\tau}\sigma \qquad (76)$$

with the ansatz

$$\sigma(t) = \sigma(\omega)e^{i\omega t} \qquad (4.12)$$

Here $\sigma(\omega) = \sigma'(\omega) + i\sigma''(\omega)$ is a complex quantity. $\sigma'(\omega)$ gives the in-phase response of the rheometer, $\sigma''(\omega)$ the out-of-phase response.
Inserting (4.11) and (4.12) into (4.7) we get

$$i\omega\sigma(\omega)e^{i\omega t} = \left(i\omega G\epsilon_0 - \frac{1}{\tau}\sigma(\omega)\right)e^{i\omega t} \qquad (4.13)$$

$$\Rightarrow \quad \sigma(\omega) = \frac{i\omega G\epsilon_0}{i\omega + \frac{1}{\tau}} \equiv G(\omega)\epsilon_0 \qquad (4.14)$$

Here we have defined a complex shear modulus

$$G(\omega) = \frac{G}{1 + \frac{1}{i\omega\tau}} \qquad (4.15)$$

and we get in the high-frequency limit

$$G(\omega{=}\infty) \equiv G_\infty = G \qquad (4.16)$$

We now write down the final form of Maxwell's relation for the relaxation time

$$\boxed{\tau = \frac{\eta}{G_\infty}}$$

For the in-phase shear response we get

$$\sigma'(\omega) = G'(\omega)\epsilon_0 = G_\infty\frac{\omega^2}{\omega^2 + \tau^{-2}}\epsilon_0 \qquad (4.17)$$

and for the out-of-phase response

$$\sigma''(\omega) = G''(\omega)\epsilon_0 = \eta\frac{\omega}{1 + (\omega\tau)^2}\epsilon_0 \qquad (4.18)$$

The maximum of $G''(\omega)$ (red line in Fig. 30) marks the transition between liquid-like behaviour at small frequencies and solid-like behaviour at high frequencies.

In Fig. 31 we show experimental measurements of Tina Hecksher and her coworkers from Roskilde University in Denmark [20] of the mechanical modulus

$$M(\omega) = K(\omega) + \frac{4}{3}G(\omega) \qquad (4.19)$$

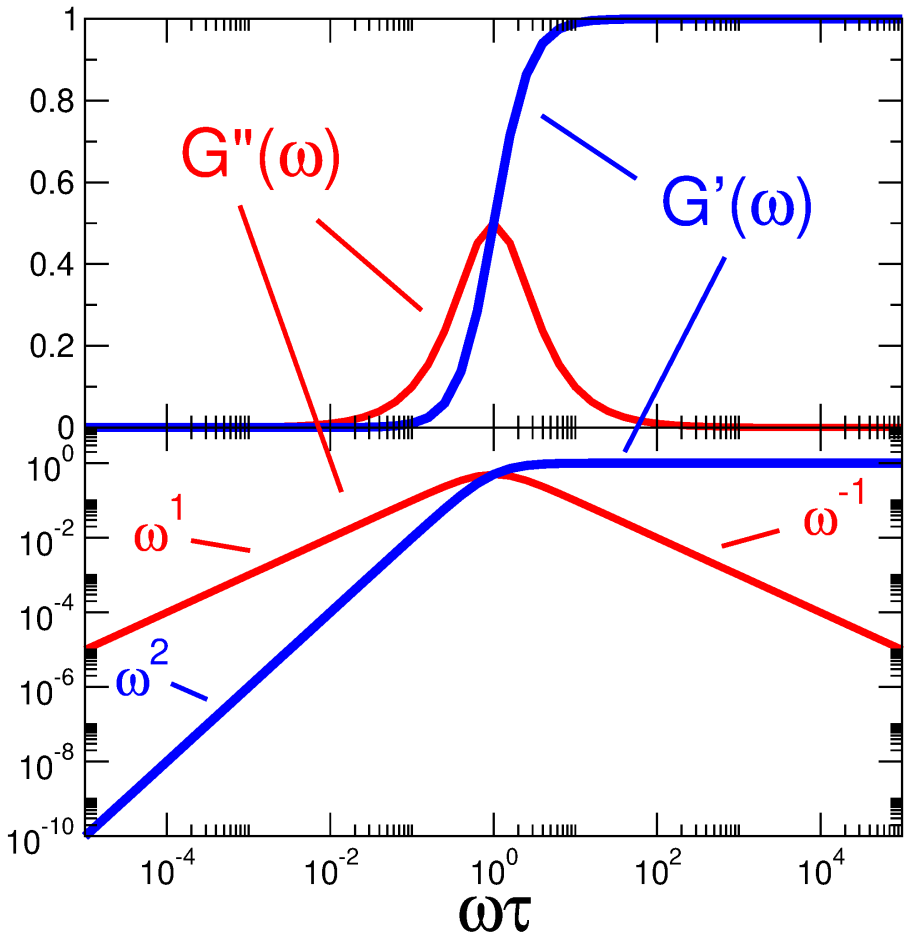

Figure 30: Out-of-phase part of the shear modulus $G''(\omega)$ as given by the Maxwell model, Equations (4.17),blue, and (4.18), red, semi-logarithmically (top), and double-logarithmically (bottom).

over a very large frequency range . Here the compression modulus $K = K(0) = \frac{1}{\kappa_T}$ is the inverse of the compressibility, intoduced above. The authors chose this combination of elastic moduli, because this is, what is measured by the high-frequency acoustic methods. At low frequency separate measurements of G and K are combined.
The compression modulus (or bulk modulus) K is finite in a liquid. Therefore $M'(\omega)$ does not start at zero, but at $K(0)$.

- The step in this function corresponds to the peak in $M''(\omega)$, which essentially comes from the peak in $G''(\omega)$. The peak maximum is at $\omega_{\max} = 1/\tau$ ("α relaxation peak") . With increasing temperature the maximum is shifted to higher and higher frequencies, corresponding to an exponential decrease of the relaxation time and therefore the viscosity.

On the other hand, if the relaxation time τ exceeds the every-day life timescale, the material is essentially frozen. We explore this in the next section.

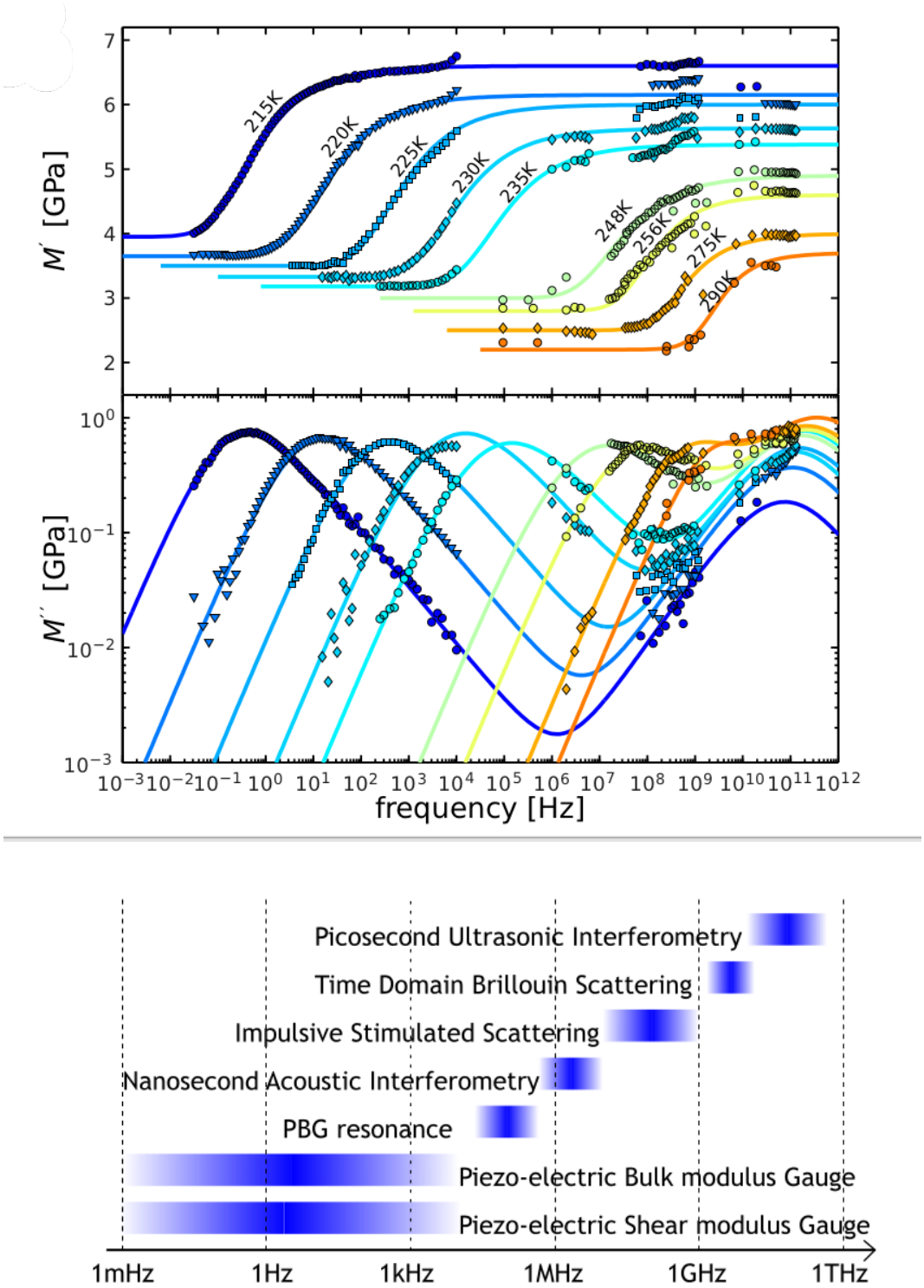

Figure 31: Top panel: In-phase part $M'(\omega)$ and out-of-phase part $M''(\omega)$ of the mechanical modulus $M(\omega) = K(\omega) + \frac{4}{3}G(\omega)$ of tetramethyl tetraphenyl trisiloxane (DC704) diffusion pump oil, obtained by seven different experimental techniques, displayed in the bottom panel; after Hecksher *et al.*, 2017 [20].

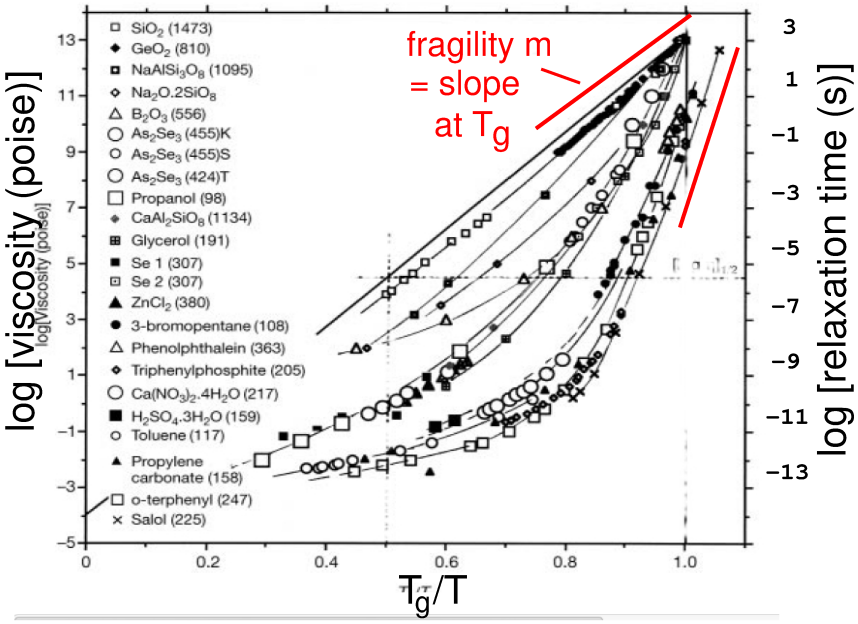

C. A. Angell 1933 - 2021

Figure 32: Angell plot for the viscosity, $\ln \eta(T) vs. T_g/T$ [21].

4.2 Glass transition, Deborah number, and the flow of mountains and church windows

- The glass-transition temperature T_g is defined to be the temperature, below which a supercooled liquid ceases to flow within the timescale of interest.

This happens if the viscosity of a material exceeds 10^{13} poise $= 10^{12}$ Pa s, or so. Because all high-viscosity materials exhibit visco-elastic behavior, we can use the Maxwellian expression for the relaxation time

$$\boxed{\tau = \frac{\eta}{G_\infty}}$$

where the shear modulus G_∞ refers to a periodic external shear stress with a very high frequency $\omega \to \infty$. Inserting a typical value for a solid shear modulus $G \sim 10^{10}$ Pa, we obtain a relaxation rate at the glass transition $\tau_g \sim 10^2$

In Fig. 32 we show the famous Angell plot [21].

- In the Angell plot the logarithm (basis 10) of the viscosity is plotted against the reduced inverse temperature T_g/T. T_g is the temperature, where $\eta = 10^{12}$Pa s.

$$\log_{10} \eta(T) \quad \text{vs.} \frac{T_g}{T}$$

A straight line in such a representation corresponds to an Arrhenius-type

temperature dependence

$$\eta(T) = \eta_0 e^{E_A/k_B T} \,, \tag{4.20}$$

where E_A is the activation energy. For the other cases the data may be well fitted by the Vogel-Fulcher-Tammann, VFT equation

$$\eta(T) = \eta_0 e^{B/(T-T_0)} \tag{4.21}$$

from which one may define a "temperature-dependent activation energy"

$$E_A(T) = Bk_B T/(T-T_0) \tag{4.22}$$

Note that $E_A(T)/k_B T$ is just the local slope in the Angell plot.

A temperature dependence as given by the VFT Equation (4.21) implies that at a certain temperature T_0 the viscosity would diverge, i.e. one would have a true solid without flow. However, in spite of theories, which involve the existence of a temperature T at which the flow ceases completely [22, 23, 24, 5], until now, there is no evidence for such a transition.
If one introduces Angell's fragility index

$$m = E_A(T_g)/k_B T_g \tag{4.23}$$

(the slope at T_g), one can state for the relaxation time at temperature T at temperatures below T_g

$$\tau(T) > \tau(T_g) e^{m(\frac{T_g}{T}-1)} \tag{4.24}$$

Here, replacing the $>$ sign with an equality would just be an Arrhenius-type extrapolation to lower temperature.

Rheologists, who like to introduce dimensionless numbers have defined the Deborah number [25] as

$$De = \tau/t \tag{4.25}$$

where t is the duration of the observation. The name refers to a citation of the bible (Judges 5,5): "The mountains poured from the face of Yahweh.." , i.e. on Yahweh's time scale the rocks are floating.

Original Hebrew Bible Judges 5,5

ה הָרִים נָזְלוּ, מִפְּנֵי יְהוָה: {ס} זֶה {ר} סִינַי--מִפְּנֵי, יְהוָה אֱלֹהֵי יִשְׂרָאֵל. {ס}

(The mountains poured out, from the face of Yahweh, and Sinai from the LORD, the God of Israel.)

Latin bible (Vulgata):
montes fluxerunt a facie Domini et Sinai a facie Domini Dei Israhel
(The mountains melted from the face of the Lord, and Sinai from the face of the Lord, the God of Israel.)

Bible English Standard Version:
The mountains quaked before the LORD,
even Sinai before the LORD, the God of Israel.

Luther-Bibel
Die Berge ergossen sich vor dem Herrn, der Sinai vor dem Herrn, dem Gott Israels.

Markus Reiner (Hebrew: מרכוס ריינר, born 5 January 1886, died 25 April 1976) was an Israeli scientist and a major figure in rheology.[1]

Biography [edit]

Reiner was born in 1886 in Czernowitz, Bukovina, then part of Austria-Hungary, and obtained a degree in Civil Engineering at the Technische Hochschule in Vienna (Vienna University of Technology). After the First World War, he immigrated to Mandatory Palestine, where he worked as a civil engineer under the British mandate. Reiner married Margalit Obernik and had two children, Ephraim and Hana. He later remarried Dr. Rivka Schoenfeld and had two daughters, Dorit and Shlomit. His granddaughter is Prof. Tal Ilan. After the founding of the state of Israel, he became a professor at the Technion (Israel Institute of Technology) in Haifa. In his honour the Technion later instituted the Markus Reiner Chair in Mechanics and Rheology.

Markus Reiner

Born	Markus Reiner 5 January 1886
Died	25 April 1976 (aged 90)
Awards	Weizmann Prize (1955)

Figure 33: Top: Original citation from the bible Judges 5,5
Bottom: Wikipedia entry on Markus Reiner, who created the discipline of Rheology and the term "Deborah number".

Figure 34: Stained glass window of Westminster Abbey in London, showing the Pentecost Event.

A related popular urban legend exists with respect to church windows: It had been found that window panes of old churches were thicker at the bottom than at the top, and it was argued that in the time scale of 1000 years the glass would have flowed downwards.
Let us calculate the relaxation time of window glass at room temperature using the formula (5.25):

$$\tau(T) > \tau(T_g) e^{m(\frac{T_g}{T} - 1)} \tag{93}$$

The fragility index m and glass transition temperature T_g of the soda lime glass of the windows of Westminster Abbey in London has been determined [26] as $m = 42$ and $T_g = 866$ K, which gives $m[T_g/T - 1] \sim 80$. So we have (taking the "=" sign instead of the "<" sign)

$$\tau/\tau_g \sim e^{80} \sim 10^{34}\,.$$

Taking $3 \cdot 10^7$ seconds for a year and $\tau_g \sim 10^2$ s, we obtain

$$\tau \sim 10^{29} \text{ years.}$$

Now the age of the universe, i.e. the time elapsed since the big bang is of the order of 10^{10} years. This means that the church windows could not possibly have flowed down appreciably in less than 1000 years.

Gulbiten et al. [26] estimate a flow velocity of 10^{-18} meter per year, which amounts to 10^{-15} m in 1000 years, which is just the diameter of an atomic nucleus. However, we should keep in mind that these numbers are a result of extrapolation.

As to mountains, they are known to float in geological history due to plate tectonics. So using his time lapse[4] God could have certainly seen the mountains flowing. This, by the way, means that the viscosity of the earth crust is much less than that of church glass.

- Anyway, we really do not know the temperature variation of viscosity of lime glass at room temperature or even lower temperatures. But we can be rather sure that glass is a solid for all relevant time scales.
- The viscosity of very low temperatures is known to be strongly affected by quantum effects, which – by the tunneling mechanism – reduces the viscosity [27].

[4] "A thousand years in your sight are like a day that has just gone by, or like a watch in the night." Psalm 90:4

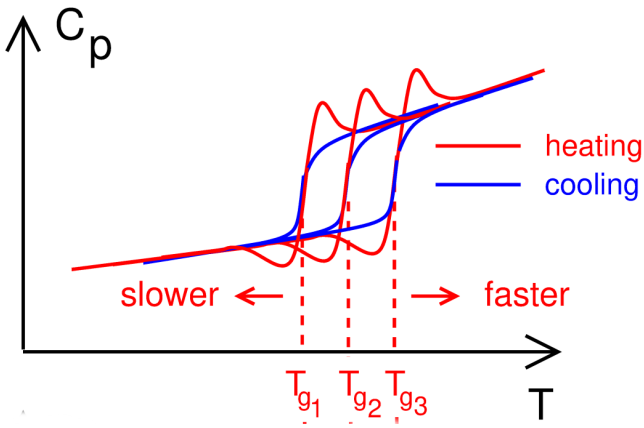

Figure 35: Cooling/heating rate dependence of T_g

4.3 Glass transition, specific heat and entropy

The glass transition is not only be characterized by the viscosity, but also by the specific heat capacity (thermodynamic glass transition). This quantity (we subsequently use the old term specific heat) shows a step-like behavior at T_g.

In Fig. 35 we have sketched the temperature dependence of the specific heat of a glass.

- It is seen that the cooling (blue) and heating curves (red) are different (hysteresis).
- The transition between the lower solid-like value and the upper one (indicated by the dashed lines) depends on the cooling (or heating) rate.
- The slower the cooling, the lower is the thermal transition temperature T_g.

- Let us recapitulate: What is heat?

Heat is the irregular thermal motion of the atoms and molecules. This motion can be vibrational or configurational. The latter dominates in gases and liquids, where the particles just move around irregularly, the former in solids, in which irregular sound waves (phonons) are thermally excited.

We have seen above that the relaxational dynamics of a highly supercooled liquid near the glass transition has its relaxational (alpha) dynamics in the sub-Hz region, whereas there is a region over many order of magnitude, which may be ascribed to kind of vibrational motion. Therefore, in an undercooled liquid we may sub-divide the heat, and also the specific heat into a liquid-like part, called configurational specific heat and a vibrational one:

$$C_V(T) = C_{V,v}(T) + C_{V,c}(T) \tag{4.26}$$

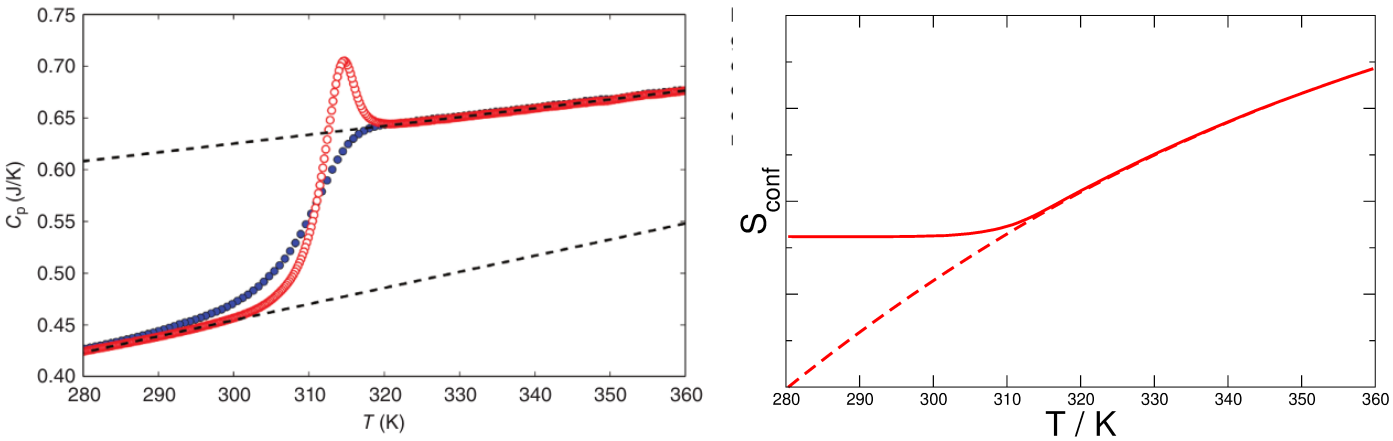

Figure 36:
Left: Specific heat capacity of poly-vinyl-acetate $\left[\text{PVAc, } (C_4H_6O_2)_n\right]$ across the glass transition, measured by differential scanning calorimetry (DSC) with heating (open circles) and cooling (filled circles) rate of 1.2 K/min. Dashed lines extrapolate the data in the liquid and the glass range after J. L. Garden and H. Guillou in [1].
Right: Configurational entropy, evaluated from the cooling data minus the extrapolated vibrational specific heat (full line), and evaluated from the upper extrapolated line minus the lower one (dashed line).

The vibrational part $C_{V,v}(T)$ is also very often identified with the specific heat of the crystal. The configurational specific heat is then the difference of that of the supercooled liquid and that of the crystal:

$$C_{V,c}(T) = C_V - C_{V,\text{cryst}} \tag{4.27}$$

It is customary in glass science to discuss the entropy associated with the thermal glass transition.

What is entropy?

If we have a look at Atkins [28], we find that a change in entropy is related to the reversible heat transfer δQ_{rev}[5]

$$dS = \frac{1}{T}\delta Q_{\text{rev}} \,. \tag{4.28}$$

We can relate the entropy S to the specific heat by considering the internal energy $U(S,V)$, for which we have (δW_{rev} is the reversible transfer of mechanical work)

$$dU = \delta Q_{\text{rev}} + \delta W_{\text{rev}} = TdS - pdV \tag{4.29}$$

where δW_{rev} is the reversible transfer of mechanical work.
For the specific heat C_V at constant volume we have

$$C_V = \left(\frac{\partial U}{\partial T}\right)_V \tag{4.30}$$

For constant volume V the entropy change is

$$dS = \frac{1}{T}dU \,, \tag{4.31}$$

[5] We use the common notation δQ_{rev} to indicate that it does not denote an exact differential, denoted d, the integral over which is path independent.

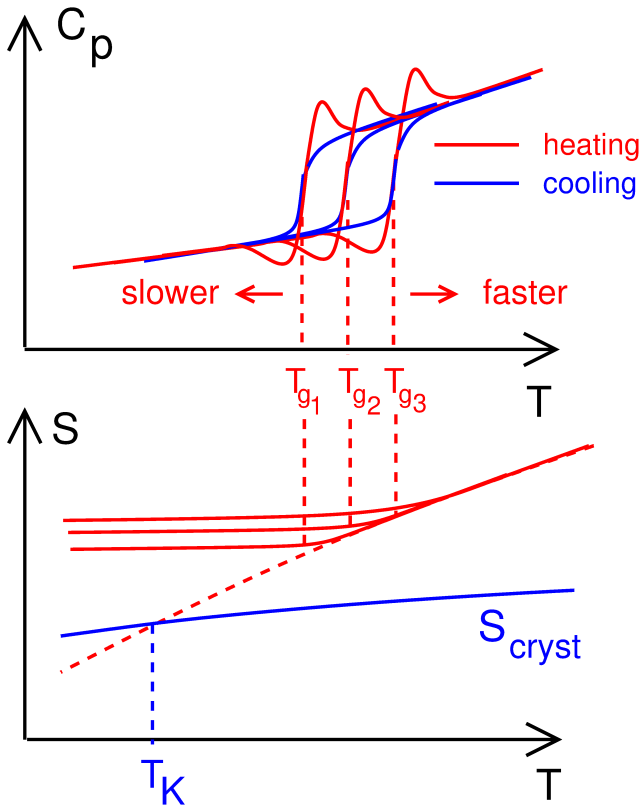

Figure 37: Cooling/heating rate dependence of T_g and Kauzmann scenario

so, the entropy is given by

$$S(T) = \int_0^T d\tilde{T}\, \frac{1}{\tilde{T}}\, C_V(\tilde{T}) \tag{4.32}$$

We now may subdivide the entropy of our glass-forming liquid into a configurational and vibrational part, following that of the heat and specific heat.

$$S = S_{\text{vib}} + S_{\text{c}} \tag{4.33}$$

In the right panel of Fig. 36 we have calculated the configurational entropy using Eq. (4.32) with a configurational specific heat obtained by subtracting the extrapolated low-temperature linear law (lower dashed line) from the specific heat data. The result is the continuous line. We could also hypothesize a much slower cooling rate, so that the entire temperature range would be still in the supercooled liquid state. So we could use as configurational specific heat the top dashed line minus the bottom dashed line. The result is the entropy drawn with dashed line in the bottom panel. For obtaining the two curves we made sure that the high-temperature entropy curves lie on top of each other. So with respect to the hypothetical curve that correspond to a much lower cooling rate, there appears something like a residual, or frozen-in entropy.

4.3.1 Kauzmann scenario

In Fig. 37 we have sketched typical $C_V(T)$ curves with three different cooling rates, corresponding to three different values of the thermally determined glass transition T_g. Below this picture we show the resulting entropy curves using the integral of Equation (4.32).

In 1948 Kauzmann [29] raised the question, what happens, if the total entropy of the supercooled liquid, which varies stronger with temperature than the vibrational one, becomes smaller than the vibrational entropy of the crystal. Or, in other words: What happens, if the configurational entropy goes to zero at a finite temperature?

This scenario plays a prominent role in recent model descriptions of the glass transition, see the next chapter. The hypothetical temperature, where the configurational entropy vanishes is called Kauzmann temperature T_K. This scenario has never been verified for experimental glasses. One always ends up with a residual entropy.

4.4 But: Is a residual entropy compatible with the 3rd law?

The debate about the existence or otherwise of a residual entropy as the temperature reaches zero goes back to the time shortly after Nernst [30] formulated the 3rd law of thermodynamics in 1906, none other than Albert Einstein [31] noted that in mixed crystals, in which two types of atoms occupying randomly the lattice sites, there should exist a residual entropy due to the frozen-in disorder. Linus Pauling [32] came to the same conclusion for the case of crystalline ice, where the water molecule have random orientation as $T \to 0$. The same seems also to apply for glasses, which exhibit a frozen-in spatial disorder. This certainly is at variance with Nernst's law, and the discussion, whether glasses feature a finite residual entropy as the temperature reaches zero, persists until now [33, 34, 35, 36, 37, 38, 39, 40, 41]. In order to be able to follow this discussion, we have to recall the statistical definition of entropy. In a microcanonical ensemble, where the energy is confined to a small interval between E and $E + \Delta E$ the entropy, according to the book on statistical physics by Landau and Lifshitz [42]

- $S = k_B \ln W,$

where W is the number of states, which exists in this energy interval. In quantum theory these states are discrete, and we may count them one by one. We only have to pay attention to possible generacies, i. e. the possibility that more than one states have the same energy. For $T \to 0$ in a quantum system, there exist no excitations to energies above the ground state, so we can state

- the 3rd law of thermodynamics (Nernst's theorem) as

$$\lim_{T\to 0} S(T) \quad \to \begin{cases} 0 & \text{ground state non-degenerate} \\ k_B \ln d & \text{ground state d-fold degenerate} \end{cases} \tag{4.34}$$

So, for a d-fold degenerate quantum system there exists a residual entropy. However we recall that a degeneracy can only occur if there exists a conserved quantity, corresponding to a quantum operator, which commutes with the Hamilton operator.

In classical theory W is proportional to the phase space volume

$$W \sim \Delta\{p_i\}\Delta\{q_i\} \tag{4.35}$$

where $p_1 \dots p_i \dots p_f$ and $q_1 \dots q_i \dots q_f$ are the f coordinates and momenta, which appear in the Hamiltonian function and span the $6f$-dimensional phase space. f is the number of degrees of freedom, and $\Delta\{p_i\}\Delta\{q_i\}$ is the phase-space volume}.

In gases and liquids the phase-space volume corresponding to a certain energy is proportional by the number of different configurations (commutations) of $f = N$ particles

$$W \sim N! \qquad \Rightarrow \qquad S \sim k_B \ln N! \sim N \ln N \tag{4.36}$$

The second equality follows from Stirling's Formula, which we derive by the following repeated integrations by part:

$$\begin{aligned}
\int_0^\infty dx x^N e^{-x} &= \underbrace{\Big|_0^\infty (-1) x^N e^{-x}}_{0} + N \int_0^\infty dx x^{N-1} e^{-x} \\
&= N(N-1) \int_0^\infty dx x^{N-2} e^{-x} \\
&= \dots \\
&= N! \int_0^\infty dx e^{-x} = N! \\
\Rightarrow \quad N! &= \int_0^\infty dx x^N e^{-x}
\end{aligned} \tag{4.37}$$

- For very large N the function $x^N e^{-x}$ has a very sharp maximum at $x = N$,
- the width around the maximum is roughly $\Delta x \sim 2N$,

So we can estimate

$$N! \sim 2N^{N+1} e^{-N} \quad \Rightarrow \quad \ln N! \sim \ln 2 + (N+1) \ln N - N \overset{N\to\infty}{\longrightarrow} N \ln N \tag{4.38}$$

- Can we apply this formula for a frozen-in system?

The answer is immediately no, because

- the system is no more in thermal equilibrium
- the momenta, which describe the motion of the particles are zero, therefore the phase-space volume is zero.

Mauro *et al.* [33, 34, 35] therefore emphasize that only those states may be counted for the configurational entropy, wich are able to establish equilibrium within the Deborah time. Therefore there should be no residual entropy below T_g. Shirai [41] refines this argument by making the separation between the vibrational and the configurational entropy dependent on the measuring time scale *viz.* the cooling rate.
However, the rest of the community, including Einstein and Pauling [31, 32, 36, 37, 38, 39, 40] use the notion of the entropy more in a sloppy way: They include the quenched, frozen-in disorder in the entropy.
In the majority of the literature the residual entropy is defined via the integral over the measured configurational part of the specific heat and used as a descriptor of the glassy state, which depends on the thermal history of the material like the residual resistivity of a metal.

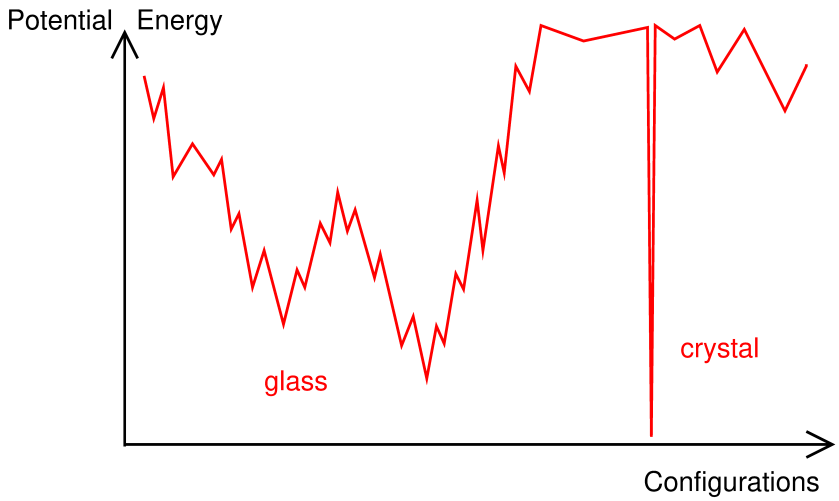

Figure 38: Sketch of the Potential-Energy-Landscape picture of Goldstein (1969)[43].

5 Theories and models for the Glass transition

A very pedagogical description of the presently available theoretical description of the glass transition has been given by Cavagna (2009) [24]. This chapter follows in large parts his description.

5.1 Energy landscape

In 1969 Martin Goldstein [43] published an article (all in text!) in which he described his – now famous – view of the transition from the supercooled liquid to a glass. He imagined the potential energy as a function of the $3N$ spatial coordinates of a supercooled liquid as a surface in a $3N+1$-dimensional space which forms a very ragged landscape, as sketched in Fig. 38. In this landscape there are a large number of local minima. The deepest one corresponds to the crystalline configuration, as indicated in the figure. Turning to phase space, the momenta, viz. the velocities of the particles contribute the thermal energy $\frac{1}{2}3Nk_BT$. Goldstein described the following scenario starting at $T = 0$ and then increasing the temperature:

- At $T = 0$, the material, which has been prevented to fall into the crystalline minimum, chooses one of the very many metastable minima of the glassy state. (Nowadays the minima of the potential-energy landscape are called inherent states [44].)
- When the temperature increases, the molecules start vibrating around the potential-energy minimum, thus providing the heat (and corresponding entropy) of the glass. This entropy is the vibrational entropy S_{vib}.
- With T increasing towards the vicinity of T_g, the thermal energy starts to allow for overcoming some of the saddles (barriers), which lead from one valley to another. The glass starts melting, and the activated barrier hopping within the potential landscape provides the finite fluidity $1/\eta(T)$.
- When the temperature is further increased beyond a limiting temperature T_x a cross-over from barrier hopping to collisional kinetic transport

takes place, and the barrier-hopping picture loses its range of application. Goldstein estimates the crossover temperature T_x to be reached if the relaxation rate becomes smaller than $\tau \sim 10^{-9}$ seconds, corresponding to a viscosity of arround 10 Pa s.

So, the applicabibily range of Goldstein's potential-energy-barrier picture is confined to temperatures below T_x. The range of the relaxation rate between T_g and T_x covers 11 orders of magnitude. But, if we have a look at the Angell plot, the corresponding temperature range, in which the relaxation time trops from $\tau = 10^2$ to 10^{-9} is rather limited. In particular, for fragile glass-forming liquids like o-terphenyl, the crossover temperature T_x is around 12 % above T_g. T_g of o-terphenyl is $\sim$ 243 K, so $T_x \sim 270$ K. In a later paragraph, we shall discuss the mode-coupling theory of Götze [22, 45, 23], which does not involve activated processes, and which predicts a vanishing fluidity at a critical temperature T_c. when experimentally measured relaxation spectra are fitted with this theory, one finds in many materials, that the would-be critical temperature T_c is around 10 % above T_g i.e. can be identified with Goldstein's T_x.

In the regime of validity of Goldstein's potential-energy-barrier model of viscous liquids, we may conclude that, indeed, the entropy may be subdivided into a vibrational and a configurational part, as done in Eq. (4.33): Most of the time the system stays down in the valley and perform vibrational motion, and occasionally there is an activated jump over a saddle into another valley. This picture has been anticipated in a way by Adam and Gibbs (1965). The Adam-Gibbs model will be described in the next subsection.

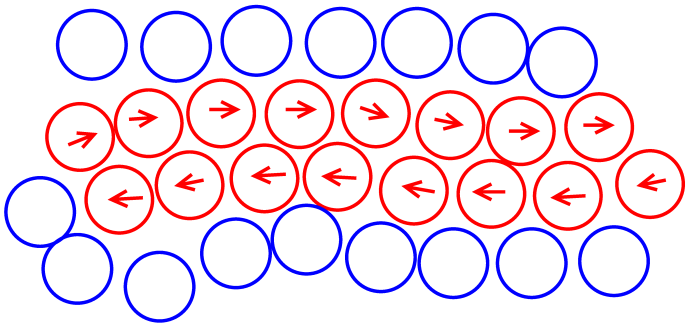

Figure 39: Sketch of a collective re-arrangement of molecules in a supercooled liquid as considered by Adam and Gibbs (1965) [46]. The 16 molecules are supposed to collectively jump backwards and forwards between two configurations.

5.2 Adam-Gibbs model

Adam and Gibbs (1965) [46] constructed a relation between the viscosity $\eta(T)$ and the configurational entropy $S_c(T)$ as follows:

They started with the expression for a collective activation event (see the sketch in Fig. (40) between different configurations, given by transition-state theory [28]:

$$\tau^{-1} = \tau_0^{-1} e^{-\Delta G_{i\to j}/k_B T} \tag{5.1}$$

where $\Delta G_{i\to j}$ is the difference in (Gibbs) free enthalpy of the z molecules involved in the collective transition given by

$$\Delta G_{i\to j} = z(T)\mu \tag{5.2}$$

Here $z(T)$ is the number of the molecules, which paricipate in the transition and μ is the chemical potential. They then argue as follows:

- The transtions which dominate the fluidity of the liquid are those with the smallest number $z^*(T)$ of collectively rearranging molecules
- This number z^* involves a rather small number of configurations ν (e.g. $\nu = 2$, see Fig. 39). ν is related to a temerature independent reference entropy $S_\nu = k_B \ln \nu$
- Because the entropy is extensive, we have for the configurational entropy per molecule

$$\Sigma(T) = \frac{1}{N} S_c(T) = \frac{1}{z^*(T)} S_\nu \quad \Rightarrow \tag{5.3}$$

$$z^*(T) = N \frac{S_\nu}{S_c(T)} \tag{5.4}$$

The configurational entropy per molecule $\Sigma(T)$ is also called complexity in connection with the generalized spin-glass models (see below).

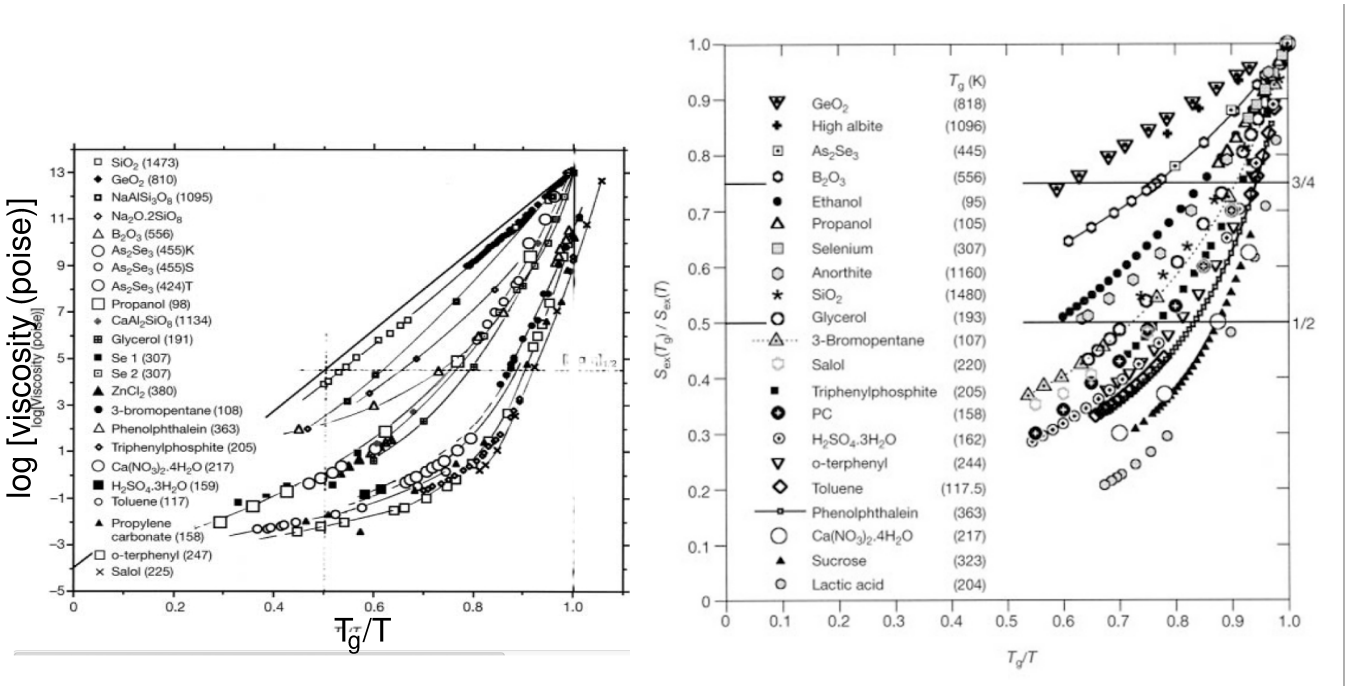

Figure 40: Left: Angell-plot: log of the viscosity against T_g/T. Right: Inverse configurational entropy vs. T_g/T.
"thermal Angell plot" [47].

We may here construct a connection with the energy-landscape picture [24]: If we identify the number of thermodynamic states (in phase space) $\mathcal{N}(T)$ with the number of valleys relevant to a certain temperature T, then $\mathcal{N}$ is given by

$$\mathcal{N}(T) = \nu^{N/z^*(T)} \tag{5.5}$$

and consequently

$$S_c(T) = k_B \ln \mathcal{N} = \frac{N}{z^*(T)} \underbrace{k_B \ln \nu}_{S_\nu},$$

which is a re-statement of Eq. (5.4) We finally arrive at Adam-Gibbs's result [46]

$$\eta(T) \sim \tau(T) \sim e^{\frac{C}{S_c(T)} \frac{\mu}{k_B T}} \tag{5.6}$$

with $C = N S_\nu$.

In Fig. (40 we reproduce a plot of Martinez and Angell (2001) [47], who collected configurational-entropy data, evaluated according to Eq. (4.32) from the configurational part of the entropy in the supercooled state (the crystalline/vibrational specific heat was subtracted). The picture is very similar to the Angell plot for the logarithm of the viscosity, verifying the model ideas of Adam and Gibbs [46].

If you compare the viscosity with the entropy Angell plot (Fig. 40) you see that the Adam-Gibbs relation (5.6) applies to all displayed data except for the paradigmatic material SiO_2. In the viscosity plot silica appears as strong, whereas it appears in the entropy plot as fragile. This may be due to the fact that in the glass transition of SiO_2 the bond-breaking mechanism, i.e. the

thermal breaking of the covalent Si-O bonds, may dominate over the Adam-Gibbs scenario.

5.2.1 Relation to the Kauzmann scenario

If we now assume, as Kauzmann as well as Adam and Gibbs, that one could define an ideal glass as a material which is prepared by a infinitely slow cooling rate, we might envisage a Kauzmann scenario

$$S_c(T) \to 0 \quad T \to T_K \tag{5.7}$$

i.e. a vanishing configurational entropy at finite temperature T_K. Then the fluidity goes to zero as in the Vogel-Fulcher-Tammann equation (4.21). We shall come across this scenario in the paraagraph on generalized spin-glass theory.

We may also associate a length scale ξ with the configurational entropy [48]. The volume occupied by z^* collectively rearranging molecules is given by

$$v^*(T) = \xi^*(T)^3 = \frac{1}{\rho_0} z^*(T) = V \frac{S_\nu}{S_c(T)} \tag{5.8}$$

where $\rho_0 = N/V$ is the number density of the molecules, and V the volume of the sample. Eqs. (5.7) and (5.8) imply a diverging length scale

$$\xi^*(T) \sim (T - T_K)^{-\alpha} \tag{5.9}$$

with $\alpha \sim \frac{1}{3}$. Therefore glass scientists are looking for such a diverging length scale in experiments and computer simulations, see below.

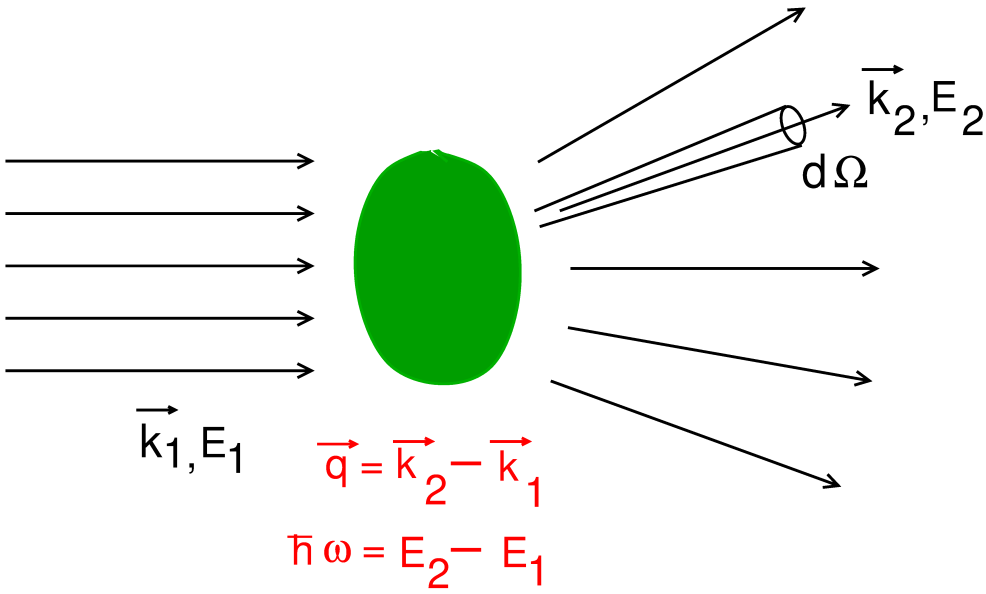

Figure 41: Scenario for inelastix X-ray or neutron scattering with in- and outgoing energies and momenta $E_1, E_2 and \hbar\mathbf{k}_1, \hbar\mathbf{k}_2$ The transferred energies and momenta are $\hbar\omega = E_2 - E_1$ and $\hbar\mathbf{q} = \hbar(\mathbf{k}_2 - \mathbf{k}_1)$.

5.3 Structural relaxation above T_g

5.3.1 Inelastic scattering and density-density correlation function

In the beginning we have shown that the structure factor $S(\mathbf{q})$, which is obtained by elastic scattering of X-rays and neutrons is given by

$$S(\mathbf{q}) = \rho_0 C_{\rho\rho}(\mathbf{q}) = \frac{1}{N} \sum_{\alpha,\beta=1}^{N} e^{i\mathbf{q}[\mathbf{r}_\alpha - \mathbf{r}_\beta]} \tag{5.10}$$

We now define time-dependent density fluctuations as

$$\rho(\mathbf{q}, t) = \frac{1}{N^{1/2}} \sum_{\alpha=1}^{N} e^{i\mathbf{q}\mathbf{r}_\alpha(t)} \tag{5.11}$$

and define a q and t dependent density-density correlation function (van Hove function) as

$$S(q, t) = \langle \rho(\mathbf{q}, t)\rho(\mathbf{q}, 0)\rangle = \frac{1}{N} \left\langle \sum_{\alpha,\beta=1}^{N} e^{i\mathbf{q}[\mathbf{r}_\alpha(t) - \mathbf{r}_\beta(0)]} \right\rangle \tag{5.12}$$

The spectrum of the density fluctuations is the Fourier transform

$$S(q, \omega) = \int_{-\infty}^{\infty} e^{i\omega t} S(\mathbf{q}, t) \tag{5.13}$$

The double-differential cross-section for inelastic neutron and X-ray scattering is related to the Fourier-transformed van-Hove function as

$$\frac{\mathrm{d}^2\sigma}{\mathrm{d}\Omega \mathrm{d}\omega} = \frac{k_2}{k_1} |f(q)|^2 S(q, \omega) \tag{5.14}$$

Here $\mathbf{k}_1/k_1$ denotes the direction of the incoming radiation and $\mathbf{k}_2/k_2$ is the vector pointing to the center of the solid-angle element $d\Omega$, see Fig. 41.

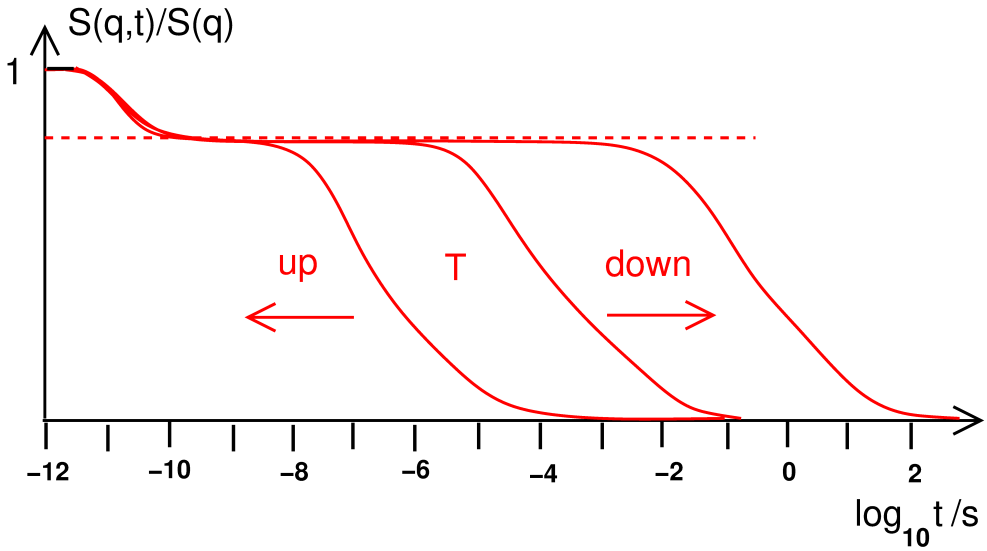

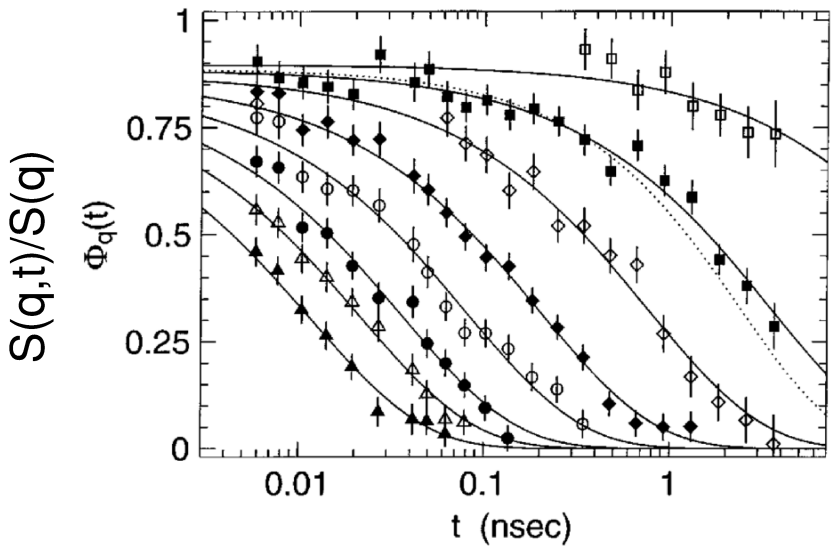

Figure 42: Top: Sketch of the behaviour of $S(q,t)$ of a glass-forming liquid for T approaching the glass temperature T_g
Bottom: neutron scattering data, Fourier-transformed from the measured $S_{\text{icoh}}(q,\omega)$ at glycerol for the temperatures (from right to left) $T = 270$ K, 293 K, 313 K, 333 K, 353 K, 393 K, 423 K, after [49].

Because for inelastic scattering the Fourier-transformed van-Hove function $S(q,\omega)$ takes the place of the static structure factor $S(q)$ for for elastic scattering, $S(q,\omega)$ is also called the dynamical structure factor.

Let us now discuss the typical behavior of the density-density correlation function of a glass-forming liquid $S(q,t)$. In Fig. 42 we show a cartoon of the typical begavior together with measured data by Wuttke et al. (1996) [49] at liquid glycerol with the help of the neutron source ILL (Institut Laue-Langevin) in Grenoble.

The decay of the correlation function is called relaxation. As we see, the relaxation occurs in a two-step fashion, as the glass-transition temperature ($T_g = 190$ K for glycerol) is approached.
What does it mean that the relaxation gets stuck in a large time interval?

- The time range with constant $S(q,t)$ function (absence of relaxation) corresponds to the absence of fluidity in this time regime
- The molecules are trapped within the cage of their neighbors, and have to wait for the accumulation of enough thermal energy to get out of the cage ("cage effect).
- There is a theory, which describes the cage effect, namely Mode-Coupling Theory.

There is another peculiarity of the relaxation approaching the glasss temperature:

- The relaxation is not exponential, but follows a stretched exponential as given by the Kohlrausch-Williams-Watts (KWW) equation

$$S(q,t) \sim e^{-t/\tau^{\beta}},, \tag{5.15}$$

  with $\beta < 1$.

This stretched-exponentially relaxation is typical for the so-called alpha relaxation, namely the decay away from the plateau. It is also observed below T_x, very near T_g.

5.3.2 Dynamical structure factor for liquids much above T_g

Away from the glass transition and for rather small values of q and ω one can use the linerized version of the Navier-Stokes equations for describing the flow. Within this description the density-density correlation function obeys a differential equation like the damped harmonic oscillator:

$$\left(\rho_m \frac{d^2}{dt^2} + q^2 \eta_L \frac{d}{dt} + \frac{q^2}{\kappa_T}\right) S(\mathbf{q},t) = 0 \tag{5.16}$$

$\rho_m = m\rho_0$ is the mass density, and η_L is the so-called longitudinal viscosity, which is composed of the shear viscosity η, and the volume (bulk viscosity η_v

$$\eta_L = \frac{4}{3}\eta + \eta_v \tag{5.17}$$

The latter describes dilatational (compressional) damping of the liquid. κ_T is the isothermal compressibility, which

$$\kappa_T = \frac{1}{m\rho_0 v_T^2} = \frac{1}{\rho_m v_T^2} \tag{5.18}$$

Dividing Eq. (A.62) through ρ_m we get

$$\left(\frac{d^2}{dt^2} + q^2\gamma \frac{d}{dt} + \Omega_0^2(q)\right) S(\mathbf{q},t) = 0 \tag{5.19}$$

with the oscillator frequency gven by

$$\Omega_0(q) = v_T q \tag{5.20}$$

and the kinematic viscosity

$$\gamma = \eta_L/\rho_m \tag{5.21}$$

In real space, where $q^2 \to -\nabla^2$ we can convert Eq. (A.63) to

$$\left(\frac{d^2}{dt^2} - \nabla^2\left(\gamma\frac{d}{dt} - v_T^2\right)\right) S(\mathbf{r},t) = 0 \tag{5.22}$$

This is a wave equation for the sound in the liquid with sound damping depending on the gradients of the density. In $\mathbf{q}$ space one defines a q dependent sound damping coefficient

$$\Gamma(q) = q^2\gamma = q^2\eta_L/\rho_m \tag{5.23}$$

As we are interested in the behavior of the dynamic structure factor $S(q,t)$ rather than in its real-space counterpart, we stick to the damped-harmonic oscillator equation (A.63) in $\mathbf{q}$ space.

- For high viscosity and time t large compared to $1/\Omega_0$, we may omit the inertia term with the double time derivative and get

$$S(q,t) = S(q,t{=}0)e^{-t/\tau} \tag{5.24}$$

$$\tau = \frac{\Gamma(q)}{\Omega_0^2(q)} = \frac{\eta_L}{v_T^2} = \eta_L\kappa_T\,. \tag{5.25}$$

- This exponential decay, with a time constant increasing with the viscosity qualitatively explains the findings depicted in Fig. 42, namely the
- shift of the relaxation to large times for $T \to T_g$, but not the stretched-exponential behavior.
- Eq. (5.25) is also very similar to Maxwell's relation for the relaxation time. Here the stiffness is the short-time bulk modulus instead of the shear modulus.

5.3.3 Response function and Fluctuation-Dissipation theorem

In rheological and specroscopical experiments one exerts an external potential $\mathcal{V}(t)$ to the system. The average density fluctuation $\langle\Delta\rho(\mathbf{q},t)\rangle$ in the presence of this perturbation may be expressed as

$$\langle\Delta\rho(\mathbf{q},t)\rangle = \int_0^t d\tilde{t}\chi(q,t-\tilde{t})\mathcal{V}(\mathbf{q},\tilde{t})\,. \tag{5.26}$$

Here $\xi(\mathbf{q},t)$ is the response function, which gives the answer of the system to the external perturbation $\mathcal{V}(q,t)$

- This answer cannot take place before the question has been posed (causality requirement):

$$\chi(\mathbf{q},t) = 0 \quad \text{for } t < 0\,.$$

If we assume that the external perturbation $\mathcal{V}(\mathbf{q},t)$ started at $t=0$ then the Fourier transforms of the relevant functions turn into a one-sided Fourier transform. So we get for the Fourier-transformed response function

$$\chi(q,\omega) = \lim_{\epsilon\to+0}\int_0^\infty dt\, e^{i\omega t}e^{-\epsilon t}\chi(q,t) = \lim_{\epsilon\to+0}\mathcal{L}_{\epsilon-i\omega}\{\chi(q,t)\} \tag{5.27}$$

where we had to put in the factor $e^{-\epsilon t}$ to guarantee the convergence.

$$\mathcal{L}_s\{f(t)\} = \int_0^\infty dt\, e^{-st}f(t)$$

is the Laplace transform discussed in the Appendix.

If we calculate the time convolution of the two functions $\chi(\mathbf{q},t)$ and $\mathcal{V}(\mathbf{q},t)$, which are both confined to $t>0$ we just get the right-hand side of Eq. (5.26), so we can reformulate, using the convolution theorem

$$\langle\Delta\rho(\mathbf{q},\omega)\rangle = \chi(\mathbf{q},\omega)\mathcal{V}(\mathbf{q},\omega) \tag{5.28}$$

- The complex function

  $$\chi(\mathbf{q},\omega) = \chi'(\mathbf{q},\omega) + i\chi''(\mathbf{q},\omega)\,,$$

  namely, as we just stated, the Laplace transform of the response function with $s=-i\omega+\epsilon$, is called the dynamical susceptibility.

- $\chi'(\mathbf{q},\omega)$ is the in-phase response,
  which follows the frequency dependence of $\mathcal{V}(\mathbf{q},t)$,
  $\chi''(\mathbf{q},\omega)$ is the out-of-phase response, delayed by a phase of $90^\circ=\pi/2$.

- The response function is related to the van-Hove function by the Fluctuation-dissipation theorem, due to R. Kubo (1957) [50]

  $$\chi(\mathbf{q},t) = -k_BT\frac{d}{dt}S(\mathbf{q},t) \tag{5.29}$$

We insert this into the one-sided Fourier transform
(omitting for notational simplicity the ϵ procedure)
and doing an integration by part

$$\begin{aligned}\frac{1}{k_BT}\chi(\mathbf{q}\omega) &= -\int_0^\infty e^{i\omega t}dt\dot{S}(q,t) = -\Big|_0^\infty e^{i\omega t}S(q,t) + i\omega\int_0^\infty e^{i\omega t}S(q,t)\\ &= S(t{=}0) + i\omega\mathcal{L}_{s=-i\omega}\{S(q,t)\}\\ &= S(t{=}0) + i\omega S(q,s{=}-i\omega)\}\end{aligned} \tag{5.30}$$

If we recognize the relation between Fourier and Laplace transform, proved in the Appendix

$$f(\omega) = 2\mathrm{Re}\{f(s{=}-i\omega)\}\,,$$

we obtain the Fluctuation-Dissipation theorem in its well-known form for the imaginary part of the dynamic susceptibility

$$S(q,\omega) = 2\mathrm{Re}\{S(q,s=-i\omega\} = \frac{2\omega}{k_BT}\chi''(\mathbf{q}\omega) \tag{5.31}$$

- This is the classical version (obtained as $\hbar\omega/k_BT \to 0$) of the quantum Fluctuation-dissipation theorem[50, 51, 2]

$$S(q,\omega) = \frac{2\hbar}{1-e^{-\hbar\omega/k_BT}}\chi''(q,\omega) \tag{5.32}$$

- The name fluctuation-dissipation theorem stems from the fact that $\chi''(q,\omega)$, the out-of phase response to $\mathcal{V}(\mathbf{q},t)$, describes the dissipation, i.e. the production of heat and entropy by the action of the external potential, whereas $S(q,\omega)$ describes the fluctuations of the density.

- The fluctuation-dissipation theorem applies to any other fluctuating dynamical variable, for example the magnetization. In this case χ is the magnetic susceptibility.

5.3.4 Damped-harmonic-oscillator expression for the dynamic structure factor much above T_g

We recall the damped-harmonic-oscillator equation of motion (A.63) for the dynamic structure factor

$$\left(\frac{d^2}{dt^2} + \Gamma(q)\frac{d}{dt} + \Omega_0^2(q)\right) S(\mathbf{q},t) = 0$$

Using $\dot{S}(q,t) = 0$ (which can be shown to hold for density fluctuations), the Laplace transform of the van-Hove function, obeying the (hydrodynamic) damped-harmonic oscillator equation (A.63) can be put into the compact form (see Appendix)

$$S(q,s) = S(q)\frac{1}{s + \dfrac{\Omega_0^2}{s+\Gamma(q)}} \tag{5.33}$$

Using the Laplace version of the Fluctuation-Dissipation theorem, and inserting the thermodynamical relation

$$S(0) = \rho_0 k_b T \kappa_T \tag{5.34}$$

we get for the dynamic susceptibility (we recall $s = -i\omega + \epsilon$; we drop the ϵ for brevity)

$$\begin{aligned}
\frac{1}{k_BT}\chi(q,s) &= S(Q) - sS(q,s) \\
&= S(q)\left(1 - \frac{s}{s + \dfrac{\Omega_0^2(q)}{s+\Gamma(q)}}\right) = S(q)\left(1 - \frac{s[s+\Gamma(q)]}{s[s+\Gamma(q)] + \Omega_0^2(q)}\right) \\
&= S(q)\frac{\Omega_0^2(q)}{s[s+\Gamma(q)] + \Omega_0^2} = q^2\frac{k_BT/m}{-\omega^2 - i\omega\Gamma(q) + v_T^2 q^2}
\end{aligned} \tag{5.35}$$

Using now the imaginary-part version of the fluctuation dissipation theorem, we obtain for the dynamical structure factor

$$
\begin{aligned}
S(q,\omega) &= \frac{1}{k_B T}\chi''(q,\omega) \\
S(q,\omega) &= q^2\frac{\omega}{m}\mathrm{Re}\left\{\frac{1}{v_T^2 q^2 - \omega^2 - i\omega\Gamma(q)}\right\} \\
&= \frac{1}{m}q^2\frac{\omega^2\Gamma(q)}{[\underbrace{v_T^2 q^2}_{\Omega_0^2} - \omega]^2 + \omega^2\Gamma(q)^2}
\end{aligned}
\tag{5.36}
$$

This function, which has two resonances at $\pm\Omega_0 = v_T q$, which are broadened by the damping coefficient $\Gamma(q)$ can be observed by Brillouin light scattering [52, 51].

5.4 Mode-coupling theory

5.4.1 Non-ergodicity and the Fluctuation-Dissipation theorem

In the beginning, we stated that the ergodic property of a dynamical variable in thermodynamics means that the time average is equal to the ensemble average. This is for systems in thermal equilibrium the case, because a point in phase space visits all phase space as time goes by.

However, if we approach the glassy state, this may not be true, because the system might get stuck in a pocked of phase space, and ergodicity is broken.

- Kubo, in his seminal paper on the statistical mechanics of irreversible processes [50] has shown that in the case of broken ergodicity the correlation function does not decay to zero:

$$\lim_{t\to\infty} \Big\langle A(t+t_0)A(t_0) \Big\rangle = F_A \geq 0 \quad \Leftrightarrow \quad \langle A \rangle \neq \overline{A} \tag{5.37}$$

  where A is a dynamical variable, $\langle A \rangle$ denotes an ensemble average, and $\overline{A}$ denotes a time average

$$\overline{A} = \lim_{\Delta t\to\infty} \frac{1}{\Delta t} \int_{-\Delta t/2}^{\Delta t/2} A(t)$$

- F_A is called non-ergodicity parameter of the non-ergodic variable A.
- In a glass the dynamical variable, which describes the configuration is the density fluctuation $\rho(q)$. So, in a glass we may expect $\rho(t)$ to become non-ergodic, and we have

$$\lim_{t\to\infty} S((q,t) = F_\rho(q) \geq 0 \tag{5.38}$$

Considering the Laplace transform of $S(q,t)$ we may split off the non-ergodicity parameter

$$\begin{aligned} S(q,t) &= \tilde{S}(q,t) + F_\rho(q) \\ S(q,s) &= \tilde{S}(q,s) + \frac{1}{s} F_\rho(q) \end{aligned} \tag{5.39}$$

and we can state

$$\lim_{t\to\infty} S(q,t) = \lim_{s\to+0} s\, S(q,t) = F_\rho(q) \tag{5.40}$$

So, in the non-ergodic glassy state the Fluctuation-Dissipation theorem takes the form [50, 23]

$$\frac{1}{k_B T}\chi(\mathbf{q}\omega) = S(t{=}0) + i\omega S(q, s{=}{-}i\omega)\} = S(t{=}0) - F_\rho(q) + i\omega \tilde{S}(q, s{=}{-}i\omega)\} \tag{5.41}$$

In particular we have for the $\omega{=}0$ value of the susceptibility

$$\frac{1}{k_B T}\chi(\omega{=}0) = S(q) - F_\rho(q) = S(q)[1 - f(q)] \tag{5.42}$$

Here we have defined a reduced non-ergodicy parameter $f(q)$.

5.4.2 The memory function

It can be shown [53, 51] that quite generally the Laplace transform of a correlation function can be represented as a continued fraction

$$C(s) = \cfrac{\nu_0}{s + \cfrac{\nu_1}{s + \dots \cfrac{\nu_n}{s + M_n(s)}}} \tag{5.43}$$

The residues $M_n(s)$ are complex functions, and the coefficients ν_n are related to the moments c_m of the spectrum

$$c_m = \frac{1}{2\pi} \int_{-\omega}^{\omega} d\omega \omega^m C(\omega) \,. \tag{5.44}$$

The first two coefficients ν_0 are (we don't need more)

$$\nu_0 = c_0 \qquad \nu_1 = c_2/c_0 \tag{5.45}$$

For the van-Hove function of the density fluctuations we have [51]

$$\nu_0(q) = c_0(q) = S(q) \tag{5.46}$$

and

$$c_2(q) = \frac{1}{m} k_B T q^2 \qquad \Rightarrow \qquad \nu_1(q) = \Omega^2(q) = \frac{1}{m} k_B T \frac{q^2}{S(q)} \tag{5.47}$$

If we terminate the continued fraction (5.43) at $n = 1$ we get

$$S(q,s) = S(q) \cfrac{1}{s + \cfrac{\Omega_0^2(q)}{s + M_1(q,s)}} \tag{5.48}$$

This, using the convolution theorem for Laplace transforms of the Appendix, can be converted to a generalized damped-harmonic-oscillator equation:

$$\boxed{\left(\frac{d^2}{dt^2} + \Omega_0^2(q)\right) S(\mathbf{q},t) + M(q,t) \circ \dot{S}(q,t) = 0} \tag{5.49}$$

with the Laplace-type version of the convolution

$$M(q,t) \circ \dot{S}(q,t) = \int_0^t d\tilde{t} M(q, t-\tilde{t}) \dot{S}(q,\tilde{t}) \tag{5.50}$$

The time version of the residual function, $M(q,t)$ is called memory function, because the dynamics at the time t keeps the memory of the previous history, represented by $\tilde{t}$.

The Memory function $M(q,t)$ can be shown to be a correlation function of random forces. Equations of motions with random forces, as one can write down for Brownian particles have been investigated by Paul Langevin, therefore Eq. (5.49) is also called generalized Langevin equation.

If we compare the generalized damped-harmonic-oscillator expression (5.49) hydrodynamic one (5.33), we see that the Laplace-transformed memory function $M(q,s)$ takes the place of the damping coefficient $\Gamma(q)$. So we may write

$$M_1(q,s) = \Gamma(q,s) = \frac{1}{\rho_m} q^2 \eta_L(q,s)\,, \tag{5.51}$$

where we have also defined a q and ω dependent longitudinal viscosity. We may solve Eq. (5.49) for $M_1(q,s)$ and insert the van-Hove function of the (non-ergodic) glass (5.39)

$$\begin{aligned} M_1(q,s) &= \Omega_0^2(q)\left(\frac{S(q,s)}{S(q)-sS(q,s)}\right) - s \\ &= \Omega_0^2(q)\left(\frac{S(q,s)+\frac{1}{s}F_\rho(q)}{S(q)-sS(q,s)-F_\rho(q)}\right) - s \end{aligned} \tag{5.52}$$

For $t \to \infty$ the memory function then takes the form (remembering (5.40)):

$$\boxed{\lim_{t\to\infty} M(q,t) = \lim_{s\to 0} sM(q,s) = \Omega_0^2(q)\left(\frac{F_\rho(q)}{S(q)-F_\rho(q)}\right) = \Omega_0^2(q)\left(\frac{f(q)}{1-f(q)}\right)} \tag{5.53}$$

Splitting off the non-ergodic contribution we can write for the memory function, viz. the sound-damping coefficient $\Gamma(q,s)$

$$M_1(q,s) = \Gamma(q,s) = \tilde{\Gamma}(q,s) + \frac{1}{s}\Omega_0^2(q)\frac{f(q)}{1-f(q)} \tag{5.54}$$

For the dynamic susceptibility we obtain in the small-q limit, where $\Omega_0(q) = v_T q$:

$$\chi(q,s) = q^2 \frac{k_B T/m}{-\omega^2 - i\omega\tilde{\Gamma}(q,s) + v_g^2 q^2} \tag{5.55}$$

with the sound velocity in the glassy state

$$v_g^2 = v_T^2\left(1 + \frac{f(o)}{1-f(0)}\right) = \frac{1}{\rho_m \kappa_T[1-f(0)]} \tag{5.56}$$

We see that in the glassy state the sound velocity is larger than in the liquid.

We can compare this with the longitudinal-sound velocity according to elasticity theory (see below in section 8)

$$v_L^2 = \frac{1}{\rho_m}\left(K + \frac{4}{3}G\right) \tag{5.57}$$

where $K = 1/\kappa_T$ is the bulk modulus. Comparing (5.56) with (5.57) we can identify

$$G = \frac{3}{4}K\frac{f(0)}{1-f(0)} \tag{5.58}$$

We may state:

- The non-ergodity parameters $f(q)$ are finite in the non-ergodic (glassy) state and zero in the ergodic (liquid) state, i.e. serves as an order parameter.
- The shear modulus G is zero in the liquid and finite in the solid. i.e. is the order parameter for any transition from a liquid to a solid.
- If the density variable $\rho(q)$ becomes non-ergodic, $f(0)$ and therefore G becomes finite, which describes a liquid-solid transition as an ergodicity-non-ergordicity transition.
- The mode-coupling theory describes this transition in a mathematical way.

5.4.3 Mode-coupling expression for the memory function

The idea of the mode-coupling approach [45, 22, 54, 23] is to express the memory function $M_1(\mathbf{q}, t)$ again in terms of the density correlation function $S(q, t)$. This is then a dynamic closure relation, and establishes a self-consistent set of equations, which can be solved for $S(q, t)$. The name "mode-coupling" comes from the theory of nonlinear media, where the nonlinearity leads to a coupling of the Fourier components of the dynamical variables. In our case this dynamical variable is the density fluctuation $\rho(\mathbf{r}, t)$, and the modes are their Fourier components $\rho(\mathbf{q}, t)$.

The decoupling procedure leading to the mode-coupling mean-field equations now proceeds performing the following steps:

- Expressing the memory function as a correlation function of fluctuating forces, using the memory function formalism of Mori and Zwanzig [55, 56, 57, 51], which is formulated in terms of the microscopic Hamilton function.
- expressing the fluctuating forces in terms of pair modes of density fluctations $\rho(\mathbf{q}_1, t)\rho(\mathbf{q}_2, t)$;
- factorizing the resulting four-point density correlation functions into products of two-point functions;
- approximating the static projection vertex (static three-point correlation function) in terms of the radial distribution, or, respectively, their Fourlier transforms, $S(k)$ (convolution approximation).
- The result for $M(q, t)$ is

$$\boxed{M(q,t) = \underbrace{\Omega_0^2(q)}_{\frac{q^2 k_B T}{m S(q)}} \int \frac{\mathrm{d}\mathbf{q}_1}{(2\pi)^3} V(\mathbf{q}, \mathbf{q}_1, \mathbf{q}_2) S(q_1, t) S(q_2, t) \Big|_{\mathbf{q}_2 = \mathbf{q} - \mathbf{q}_1}} \tag{5.59}$$

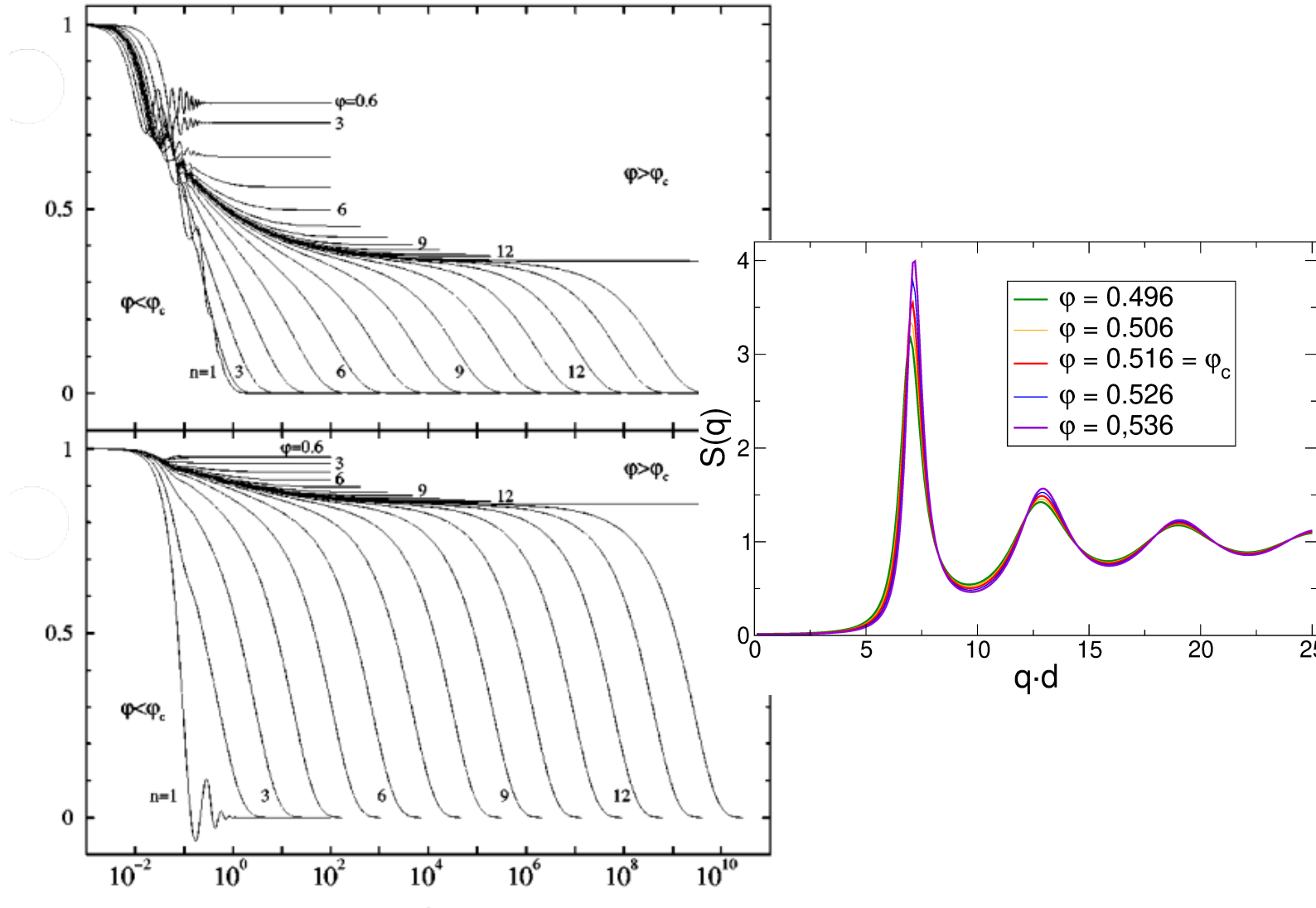

Figure 43: Solution of the Mode-coupling equations with hard-sphere structure factors $S(q)$ as input. The hard-sphere structure factors depend only on the packing fraction $\varphi = \frac{\pi}{6} d^3 \rho_0$, where d is the hard-sphere diameter [54]. The values of φ are parametrizes in terms of an integer n as $varphi = \varphi_c(1 \pm 10^{-n/3})$. Top: $qd = 3.4$, bottom: qd =7.0
The right panel shows $S(q)$ for packing fractions $\varphi_c = 0.516$ and values above (glass) and below (liquid), corresponding to $n = 6$ and 12.

The vertex function $V(\mathbf{q}, \mathbf{q}_1, \mathbf{q}_2)$ is given by

$$V(\mathbf{q}, \mathbf{q}_1, \mathbf{q}_2) = \frac{1}{\rho_0} S(q) W(\mathbf{q}, \mathbf{q}_1, \mathbf{q}_2)^2 \tag{5.60}$$

$$W(\mathbf{q}, \mathbf{q}_1, \mathbf{q}_2) = \frac{1}{q^2} \mathbf{q} \cdot [\mathbf{q}_1 \rho_0 c(q_1) + \mathbf{q}_2 \rho_0 c(q_2)], \quad \text{where} \quad c(q) = \frac{1}{\rho_0} \left(1 - \frac{1}{S(q)}\right)$$

is the direct correlation function.

- The mode-coupling equations have as input
  - the state variables mass m, density ρ_0, temperature T;
  - the static structure factor $S(q)$

The vertex $V_{\mathbf{qkp}}$ depends only on the static structure factor $S(q)$ and on the other known functions of q. (5.49) together with (5.59) constitute a closed set of equations which can be solved for $S(q, t)$ with the initial conditions

$$S(q, t{=}0) = S(q) \qquad \dot{S}(q, t{=}0) = 0\,. \tag{5.61}$$

- Hard-sphere structure factor:

The structure factor of $S(q)$simple liquids like methane or liquid metals can be well described by the structure factor of hard spheres with diameter d (see the upcoming seminar talk). Hard-sphere fluids characterized by d and the density ρ_0. They form together a single parameter, namely the packing fraction, which is the volume filled with matter, $\frac{\pi}{6}Nd^3$ divided by the total volume:

$$\varphi = \frac{\pi}{6}Nd^3/V = \frac{\pi}{6}\rho_0 d^3 \tag{5.62}$$

In Fig. 43 we have plotted the density correlation function divided by the structure factor $S(q,t)/S(q)$ against t for $qd = 3.4$ and $qd = 7.0$ and various values of the packing fraction φ. It turns out that at a critical packing fraction φ_c a egodicity-non-ergodicity transition takes place, i.e. for $\varphi \geq \varphi_c$ the normalized density correlation function does not decay to zero, but to a finite value $f(q)$, which we have called non-ergodicity parameter

The values of φ have been fine-tuned around φ_c in multiplicative steps of $10^{-1/3}$. The integers n in the plot refer to $varphi = \varphi_c(1 \pm 10^{-n/3})$.

We observe the following features:

- Coming from the liquid side, with increasing φ a characteristic plateau is built up.
- The plateau represents a temporary glassy state within the time regime $t < \tau$, similar to the ideas of Maxwell and also in the spirit of the Deborah number.
- In the glassy state the non-ergodicity parameter $f(q)$ increases with increasing packing fraction φ.
- In liquid metals and other simple liquids the packing fraction φ decreases with increasing temperature T. Therefore one can identify a critical Temperature T_c as via $\varphi(T_c) = \varphi_c$.
- Relaxation towards the plateau $f(q)$:

$$\frac{1}{S(q)}S(q,t) - f(q) \sim t^{-a} \qquad \beta \text{ relaxation}$$

- Relaxation away from the plateau $f(q)$:

$$\frac{1}{S(q)}S(q,t) - f(q) \sim t^{b} \qquad \alpha \text{ relaxation}$$

- The fact that the length of the plateau $\tau(\varphi)$ in the logarithmic plot increases by equal amounts means that the critical point is approaced by a power law

$$\tau(\varphi) \sim \frac{1}{(\varphi - \varphi_c)^\gamma} \qquad \gamma = \frac{1}{2a} + \frac{1}{2b} \tag{5.63}$$

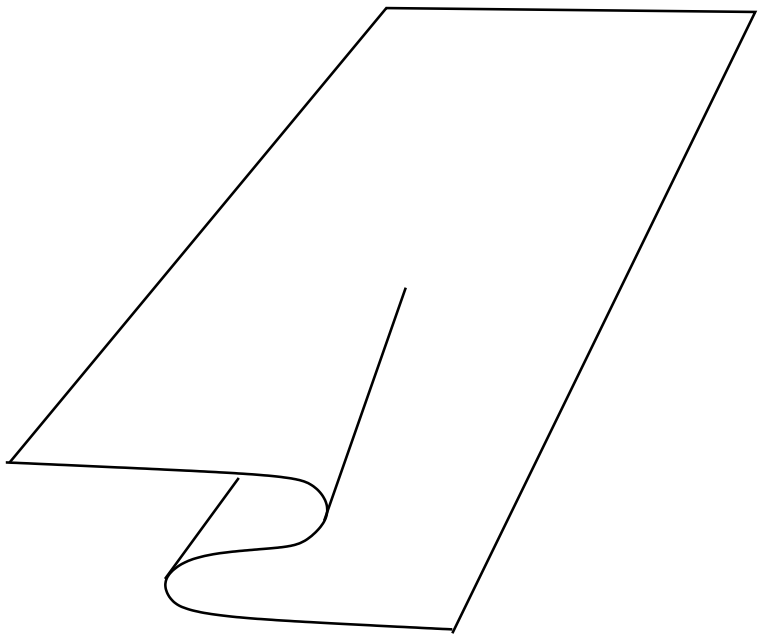

Figure 44: A fold singularity as defined in catastrophe theory

5.4.4 Phenomenological Mode-Coupling Theory

From the foregoing it is clear that the derivation of the mode-coupling equations (5.49) together with (5.59) applies for simple hard-sphere-like one-component liquids. It has been tested against computer simulations of such liquids as well as experiments on hard-sphere colloid solutions [58]
However, many experimental data on quite more complicated glass-forming liquids like ortho-terphenyle, Potassium-Calcium Nitrate or Glycerol show the same critical behavior as predicted by the original mode-coupling equations . W. Götze (2012) [23] therefore proposed the following generalized phenomenological mode-coupling theory (MCT):

$$m_q(t) = M(q,t)/\Omega_0^2(q) = (\mathcal{F}_q\{\vec{V}, \phi(k,t)\} \tag{5.64}$$

with

$$\mathcal{F}_q\{\vec{V}, x_k\} = \sum_{m=1}^{m_0} \frac{1}{m!} \sum_{k_1 \cdots k_m} V^{(m)}(q, k_1 \cdots k_m) x_{k_1} \cdots x_{k_m} \tag{5.65}$$

i. e. we have

$$m_q(t) = \sum_k V^{(1)}(q,k)\phi(k,t) + \frac{1}{2}\sum_{k_1,k_2} V^{(2)}(q,k_1,k_2)\phi(k_1,t)\phi(k_2,t) + \cdots \tag{5.66}$$

The search for non-ergodic solutions with $\phi(q, t \to \infty) = f_q \neq 0$ within this generalized set of mode-coupling equations can be shown to be equivalent to the search of topological singularities in the parameter space of the coefficients $V^{(m)}(q, k_1 \cdots k_m)$. Such singularities are the subject of the mathematical discipline "catastrophe theory", or, more modestly, the theory of bifurcations, developed by [59] and [60]. The singularities relevant for the MCT glass transition are of the simplest type, namely the *fold* singularity or A_2 singularity,

which can be visualized by crumpling a piece of paper. Near the singularity the dynamics is dominated by a single eigenvalue of the stability matrix ("reduction theorem"), from which follows that the critical fluctuations are governed by a single function $G(t)$, and the wavevector q appears only in a prefactor (factorization theorem, [61, 23])

$$\frac{1}{S(q)}S(q,t) = \phi(q,t) = f_c(q) + h(q)G(t) \tag{5.67}$$

Therefore the critical dynamics can be discussed with the help of a much simpler version of mode-coupling theory: the so-called schematic model.

5.4.5 Schematic Model

We study the following q independent mode-coupling equations ("F_{12} model"):

- No q dependence
- Reduced correlation and memory functions

$$\phi(t) = \frac{S(t)}{S(t=0)} \qquad m(t) = \frac{1}{\Omega^2}M(t)$$

- schematic mode-coupling equation

$$\boxed{\frac{\mathrm{d}^2}{\mathrm{d}t^2}\phi(t) + \Omega^2 \int_0^t \mathrm{d}\tau m(t-\tau)\frac{\mathrm{d}}{\mathrm{d}\tau}\phi(\tau) + \Omega^2\phi(t) = 0, \tag{5.68}}$$

- Memory function

$$m(t) = \lambda_1\phi(t) + \lambda_2\phi(t)^2 \tag{5.69}$$

- Boundary conditions

$$\phi(0) = 1 \quad \text{and} \quad \dot{\phi}(0) = 0\,.$$

  - λ_2 now takes the place of the structure factor $S(q_{\max})$, i.e the influence of the packing fraction φ or the temperature T
  - λ_1 is an auxiliary parameter, representing the influence of other q or higher-order terms.

(5.68) and (5.69) can be reformulated for the Laplace transforms as follows:

$$\frac{\phi(s)}{1-s\phi(z)} - \frac{s}{\Omega^2} = m(s) = \lambda_1\phi(s) + \lambda_2\mathcal{L}_s\{\phi(t)^2\} \tag{5.70}$$

We are now looking for non-ergodic asymptotic solutions

$$f \equiv \phi(t\to\infty) = s\phi(s)|_{s\to 0}$$

of (5.70). Such solutions must obey the equation

$$\frac{f}{1-f} = \lambda_1 f + \lambda_2 f^2 \tag{5.71}$$

We observe

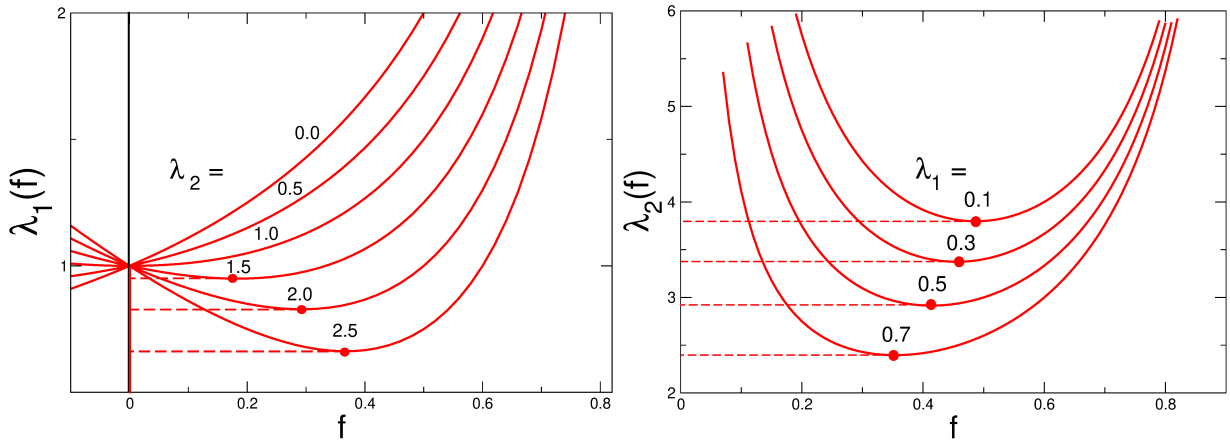

Figure 45: Left: the function $\lambda_1(f) = \frac{1}{1-f} - \lambda_2 f$ with λ_2 as parameter.
Right: the function $\lambda_2(f) = \frac{1}{1-f} - \lambda_1 f$ with λ_1 as parameter, for $\lambda_1 > 1$ (discontinuous non-ergodicity transition, type B).

- $f \equiv 0$ is always a solution of this equation.
- It can be shown that if there are several solutions to the mode-coupling equations, it is always the largest one which will be taken by the physical system (and also by the mathematical iteration).
- f cannot be smaller than 0, so that we are looking for nonergodic solutions with $f > 0$ which are the solution of

$$\frac{1}{1-f} = \lambda_1 + \lambda_2 f \tag{5.72}$$

If we inspect the left panel of Fig. 45 in which the function $\lambda_1(f) = \frac{1}{1-f} - \lambda_2 f$ is plotted for different values of λ_2 we observe

- for $\lambda_2 < 1$ the minimum is situated at negative values of f,
- for $\lambda_2 > 1$ the minimum is in the positive f regime.

If we now increase λ_1 for a certain fixed value of λ_2 and look for the largest value of f at a given pair (λ_1, λ_2) we see that

- for $\lambda_2 < 1$ there is a *continuous* transition to a nonergodic state (*"Type A transition"*),
- for for $\lambda_2 > 1$ we have a *discontinuous* one (*"Type B transition"*).

In the left panel of Fig. 47 we show the phase diagram in the $\lambda_1 - \lambda_2$ parameter plane. The type-A transition line is just given by $\lambda_1(\lambda_2) = 1$.

The type-B line is given by

$$\frac{d}{df}\lambda_1(f) = 0 = \frac{1}{(1-f)^2} - \lambda_2 \quad \Rightarrow \quad \lambda_{2,c} = \frac{1}{(1-f_c)^2}\,. \tag{5.73}$$

We stated above that in the schematic model the parameter λ_2 represents $S(q_0)$ of the q dependent mode-coupling theory, so increasing λ_2 means increasing packing fraction or decreasing temperature.

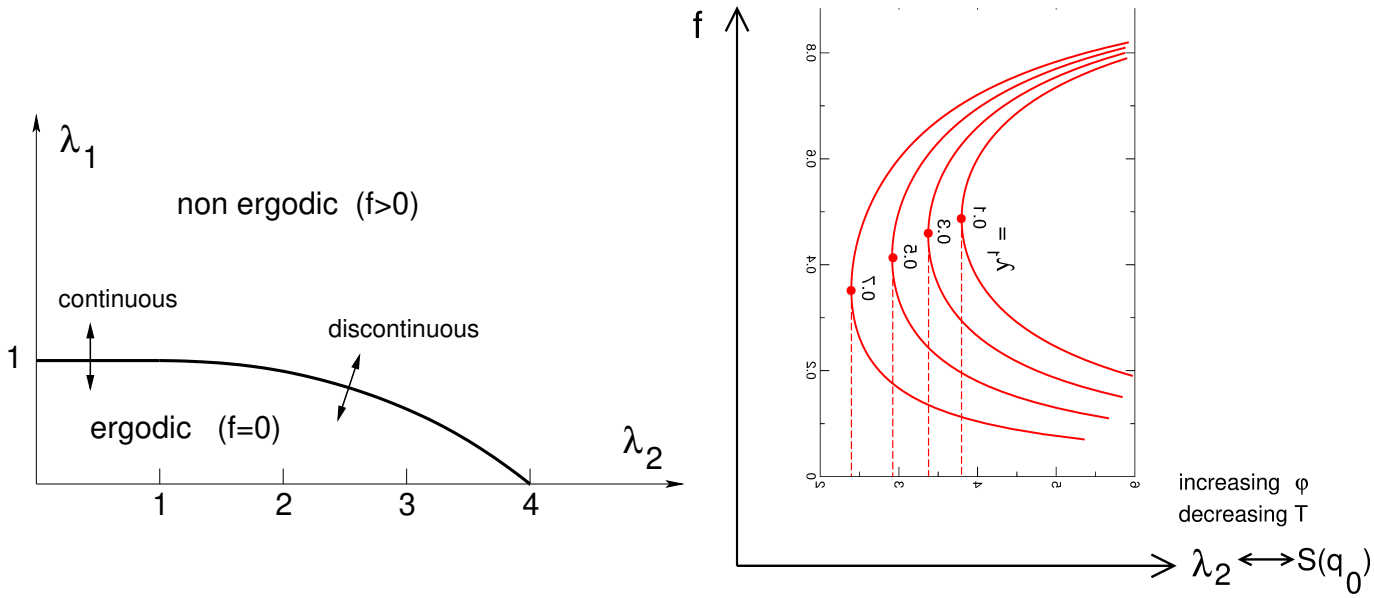

Figure 46: Left: Phase diagram of the F12 model
Right: Non-ergodicity parameter $f(\lambda 2)$ with λ_1 as parameter, i.e. inversion of the right panel of Fig. 45; λ_2 signifies an increase with density or a decrease with temperature.

In the right panel of Fig. 47 we again show the right panel of Fig. 46, but with swapped axes, i.e. $f(\lambda_2)$. We see that

- the non-ergodicity parameter f is predicted to exhibit a square-root singularity.

5.4.6 Non-ergodicity parameter as Debye-Waller factor

If we insert the contribution of the non-ergodicity factor to the Laplace transform of the density correlation function

$$S_{\rm ne}(q,s) = \frac{1}{s} f(q)\Big|_{s\,=\,\epsilon - i\omega,\ \ \epsilon \to 0}$$

into the formula for the dynamic structure factor

$$S(q,\omega) = {\rm Re}\Big\{ S(q,s) \Big\}_{s\,=\,\epsilon - i\omega,\ \ \epsilon \to 0}$$

we get

$$\begin{aligned} S_{\rm ne}(q,\omega) &= \lim_{\epsilon\to 0} f(q)\ {\rm Re}\Big\{ \frac{1}{\epsilon - i\omega} \Big\} \\ &= \lim_{\epsilon\to 0} f(q)\ \frac{\epsilon}{\epsilon^2 + \omega^2} \\ &= \pi\, f(q)\delta(\omega) \end{aligned} \tag{5.74}$$

This means that after the liquid has been transformed to a solid the scattering law $S(q,\omega)$ acquires

- an infinitely narrow central peak,
  indicating that

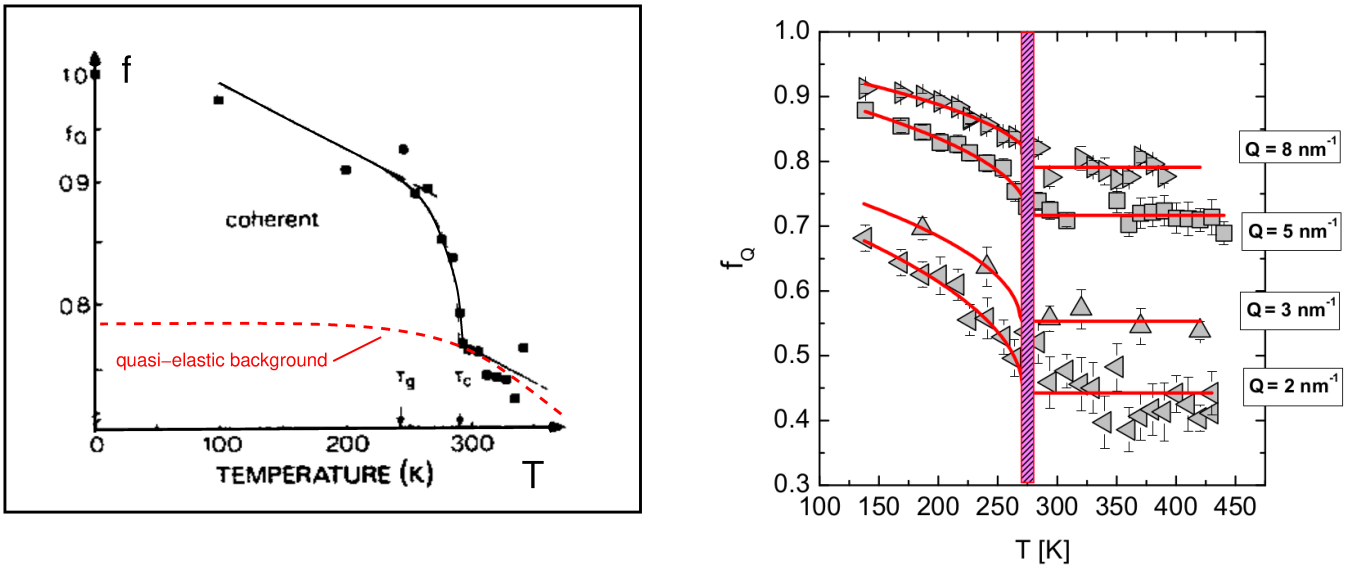

Figure 47: Left: Debye-Waller factor of o-terphenyl as a function of temperature measured with inelastic neutron scattering [62]
Right: Debye-Waller factor of salol as a function of temperature measured with inelastic X-ray scattering [63]

- scattering from a solid involves a recoilless contribution (Mössbauer effect).
- $f(q)$ is called Debye-Waller factor.
- The mode-coupling theory predicts that the Debye-Waller factor of a glass exhibits a square-root singularity as a function of temperature.

In Fig. 47 we show measured Debye-Wallerfactors for ortho-terphenyl (inelastic neutron scattering [62]) and for salol (inelastic X-ray scattering [63]) as a function of temperature. If one disregards the background (which comes from quasi-elastic scattering due to diffusional modes), the square-root behavior, like the one depicted in the right panel of Fig. 46.

5.4.7 Fractal relaxation dynamics

- Relaxation right at $\lambda_{2,c}$:

We would now like to study the dynamics right on the B-type transition line. In order to do so we divide the correlation function up as follows:

$$\phi(t) = f_c + hG(t) \qquad \Leftrightarrow \qquad s\phi(s) = f_c + hsG(s) \tag{5.75}$$

and treat $h|sG(s)|$ as a small parameter.

Expanding both sides of (5.70) w. r. to $|hsG()|$, and setting

$$\lambda \equiv 1 - f_c = \sqrt{1/\lambda_2} \tag{5.76}$$

we obtain the following equation of motion:

$$\boxed{sG^2(s) - \lambda\mathcal{L}_s\{G(t)^2\} - \lambda^3 s = 0} \tag{5.77}$$

Before we proceed we take a look at the Gamma function [64]

- Gamma function:

$$\Gamma(z) = \int_0^\infty dt\, t^{z-1}e^{-t}$$

- For $z = n$ (integer) we obviously have

$$\Gamma(n) = \int_0^\infty dt\, t^{n-1}e^{-t} = (n-1)!$$

- $\Rightarrow$

$$\begin{aligned}\mathcal{L}_s\{t^{-x}\} &= \int_0^\infty dt\, t^{-x}e^{-st} \\ &= \frac{1}{s^{1-x}}\int_0^\infty d(st)\,(st)^{-x}e^{-st} \\ &= \frac{1}{s^{1-x}}\Gamma(1-x)\end{aligned} \tag{5.78}$$

We make now the ansatz

$$\boxed{G(t) = A(t/t_0)^{-x} \quad \Leftrightarrow \quad G(s) = \frac{1}{s}\Gamma(1-x)(st_0)^x} \tag{5.79}$$

We have also

$$\mathcal{L}_s\{G(t)^2\} = \frac{1}{s}\Gamma(1-2x)(st_0)^{2x} \tag{5.80}$$

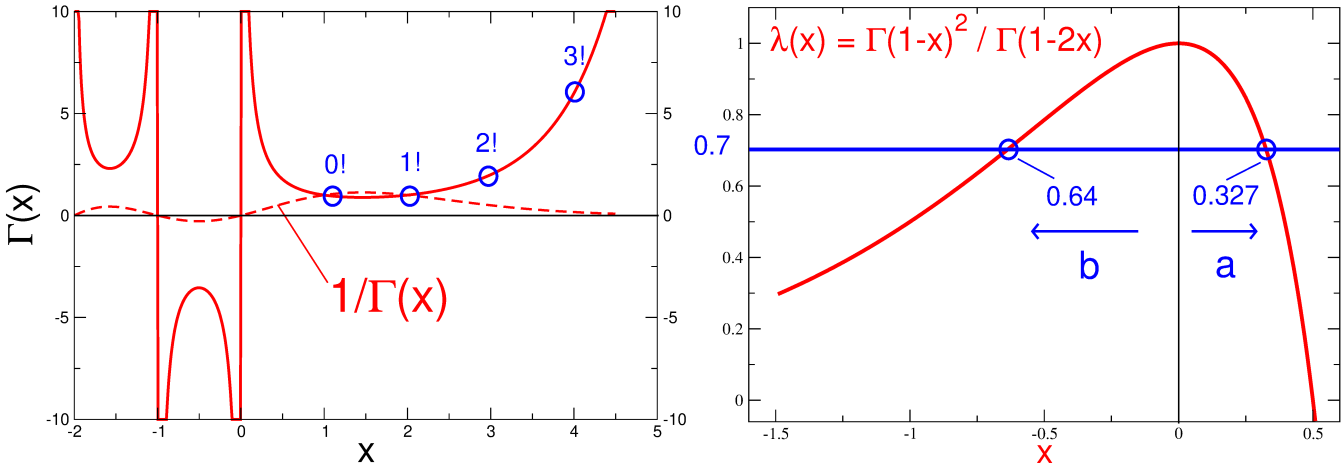

Figure 48: Left: The gamma function $\Gamma(x)$ (full line) and its inverse $1/\Gamma(x)$ (dashed line). Right: The function $\lambda(x) = \Gamma(1-x)^2/\Gamma(1-2x)$.

For $s \to 0$ the "regular term" in (5.77) $\lambda^3(s$ can be neglected as $s \to 0$.

- Then (5.79) provides an asymptotic solution of (5.77), provided

$$\boxed{\lambda \equiv \lambda(x) = \Gamma(1-x)^2/\Gamma(1-2x) \qquad (5.81)}$$

It is important to note that the solution – once the regular terms can be neglected – is not affected by changing the time scale t_0 (scale invariance). jj

In Fig. 48 we have plotted the function $\lambda(x)$. We can see from the graph of the function $\lambda(x)$ that,

- if we require $x \equiv a > 0$ and $\lambda > 0$, the value of a must be less than 0.5.

The "critical" relaxation law

$$\phi(t) = f_c + A(t/t_0)^{-a} \qquad (5.82)$$

is called β relaxation and holds on both sides of the (idealized) glass transition.

- Relaxation in the glass-forming liquid, away from $\lambda_{2,c}$

Now we want to study the dynamics in the supercooled liquid regime.

In order to do so we define a separation parameter σ, which measures the distance from the critical line

$$\sigma \propto |\lambda_1 - \lambda_{1,c}| \quad \text{or} \quad \sigma \propto |T - T_c| \qquad (5.83)$$

A little away from $f = f_c$ one gets the scaling equation

$$\boxed{sG^2(s) - \lambda\mathcal{L}_s\{G(t)^2\} = \frac{1}{s}\lambda^4(1-\lambda)\sigma \qquad (5.84)}$$

We now are asking at which time scale the system realizes that it is away from the critical line and at which one it doesn't.

Let's therefore insert the β-scaling solution

$$G(t) = A(t/t_0)^{-a} \quad \Leftrightarrow \quad G(s) = \frac{1}{s}\Gamma(1-a)(st_0)^a \tag{5.85}$$

into Eq. (5.84):

$$\begin{aligned} \frac{1}{s}\Gamma^2(1-a)(st_0)^{2a} - \frac{\lambda}{s}\Gamma(1-2a)(st_0)^{2a} &= \frac{1}{s}\lambda^4(1-\lambda)\sigma \\ \Rightarrow \left[\Gamma^2(1-a) - \lambda\Gamma(1-2a)\right](st_0)^{2a} &= \lambda^4(1-\lambda)\sigma \end{aligned} \tag{5.86}$$

The characteristic time which separates these regimes is obviously

$$t_\sigma = \frac{1}{\omega_\sigma} = \frac{\tilde{t}_0}{|\sigma|^{\frac{1}{2a}}} \tag{5.87}$$

where we now have defined a "microscopic" time scale $\tilde{t}_0$.

As we are now in the liquid phase in which we know that eventually the function $\phi(t)$ decreases away from $\phi(t) = f$ like a power law

$$G(t) = \phi(t) - f \propto -(t/\tau)^b \tag{5.88}$$

- This relaxation is the α relaxation, and τ is the α relaxation time.

It is the time τ, at which the system realizes that it is not at criticallity but in the egodic liquid state.

If we insert this time dependence of $G(t)$ into eq. (5.84), we see that this time τ increases with σ as

$$\frac{\tau}{t_\sigma} = \frac{\tau}{\tilde{t}_0}\sigma^{\frac{1}{2a}} = \sigma^{-\frac{1}{2b}} \tag{5.89}$$

which implies

$$1/\tau = \frac{1}{t_0}|\sigma|^\gamma \qquad \gamma = \frac{1}{2a} + \frac{1}{2b}. \tag{5.90}$$

Note that the two critical exponents are related by (5.80), i. e.

$$\lambda = \Gamma(1-a)^2/\Gamma(1-2a) = \Gamma(1+b)^2/\Gamma(1+2b) \tag{5.91}$$

The critical law (5.90) is that corresponding to structural relaxation, i. e. the diffusivity and the inverse viscosity go to zero accordingly.

- It turns out that the entire remaining time dependence is governed by the α relaxation scale;
- the scaling function outside the $-t^b$ regime can be well approximated by a stretched exponential

$$\phi(t) \propto e^{-(t/\tau)^\beta} \tag{5.92}$$

  where the exponent β must be determined numerically and has values near 0.5.

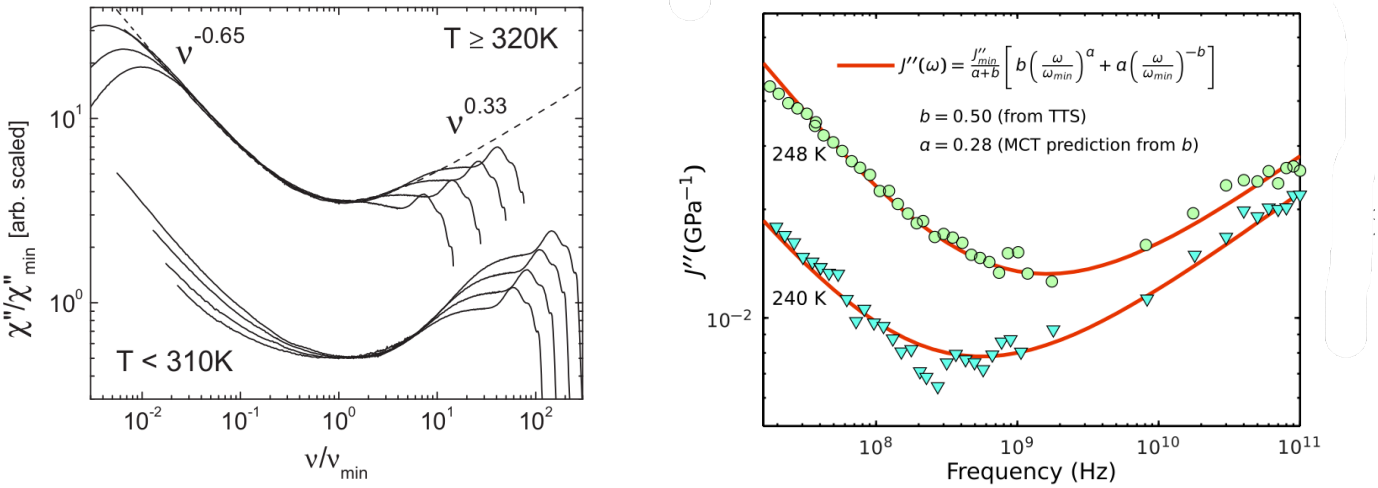

Figure 49: Experimental data of the dynamic susceptibility measured on diffusion pump oil DC 704 [20], and on and o-terphenyl [65].

- Dynamic susceptibility

We recall the Laplace transforms of the β and α relaxation laws

$$G_\alpha(s) \sim s^{-(b+1)}\Big|_{s=-i\omega} \qquad G_\alpha(s) \sim s^{a-1}\Big|_{s=-i\omega} \tag{5.93}$$

What is i^x ??

$$i^x = e^{ix\frac{\pi}{2}} = \cos(x\frac{\pi}{2}) + i\sin(x\frac{\pi}{2})$$

leading to

$$S_\alpha(s) \sim \mathrm{Re}\{G_\alpha(s{=}-i\omega)\} \sim \omega^{-(b+1)} \qquad S_\beta(s) \sim \mathrm{Re}\{G_\beta(s{=}-i\omega)\} \sim \omega^{a-1}$$

Inserting this into the fluctuation-dissipation theorem

$$\chi''(\omega) \sim \omega S(\omega) \tag{5.94}$$

we obtain

$$\boxed{\chi''_\alpha(\omega) \propto \omega^{-b} \qquad \chi''_\beta(\omega) \propto \omega^{a}} \tag{5.95}$$

- Between the α-decrease of $\chi''(\omega$ and the β-increase there is a characteristic minimum, which is observed in almost all glass-forming liquids
- At lower frequency the stretched-exponential α relaxation is converted to an asymmetric α peak.

In Fig 49 we show susceptility data of the dynamic susceptibility measured on diffusion pump oil DC 704 [20], and on and o-terphenyl [65] with the characteristic minimum and the two fractal scaling laws $\chi''_\alpha(\omega) \sim \omega^{-b}$ and $\chi''_\beta(\omega) \sim \omega^{a}$

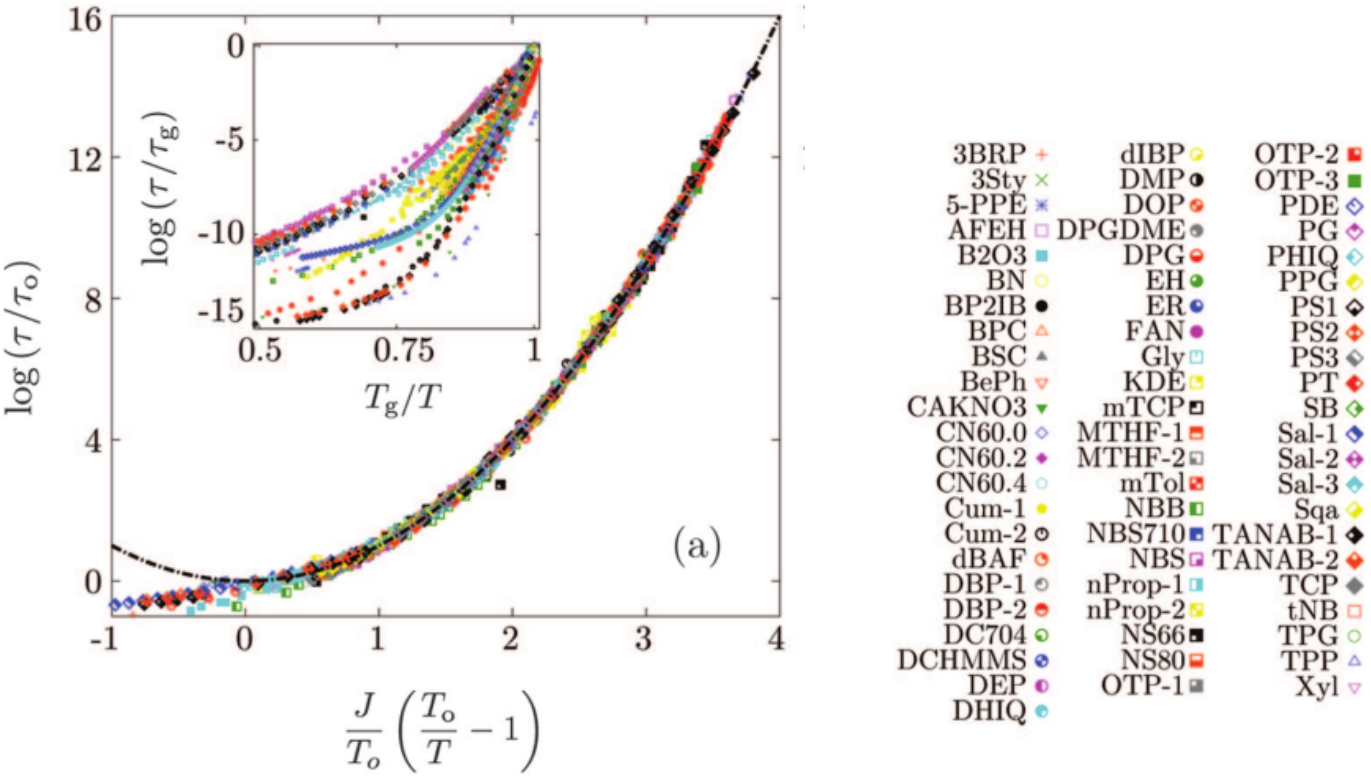

Figure 50: Universal plot of the temperature dependence of the viscosity of 67 glasses [66].

5.5 Dynamic facilitation

- The dynamic-facilitation approach [67, 66] establishes dynamic rules for the activated hopping motion of particles:
  - kinetic random-walk (Ising) model with activated transition rates;
  - A particle can only move if another particle makes room;
  - All motions depend on previous motions;
  - The glass transition is just a freezing out of the kinetics
- Evaluation of such a model gives as temperature dependence for the viscosity

$$\frac{\eta(T)}{\eta_0} = \frac{\tau(T)}{\tau_0} = \left[\frac{T_0}{T}\left(\frac{T_0}{T} - 1\right)\right]^2 \tag{5.96}$$

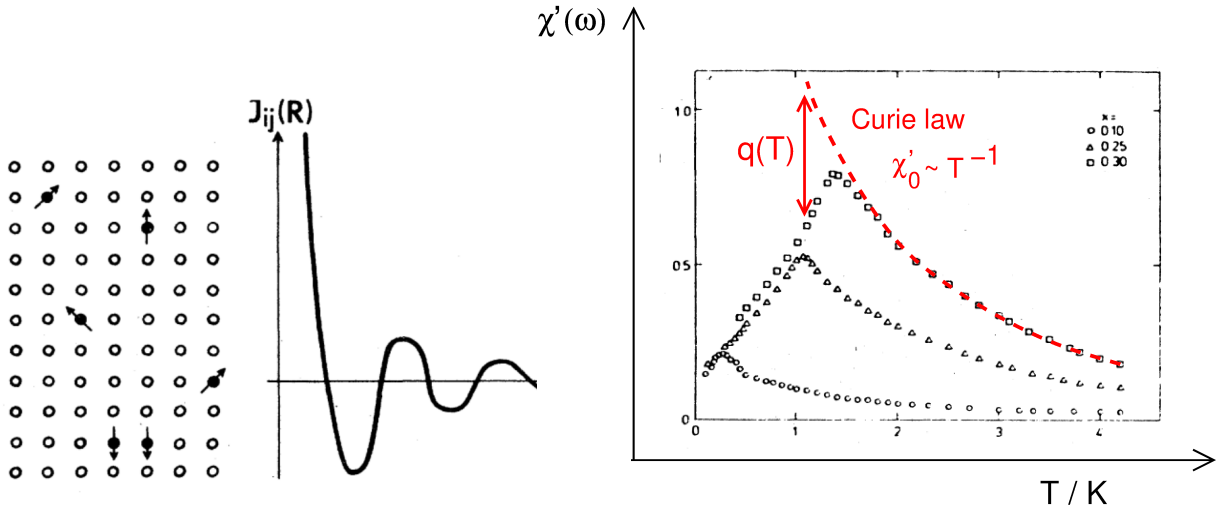

Figure 51: Left Ruderman-Kittel-Kasuya-Yosida (RKKY) interaction between parametic impurities in a nonmagnetic metallic host; Right: Real part of the low-frequency (117 Hz) magnetic susceptibility $\chi'(\omega)$ of $Eu_xSr_{1-x}S$ as a function of temperature for the Eu concentrations $x = 0.10$, 0.25, 0.30 (from bottom to top) Both figures are taken from [12].

5.6 Generalized spin glasses

The following brief account on the spin-glass-type interpretation of the structural glass transition is mainly based on the review articles [68, 24, 5, 69].

5.6.1 The non-ergodic spin-glass phase

In the left panel of Fig. 51 we recall, what is meant by spin glasses, mentioned in the introduction: A random alloy is formed from a nonmagnetic metal with a metallic atoms carrying magnetic moments (spins). This gives rise to an indirect exchange interaction between the spins, which oscillates around zero as a function of the distance between the spins.

$$\mathcal{H} = -\sum_{i\neq j} J(|\mathbf{r}_i - \mathbf{r}_j|)\mathbf{s}_i \cdot \mathbf{s}_j \quad \text{with} \quad J(r) \sim \frac{1}{r^3}\cos(2k_F r)\,, \tag{5.97}$$

where k_F is the electronic wavenumber at the Fermi edge.

- Very often the spins cannot align according to the interaction;
- This leads to frustration, and
- a frozen-in phase with immobile spins (spin glass) below a critical temperature T_K.

The critical temperature is detected as a cusp in the magnetic susceptibility. The spin-glass phase is a non-ergodic phase, in which the spin-spin correlation function does not decay towards zero, leading to a susceptibility

$$\chi(T) = \chi_0(T) - q(T) \tag{5.98}$$

where $\chi_0(T) \sim T^{-1}$ is the non-interacting Curie susceptibility and

$$q(T) = \lim_{t\to\infty} \left\langle \frac{1}{N}\sum_{i=1}^{N} \mathbf{s}_i(t_0+t)\cdot\mathbf{s}_i(t_0) \right\rangle \tag{5.99}$$

is the non-ergodicity parameter (S. F. Edwards, P. W. Anderson [70], which serves – like in the structural glass transition – as order parameter.

5.6.2 Quenched disorder, self-averaging, and the replica trick

As stated in the beginning, in glasses, which featured quenched, i.e. frozen-in disorder, one encounters the

- self-averaging property

$$\overline{A\{\mathbf{r}_i\}} = \frac{1}{N}\sum_{i=1}^{N} A\{\mathbf{r}_i\} = \langle A\{\mathbf{r}_i\}\rangle\,,$$

  where $\langle \dots \rangle$ denotes an ensemble average.

In order to calculate thermodynamic quantities in a quenched-disordered system certain rules of game must be obeyed:

- extensive physical properties are assumed to be self-averaging and have to be averaged over the quenched disorder.
- The partition function

$$\mathcal{Z} \sim \sum_{s_i} e^{-\mathcal{H}\{s_i\}/k_B T}$$

  is not self-averaging, but instead the free energy

$$\mathcal{F} = -\ln \mathcal{Z}\,.$$

- Therefore the free energy, the logarithm of the partition function must be quenched-averaged.
- Field theorists don't like to do this, because they are only able to do Gaussian integrals.
- Therefore they invented [71] the

Replica trick

$$\boxed{\ln z = \int_1^z dx \frac{1}{x} = \lim_{n\to 0}\int_1^z dx x^{n-1} = \lim_{n\to 0}\frac{1}{n}\left[z^n - 1\right]} \tag{5.100}$$

5.6.3 Mean-field spin-glass model and generalizations

Sherrington-Kirkpatrick model [72]:

$$\mathcal{H} = -\sum_{i\neq j} J_{ij} s_i s_j \qquad P(J_{ij}) \sim e^{-\frac{1}{2\sigma^2}[J_{ij}]^2} \qquad s_{i,j} = \pm 1 \text{ (Ising model)} \tag{5.101}$$

Generalizations for higher order and more spin variables:

$$\mathcal{H} = -\sum_{i\neq j\neq k} J_{ijk} s_i s_j s_k \qquad P(J_{ijk}) \sim e^{-\frac{1}{2\sigma^2}[J_{ijk}]^2} \qquad s_{i,j,k} = 0, 1, \dots \tag{5.102}$$

- Every spin s_i interacts with every other spin s_j (mean-field spin glass model)
- This mean-field feature enables
  - To calculate the free energy $\mathcal{F}$ and the associated thermodynamics exactly
  - To evaluate the dynamics of the spin correlations using a Langevin equation for the spins

$$\frac{\partial}{\partial t} s_i(t) = -\frac{\partial \mathcal{H}}{\partial s_i} + \xi_i(t)$$

  where $xi_i(t)$ is a random force.

Results for the generalized spin models [68, 24]:

- The many replicas enable the identification of many different glass configurations
- There are two transitions:
  - a thermodynamic transition at T_K,
  - a dynamic transition at $T_d > T_K$.
- Above T_d the spin correlation function obeys the mode-coupling equations, i.e. features a two-step relaxation with a plateau increasing as $[T_K - T]^\gamma$.
- Below T_d replica-symmetry breaking occurs. i.e. non-vanishing non-ergodic overlaps between different replicas a and b appear:

$$q_{ab} = \frac{1}{N} \left\langle \sum_{i=1}^{N} s_i^{(a)} s_i^{(b)} \right\rangle$$

  - leading to a field of infinitely many order parameters q_α and a
  - free-energy landscape like Goldstein's potential-energy landscape
- T_d marks a cross-over from
  - saddle-dominated dynamics for $T > T_d$ and
  - dynamics inside of one metastable state for $T < T_d$.
- For $T_c < T < T_K$ the metastable states feature a configurational entropy, which vanishes at T_K (Kauzmann-Adam-Gibbs scenario).
- Therefore the generalized spin glasses may serve as qualitative models for the structural glass transition, unifying the Kauzmann-Adam-Gibbs scenario and the Mode-coupling two-step relaxation.
- Activated processes, which appear below T_d in real glasses are absent.

5.7 Mosaic Approach, Random-First-Order Theory (RFOT)

The – presently – most popular of the glass transition, the mosaic or RFOT [73] description[6] tries to incorporate the activated processes into the generalized-spin-glass model:

- It is assumed that for infinitely slow cooling the supercooled liquid would undergo a glass transition at a Kauzmann temperature T_K.
- This transition is supposed to have the same characteristics as that for the $p \geq 3$ generalized spin models, i.e.
  - it is first-order (discontinuous)
  - there is a low-temperature ground state
- The liquid for $T > T_K$ is supposed to consist of patches in a mosaic-like fashion
- These patches have a surface tension like crystallites, which provide the barriers for thermal activation.
- As the temperature passes $T_d \approx T_c$ from above, the dynamics crosses from saddle-dominated to valley-dominated, each valley corresponding to a different state in the replica-spinglass theory.
- Going from T_d to T_K the patches increase like in the Adam-Gibbs theory, corresponding to a decreasing configurational entropy.

5.8 Summary

Experimental features of the glass transition:

(1) Super-Arrhenius T dependence of the viscosity

(2) Step-like temperature dependence of spec. heat and compressibility

(3) Two-step relaxation

(4) Fractal relaxational time dependence

(5) Cross-over from non-activated to activated relaxation

(6) Dynamic heterogeneity in the activated regime

In the table below we show, which of the models/theories accounts for these features. The mosaic-RFOT addresses all these features, but unfortulately, whithout rigor.

	(1)	(2)	(3)	(4)	(5)	(6)
Adam-Gibbs	x					
Mode-Coupling	x	x	x	x		
Dynamic facilitation	x					
Generalized spinglass			x	x	x	
Mosaic (RFOT)	x	x	x	x	x	x

[6] I don't use the word "theory" myself, because the approach is – for my taste – too much based on hand-waving

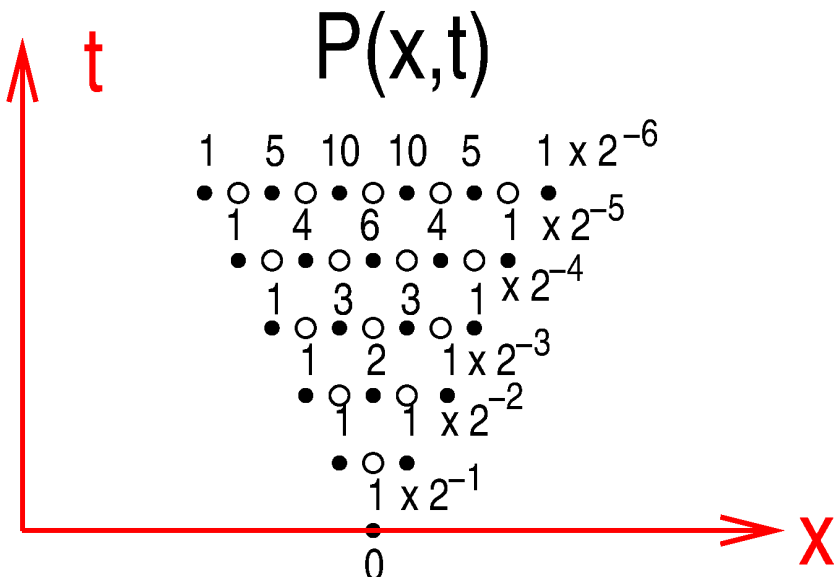

Figure 52: Pascal's triangle for a 1d random walk. The number of ways a time-space point can be reached from the bottom is given by Pascal's algorithm, i.e. each number is the sum of the two numbers underneath.

6 Diffusion and electric conduction in glasses

6.1 Random walk on a lattice and the diffusion equation

The motion of a Brownian particle can be visualized by that of a "random walker", e.g. by a drunken person, who changes its direction at random after every step. The statistics of such a motion can be easily worked out on a lattice:

- one-dimensional lattice with lattice constant a.
- The time steps are called τ.
- The propabilities to walk to the left or to the right are

$$P(x = a, t = \tau) = P(x = -a, t = \tau) = \frac{1}{2} \tag{6.1}$$

- The probabilities for the νth time step are $(1/2)^\nu$ times the number of ways one can reach the site $x_n = na$ on the triangle:

$$P(x_n, \nu\tau) = \left(\frac{1}{2}\right)^\nu \binom{\nu}{k_{n,\nu}} \qquad k_{n,\nu} = \left[\frac{1}{2}(n+\nu)\right], \tag{6.2}$$

where

$$\binom{\nu}{k} = \frac{\nu!}{k!(\nu-k)!} \tag{6.3}$$

is the binomial coefficient and $[x]$ is the smallest integer κ with $\kappa \geq x$. It is worth wile to note that at an even/odd time step ν only even/odd random walk sites x_n can be reached.

We consider now the recursion formula for the binomial coefficients

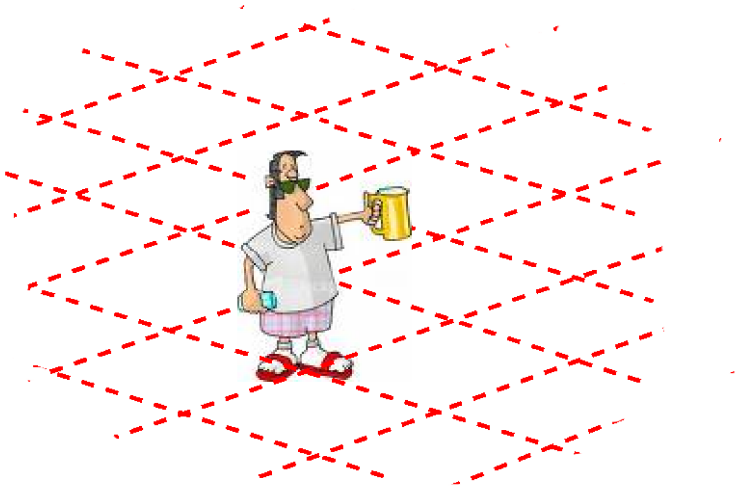

Figure 53: A random walker on a two-dimensional lattice

$$
\begin{aligned}
\binom{\nu+1}{k} &= \frac{(\nu+1)!}{k!(\nu+1-k)!} = \frac{\nu!}{k!(\nu+1-k)!}(\nu+1-k+k) \\
&= \frac{\nu!}{k!(\nu+1-k)!}(\nu+1-k) + \frac{\nu!}{k!(\nu+1-k)!}k \\
&= \frac{\nu!}{k!(\nu-k)!} + \frac{\nu!}{(k-1)!(\nu+1-k)!} \\
&= \binom{\nu}{k} + \binom{\nu}{k-1} \qquad (6.4)
\end{aligned}
$$

We re-write this recursion formula with the help of the probabilities $P(nx, \nu\tau)$:

$$
\begin{aligned}
P(x_n, t+\tau) &= \left(\frac{1}{2}\right)^{\nu+1} \binom{\nu+1}{k_{n,[\nu+1]}} \\
&= \frac{1}{2}\left(\frac{1}{2}\right)^{\nu} \left(\binom{\nu}{k_{n,[\nu+1]}} + \binom{\nu}{k_{n,[\nu+1]}-1} \right) \\
&= \frac{1}{2}P(x_{n+1}, t) + \frac{1}{2}P(x_{n-1}, t) \qquad (6.5)
\end{aligned}
$$

This can be re-written as

$$
\begin{aligned}
\frac{P(x_n, t+\tau) - P(x,t)}{\tau} &= W\Big(P(x_n+a) + P(x_n-a,t) - 2P(x,t)\Big) \\
&= D\left(\frac{P(x_n+a) + P(x_n-a,t) - 2P(x,t)}{a^2}\right) \qquad (6.6)
\end{aligned}
$$

with

$$
W = \frac{1}{2\tau} \quad \text{and} \quad D = Wa^2 = \frac{a^2}{2\tau} \qquad (6.7)
$$

From the first line we obtain at time scales $t \ll \tau$

$$\frac{\partial}{\partial t} P(x_n, t) = W\Big(P(x_n + a) + P(x_n - a, t) - 2P(x, t)\Big) \tag{6.8}$$

This is a master equation for a continuous-time random walk. We shall come back to the master equation when we shall consider disordered systems.

We now go over not only to to a large time scale, but also to a large space scale, i.e. we take now the double limit $\tau \to 0$ and $a \to 0$ keeping the ratio $D = a^2/2\tau$ fixed. This leads to

$$\frac{\partial P(x, t)}{\partial t} = D \frac{\partial^2}{\partial x^2} P(x, t) \tag{6.9}$$

This is the equation of motion for one-dimensional diffusion

6.1.1 Generalization to three dimensions

The three-dimensional versions of the master equation and the diffusion equation are just the superposition of the motion in x- y- and z direction:

$$\frac{\partial}{\partial t} P(\mathbf{r}_n, t) = \sum_{m = \text{n.N. of } \mathbf{r}_n} W\Big(P(\mathbf{r}_m, t - P(\mathbf{r}_n, t)\Big) \tag{6.10}$$

where n.N. means "nearest neighbour".

The diffusion equation is in three dimensions

$$\frac{\partial}{\partial t} P(\mathbf{r}, t) = D\, \nabla^2 P(\mathbf{r}, t) \tag{6.11}$$

The probability density $P(x, t)$ can also be re-interpreted as a real density of diffusing carriers,

$$P(\mathbf{r}, t) = \rho(\mathbf{r}, t)\,,$$

which is related to the current density $\mathbf{j}(\mathbf{r}, t)$ by

- the continuity equation

$$\frac{\partial}{\partial t} \rho(\mathbf{r}, t) + \nabla \mathbf{j}(\mathbf{r}, t) = 0 \tag{6.12}$$

- Combined with Fick's law

$$\mathbf{j}(\mathbf{r}, t) = -D \nabla \rho(\mathbf{r}, t) \tag{6.13}$$

- we obtain again the diffusion equation (6.11).

6.1.2 Solution of the diffusion equation by Laplace and Fourier transform

A spatial Fourier transform of (6.11) gives

$$\frac{\partial}{\partial t}P(\mathbf{q},t) = -Dq^2\,P(\mathbf{q},t) \tag{6.14}$$

Now we make the Laplace transform:

$$s\,P(\mathbf{q},s) - P(\mathbf{q},t{=}0) = -Dq^2\,P(\mathbf{q},s) \tag{6.15}$$

which gives the solution

$$P(\mathbf{q},s) = \frac{P(\mathbf{q},t{=}0)}{s+Dq^2} = P(\mathbf{q},t{=}0)G(\mathbf{q},s) \tag{6.16}$$

with

$$\tag{6.17}$$

Because

$$\mathcal{L}\{e^{-\lambda t}\} = \frac{1}{s+\lambda}$$

we obtain

$$P(\mathbf{q},t) = P(\mathbf{q},t{=}0)e^{-Dq^2} = P(\mathbf{q},t{=}0)G(\mathbf{q},t) \tag{6.18}$$

Now we use the convolution theorem for the spatial Fourier transform to get the solution

$$P(\mathbf{r},t) = \int d^3\tilde{\mathbf{r}}\,P(\tilde{\mathbf{r}},t{=}0)G(\mathbf{r},\tilde{\mathbf{r}},t) \tag{6.19}$$

with

$$G(\mathbf{r}_1,\mathbf{r}_2,t) = G(\underbrace{\mathbf{r}_1-\mathbf{r}_2}_{\mathbf{r}},t) = \frac{1}{(2\pi)^3}\int_{-\infty}^{\infty} d^3\mathbf{q}\,e^{-Dq^2} = \frac{1}{(\sqrt{4\pi Dt})^3}e^{-(\mathbf{r})^2/4Dt} \tag{6.20}$$

- $G(\mathbf{r}_1,\mathbf{r}_2,t)$ is the Green's function, which obeys the inhomogeneous diffusion equation

  $$\left(\frac{\partial}{\partial t} - D\nabla^2_{\mathbf{r}_1}\right)G(\mathbf{r}_1,\mathbf{r}_2,t) = \delta(\mathbf{r}_1-\mathbf{r}_2)\delta(t) \tag{6.21}$$

  $G(\mathbf{r},t) \equiv P_0(\mathbf{r},t)$ is the propagator, which gives the probability for a random walker to appear at $\mathbf{r}$ at time t if it started initially at the origin $\mathbf{r}=\mathbf{0}$, and is therefore also called propagator.

6.1.3 Mean-squared distance

The mean-squared distance walked by the particle can be calculated as follows

$$\begin{aligned}\overline{\Delta\mathbf{r}^2}(t) &= \overline{\big(\underbrace{\mathbf{r}_1-\mathbf{r}_2}_{\mathbf{r}}\big)^2} = \int_{-\infty}^{\infty} d^3\mathbf{r}r^2G(\mathbf{r},t) \qquad (6.22)\\ &= \int_{-\infty}^{\infty}dx\int_{-\infty}^{\infty}dy\int_{-\infty}^{\infty}dz(x^2+y^2+z^2) = \frac{1}{(\sqrt{4\pi Dt})^3}e^{-(x^2+y^2+z^2)^2/4Dt}\\ &= 6Dt\end{aligned}$$

Here we have used the identity for the variance σ^2 of a Gaussian

$$\int_{-\infty}^{\infty} dx x^2 \frac{1}{\sigma\sqrt{2\pi}} e^{\frac{1}{2}r^2/\sigma^2} = \sigma^2 \tag{6.23}$$

6.2 AC conduction and velocity autocorrelation

6.2.1 Relation between velocity autocorrelation function and mean-square distance

The distance walked by a random walker and its velocity are related by

$$\mathbf{v}(t) = \dot{\mathbf{r}}(t) \quad \Rightarrow \quad \Delta\mathbf{r}(t) = \mathbf{r}(t) - \mathbf{r}(0) = \int_0^t \mathbf{v}(t) \tag{6.24}$$

We now perform the following integration by part

$$\int_0^t d\tilde{t}\, \Delta\mathbf{r}(t) \cdot \mathbf{v}(t) = \Delta\mathbf{r}^2(t) - \int_0^t d\tilde{t}\, \mathbf{v}(t) \cdot \Delta\mathbf{r}(t) \tag{6.25}$$

$\Rightarrow$

$$\Delta\mathbf{r}^2(t) = 2\int_0^t d\tilde{t}\, \mathbf{v}(t) \cdot \Delta\mathbf{r}(t) = 2\int_0^t d\tilde{t} \int_0^{\tilde{t}} d\tilde{\tilde{t}}\, \mathbf{v}(\tilde{t}) \cdot \mathbf{v}(\tilde{\tilde{t}}) \tag{6.26}$$

$\Rightarrow$

$$\begin{aligned}
\overline{\Delta\mathbf{r}^2(t)} &= 2\int_0^t d\tilde{t} \int_0^{\tilde{t}} d\tilde{\tilde{t}}\, \overline{\mathbf{v}(\tilde{t}) \cdot \mathbf{v}(\tilde{\tilde{t}})} \\
&= 6\int_0^t d\tilde{t} \int_0^{\tilde{t}} d\tilde{\tilde{t}}\, \overline{v_x(\tilde{t}) v_x(\tilde{\tilde{t}})} \\
&= 6\int_0^t d\tilde{t} \int_0^{\tilde{t}} d\tilde{\tilde{t}} Z(\underbrace{\tilde{t} - \tilde{\tilde{t}}}_{\tau}) \\
&= 6\int_0^t d\tilde{t} \int_0^{\tilde{t}} d\tau\, Z(\tau)
\end{aligned} \tag{6.27}$$

$\Rightarrow$

$$\boxed{Z(t) = \overline{v_x(t+t_0) v_x(t_0)} = \frac{1}{6}\frac{d^2}{dt^2}\overline{\Delta\mathbf{r}^2}(t)\,,} \tag{6.28}$$

where we have used

$$\overline{v_x(t+t_0) v_x(t_0)} = \overline{v_y(t+t_0) v_y(t_0)} = \overline{v_z(t+t_0) v_z(t_0)} \tag{6.29}$$

- This relation holds for any $\overline{\Delta\mathbf{r}^2}(t)$.

  Let us insert the mean distance walked of the random walk: into Eq. (6.28):

  $$\overline{\Delta\mathbf{r}^2}(t) = 6Dt \quad \Rightarrow \quad Z(t) = 0$$

$\Rightarrow$ The velocity autocorrelation of a random is zero, or: the random walk has uncorrelated velocities.

Now let us assume a random walk with initially correlated velocities. This may be a random flight of a fly with a mean constant velocity v_0, with randomly changed direction. (A similar model underlies the kinetic theory of gases, where the molecules are supposed to have a mean velocities and the flight direction is changed after a collision.)

$$Z(t) = v_0^2 e^{-t/\tau_c} \tag{6.30}$$

where τ_c is the correlation time. Inserting this into Eq. (6.27) we get

$$\begin{aligned} \overline{\Delta \mathbf{r}^2}(t) &= 6v_0^2 \int_0^t d\tilde{t} \int_0^{\tilde{t}} d\tau e^{-t/\tau_c} = 6v_0^2 \int_0^t d\tilde{t} \tau_c \left(1 - e^{-\tilde{t}/\tau_c}\right) \\ &= 6v_0^2 \left[\tau_c t + \tau_c^2 \left(e^{-t/\tau_c} - 1\right)\right] \end{aligned} \tag{6.31}$$

- For times $t \gg \tau_c$ we get a random walk law with a diffusion coefficient $D = v_0^2 \tau$.
- For small times $t \ll \tau_c$ we can expand the exponential to obtain the ballistic law

$$\overline{\Delta \mathbf{r}^2}(t) = 6v_0^2 \left[\tau_c t + \tau_c^2 \left(-\frac{t}{\tau_c} + \frac{1}{2}\left(\frac{t}{\tau_c}\right)^2 \right)\right] = 3\left(\frac{v_0}{\tau_c}\right)^2 t^2 \tag{6.32}$$

6.2.2 Kubo formula and the Nernst-Einstein relation for the conductivity

Taking the first time derivative of the mean-square distance of Eq. (6.27) we obtain

$$\frac{d}{dt}\overline{\Delta \mathbf{r}^2}(t) = 6 \int_0^t d\tau Z(\tau) \tag{6.33}$$

For large time $t \to \infty$ this must become equal to $6D$. Therefore we obtain the Kubo formula for the diffusivity

$$\boxed{D = \int_0^\infty d\tau Z(\tau)} \tag{6.34}$$

We may generalize this for the Laplace transform of $Z(t)$

$$\boxed{D(s) = \int_0^\infty d\tau e^{-s\tau} Z(\tau)} \tag{6.35}$$

- The Laplace transform of the velocity autocorrelation function may be iterpreted as a generalized, complex, frequency-dependent diffusivity.
- This quantity is related to the dynamic conductivity $\sigma(\omega)$ by the Nernst-Einstein relation

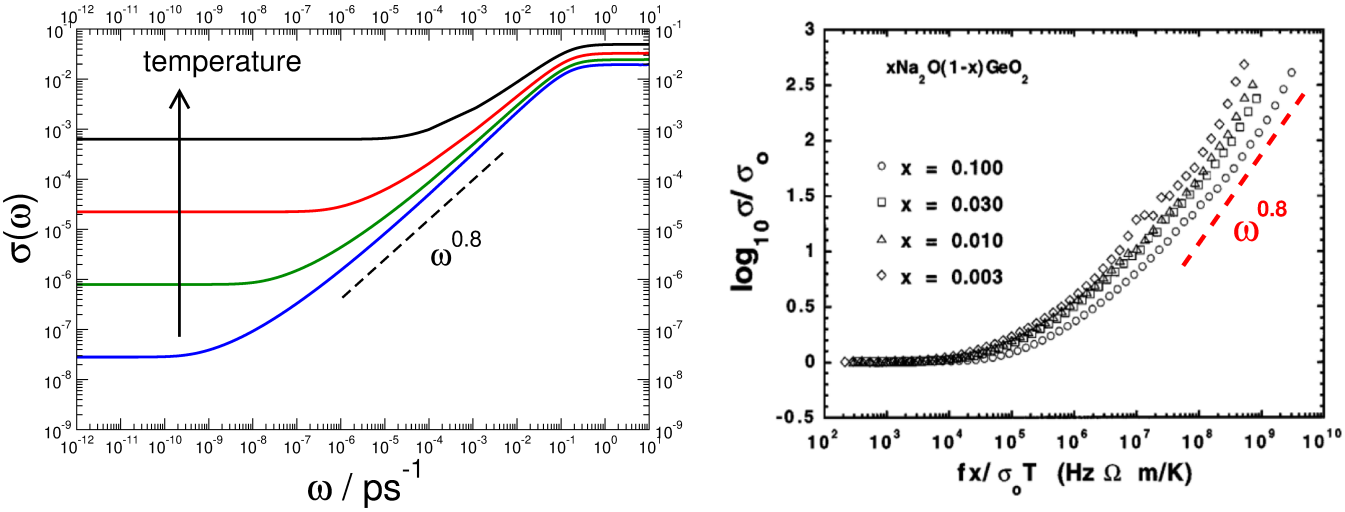

Figure 54: Left: sketch of the typical behaviour of the AC conductivity in glasses and amorphous semiconductors as a function of frequency and temperature.
Right: Measured AC conductivity of $(Na_2O)_x(GeO_2)_{1-x}$ glass glass as a function of frequency for different compositions x. The data have been divided by the DC conductivity $\sigma(0)$. The frequency has also been scaled by $\sigma(0)$.

$$\sigma(\omega) = \sigma'(\omega) + i\sigma''(\omega) = q^2 \frac{\partial n}{\partial \mu} D(s)\Big|_{s=\epsilon - i\omega}, \tag{6.36}$$

The real part, $\sigma'(\omega)$ is the AC conductivity, n is the number density of carriers of charge q, and μ is the chemical potential

- For degenerate statistics (electrons) we have

$$\frac{\partial n}{\partial \mu} = N(E_F)\,, \tag{6.37}$$

where $N(E_F)$ is the electronic density of states at the Fermi energy E_f.

- For non-degenerate, classical statistics (ions) we have

$$\frac{\partial n}{\partial \mu} = \frac{n}{k_B T} \tag{6.38}$$

For electronic hopping transport in amorphous semiconductors (e. G. OLEDs) one uses degenerate statistics, for ionic transport in glasses one uses classical statistics.

6.2.3 AC conductivity of amorphous solids and anomalous diffusion

- It has been noted quite a time ago [74, 75] that both in amorphous semiconductors, as well as in ionically conducting glasses, beyond a characteristic frequency ω^* the conductivity exhibits a strong frequency dependence, which may be characterized as

$$\sigma'(\omega) \sim \omega^{\nu} \tag{6.39}$$

with $0 \leq \nu \leq 1$.

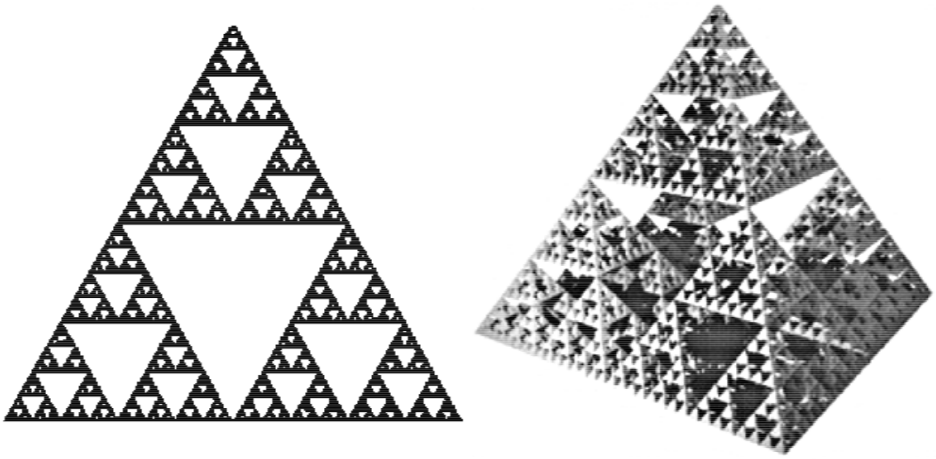

Figure 55: Left: Sierpinski triangle, Right: Sierpinski pyramide

In the left panel of Fig. 54 we show a schematic sketch of the typical frequency and temperature of the conductivity. In the right panel we show the conductivity vx. frequency for various compositions x of $(Na_2O)_x(GeO_2)_{1-x}$ glass in a universal plot, i.e. the conductivity and the frequency has been re-scaled in such a way that the data fall approximately on top of each other.

- The data show a cross-over from the DC (frequency-independent) behaviour to a ω^ν behaviour.

We now show that such a frequency dependence can be characterized as anomalous diffusion.

- Anomalous diffusion is characterized by a mean square distance walked, which increases sublinearly with time:

$$\overline{\Delta \mathbf{r}^2}(t) \sim t^\alpha \quad 0 \leq \alpha \leq 1 \tag{6.40}$$

We recall relation (6.28) between the velocity autocorrelation and the mean-square distance:

$$Z(t) \sim \frac{d^2}{dt^2}\overline{\Delta \mathbf{r}^2}(t) \sim t^{\alpha-2}$$

The Laplace transform of this is

$$\begin{aligned} Z(s) &= D(s) = \int_0^\infty dt e^{-st} t^{\alpha-2} \\ Z(s) &= D(s) = s^{1-\alpha} \underbrace{\int_0^\infty d(st) e^{-st} t^{\alpha-2}}_{\Gamma(\alpha-1)} \end{aligned} \tag{6.41}$$

This leads to $\sigma'(\omega) \sim \omega^\nu$ with $\nu = 1 - \alpha$

6.3 Models for anomalous diffusion

6.3.1 Diffusion on a fractal

We discussed in section 3.2 the scaling properties of fractals, i.e. self-similar objects. We said that the mass M of a fractal object scales in an odd way

with the length scale L

$$M(L) \sim L^{d_f}$$

, where d_f is the fractal dimension and is a real number smaller than the imbedding dimension d.

Alexander and Orbach [76, 77] and Rammal [78] showed that another time-scale related scaling exists, which is governed by the spectral dimension d_s with

$$d_s < d_f < d\,. \tag{6.42}$$

- In fractals one has always anomalous diffusion with

$$\overline{\Delta \mathbf{r}^2}(t) \sim t^{\alpha} \qquad\qquad \alpha = \frac{d_s}{d_f} \tag{6.43}$$

	d_s	d_f	α	$\nu = 1-\alpha$	d
Percolation	1.33	1.896	0.7	0.3	2
Percolation	1.33	2.48	0.54	0.46	3
Sierpinski triangle	1.364	1.584	0.86	0.14	2
Sierpinski pyramide	1.547	2	0.774	0.22	3

We observe that the AC conductivity exponents ν of the fractals are rather low, so models in terms of fractal ionic (or electronic) channels inside of the glassy structure do not appear to be appropriate.

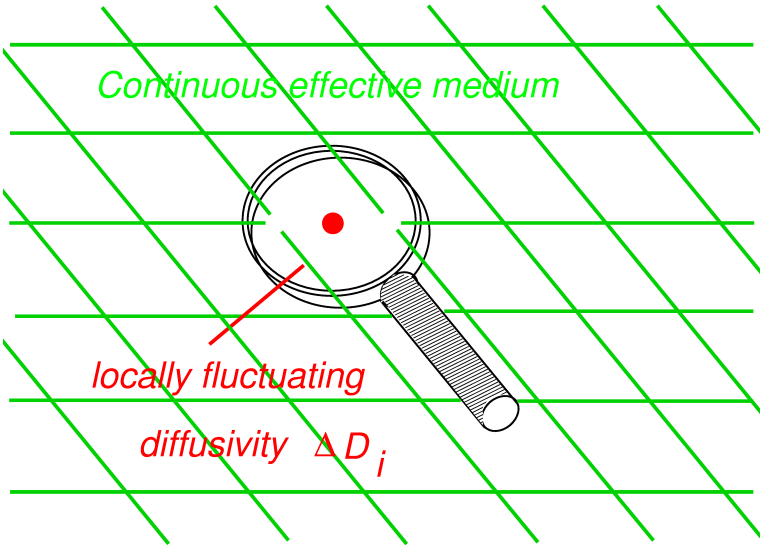

Figure 56: Visualization of the CPA procedure.

6.3.2 Spatially fluctuating diffusivity and the coherent-potential approximation (CPA)

- Model We assume, that due to the structural disorder the diffusivity exhibit spatial variations (fluctuations), which can be described by a stochastic diffusion equation

$$\frac{d}{dt}\rho(\mathbf{r},t) = \nabla \cdot D(\mathbf{r}) \cdot \nabla\rho(\mathbf{r},t) \tag{6.44}$$

  subject to a given statistics of $D(\mathbf{r})$

- to simplify the model we consider a coarse-grained patchwork of regions in the space inside of which $D(\mathbf{r})$ is constant

- From patch to patch we assume that the local diffusivity $D(\mathbf{r}_i)$ (rr_i is the midpoint of the patch) take different values.

- More specifically we consider spatially varying activation energies E_i according to

$$D(\mathbf{r}_i) \equiv D_i = D_0 e^{-E_i/k_B T} \tag{6.45}$$

  with a given distribution $P(E_i)$.

The solution of this model can be obtained by means of the coherent-potential approximation (CPA) which converts $D(\mathbf{r}_i)$ to the complex, frequency-dependent function $D(\omega)$, which can be inserted into the Laplace-transformed diffusion equation of the effective medium

$$\mathcal{L}\left\{\frac{d}{dt}G(\mathbf{r},t)\right\}_s = sG(\mathbf{r},s) - \nabla^2 D(s)G(\mathbf{r},s) = \delta(\mathbf{r}) \tag{6.46}$$

which is solved in Fourier space by

$$G(\mathbf{q},s) = \frac{1}{s + q^2 D(s)} \tag{6.47}$$

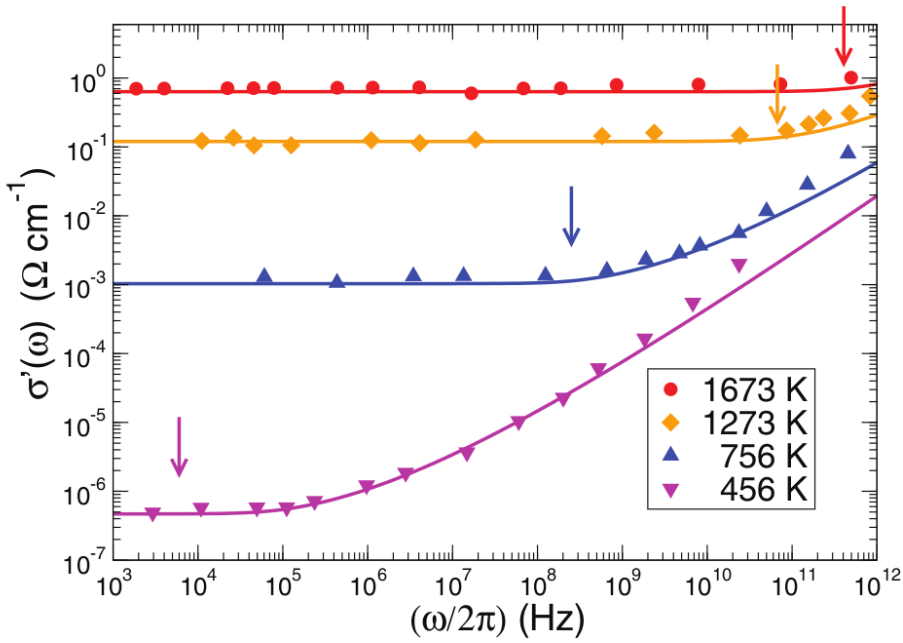

Figure 57: CPA calculation of the AC conductivity using a constant activation energy distribution $P(E)$, compared with data on Sodium-Trisilicate glass $Na_2O{\cdot}3SiO_2$, compiled by Wong and Angell [75]. The arrows mark the cross-over from DC to AC behaviour, i.e. from normal to anomalous diffusion.

- We consider now a single patch inside our patchwork (see Fig. 56) and postulate that on the average replacement of $D(\omega)$ with $D(\mathbf{r})$ should have no effect.

- This leads to the CPA equation (see [79, 80] for the CPA for electrons in a random potential and [81, 82, 83, 84] for the diffusion problem, and the Appendix A.3 below):

$$\left\langle \frac{D_i - D(s)}{1 + \frac{1}{3}[D_i - D(s)]\Lambda(s)} \right\rangle = 0 \tag{6.48}$$

  Here $\langle \dots \rangle$ denotes an average over the distribution density $P(D_i)$ of the local diffusivities D_i or that of the local activation energies $P(E_i)$.

Eq. (6.48) is an implicit equation for the dynamic diffusivity $D(s)$, which can be solved iteratively with $P(D_i)$ or $P(E_i)$ as input.

The function $\Lambda(s)$ is related to the local dynamic susceptibility $\chi(s)$ as

$$\tilde{\chi}(s) = \frac{\nu}{k_B T}\chi(s) = \nu \int_{|\mathbf{q}|\le q_\xi} d^3\mathbf{q} \frac{D(s)q^2}{s + q^2 D(s)} = D(s)\Lambda(s) \tag{6.49}$$

ν is a normalization factor [84] in order to guarantee that the $\mathbf{q}$ integration over 1 with $|\mathbf{q}| < q_\xi$ equals 1 :

$$1 = \nu \int_{|\mathbf{q}|\le q_\xi} d^3\mathbf{q}\, 1 = 4\pi\nu \int_0^{q_\xi} dq q^2 = \frac{4}{3}\pi\nu q_\xi^3 \quad \Rightarrow \quad \nu = \frac{3}{4\pi q_\xi^3}\,. \tag{6.50}$$

The reduced susceptibility function $\tilde{\chi}(s))$ is now given by

$$\tilde{\chi}(s) = D(s)\Lambda(s) = \frac{3}{q_\xi^3}\int_0^{q_\xi} dq q^2 \frac{q^2 D(s)}{s + q^2 D(s)} \tag{6.51}$$

and we have

$$\tilde{\chi}(0) = D(0)\Lambda(0) = 1 \tag{6.52}$$

In Fig. 57 we have plotted the result of a CPA calculation with a distribution density

$$P(E) = \text{const. for } E \leq E_0 \tag{6.53}$$

We can see from the plot that this calculation accounds well to the AC conductivity data of $Na_2O{\cdot}3\ SiO_2$ [75] over 12 orders of magnitude and an extended temperature range.

6.3.3 DC conductivity, random resistor networks and percolation

The present paragraph is based on Refs. citekirkpatrick73,efros73,kohler13.

Instead of a locally fluctuating diffusivity $D(\mathbf{r})$ we consider a locally fluctuating conductivity, which obeys the equation

$$\mathbf{j}(\mathbf{r}) = \sigma(\mathbf{r})\nabla V(\mathbf{r}) \tag{6.54}$$

In the absence of local charges we have

$$\nabla \cdot \mathbf{j}(\mathbf{r}) = 0 = \nabla\sigma(\mathbf{r})\nabla V(\mathbf{r})\,. \tag{6.55}$$

We can discretize Eq. (6.55) on a cubic lattice with lattice constant a to obtain

$$0 = \sum_{j\,\text{n.N.of}\,i} g_{ij}[V_j - V_i] \tag{6.56}$$

These equations constitute Kirchhoff's equations of a random resistor network with local node voltages V_i and local conductances g_{ij} given by

$$g_{ij} \sim \sigma(\boldsymbol{\rho}_{ij}) \tag{6.57}$$

where $\boldsymbol{\rho}_{ij} = \frac{1}{2}\big[\mathbf{r}_i + \mathbf{r}_j\big]$ is the center of gravity between neighbouring sites $\mathbf{r}_i$ and $\mathbf{r}_j$.

We can also consider the DC diffusion equation with spatially fluctuating diffusivity $D(\mathbf{r})$

$$0 = \nabla \cdot D(\mathbf{r}) \cdot \nabla P(\mathbf{r}, \omega{=}0) \tag{6.58}$$

and discretize it on a cubic lattice

$$0 = \sum_{j\,\text{n.N.of}\,i} W_{ij}[P_j - P_i] \tag{6.59}$$

with

$$W_{ij} \sim D(\boldsymbol{\rho}_{ij}) \tag{6.60}$$

Certainly $\sigma(\mathbf{r})$ obeys the Nernst-Einstein relation

$$\sigma(\mathbf{r}) \sim D(\mathbf{r}) \tag{6.61}$$

so that we have in the same way

$$g_{ij} \sim W_{ij} \tag{6.62}$$

- The discretized local conductivities and local diffusivities constitute a random resistor network with local resistances

$$R_{ij} = \frac{1}{g_{ij}} \, .$$

Question:

- What is the resulting conductance of the random network, viz.
- What is the resulting conductivity of a glass with locally fluctuating conductances?

$$g_{ij} \sim e^{-E_{ij}/k_B T} \tag{6.63}$$

Some authors in the early time of the investigation of diffusion in glasses [85, 86] suggested to average over the local conductances, e.g. with a Gaussian distribution

$$\langle g \rangle \sim \int dE \frac{1}{\sqrt{2\pi}\gamma} e^{-\frac{1}{2\gamma}(E-E_0)^2} e^{-E/k_B T} = e^{-E_0/k_B T} e^{\frac{1}{2}\frac{\gamma}{[k_B T]^2}} \tag{6.64}$$

This would produce a non-Arrhenius temperature dependence, which is not observed in any ionically conducting glasses. Furthermore such an average over the individual conductance would correspond to a parralel equivalent circuit.

- In random resistor networks neither a parralel equivalent network nor a serial equivalent network is correct [87].
- Instead the current follows the proverbial path of least resistance.
- For exponentially fluctuating resistances the resistance of the entire network can be obtained by the following

Percolation construction [88, 89]:

1. We remove all resistances from the network and sort them according to their values

$$R_{ij} = R_0 e^{E_{ij/k_B T}} \, ;$$

2. we start soldering the smallest resistances into the network, corresponding to small values of E_{ij} below a threshold value E^*;
3. we increase E^* and solder the corresponding resistances into the network;

4. at a certain value of $E^* = E_c$ a current will pass through the network. The resistance of the network is now

$$R = R_c = \frac{1}{g_c} = R_0 e^{E_c/k_B T} \tag{6.65}$$

5. Now we solder the remaining higher resistances into the network. The resistance remains the same, because the current takes the path of lowest resistance.

- Notice that the temperature dependence of the conductance, and hence of the conductivity of the sample, follows an Arrhenius law

$$\sigma(T) \sim e^{-E_c/k_B T} \tag{6.66}$$

independently on the form of the distribution.

6.4 CPA and percolation

We re-write our CPA equation (6.48) as follows

$$0 = \left\langle \frac{D_i - D(s)}{1 + \frac{1}{3}[D_i - D(s)]\Lambda(s)} \right\rangle \tag{6.67}$$

$$\Rightarrow$$

$$\begin{aligned} D(s) \left\langle \frac{1}{1 + \frac{1}{3}[D_i - D(s)]\Lambda(s)} \right\rangle &= \left\langle \frac{D_i}{1 + \frac{1}{3}[D_i - D(s)]\Lambda(s)} \right\rangle \\ &= D(s) \left\langle \frac{1 + \frac{1}{3}[D_i - D(s)]\Lambda(s) - \frac{1}{3}[D_i - D(s)]\Lambda(s)}{1 + \frac{1}{3}[D_i - D(s)]\Lambda(s)} \right\rangle \\ &= D(s) - \frac{1}{3}\Lambda(s) \underbrace{\left\langle \frac{D_i - D(s)}{1 + \frac{1}{3}[D_i - D(s)]\Lambda(s)} \right\rangle}_{=0} = D(s) \end{aligned} \tag{6.68}$$

We obtain

$$D(s) = \left\langle \frac{D_i}{1 + \frac{1}{3}[D_i - D(s)]\Lambda(s)} \right\rangle \tag{6.69}$$

and, by comparing the first line of Eq. (6.68) with Eq. (6.69)

$$1 = \left\langle \frac{1}{1 + \frac{1}{3}[D_i - D(s)]\Lambda(s)} \right\rangle \tag{6.70}$$

We consider now a system, in which a concentration p of the local diffusies have a certain value D_0 and the rest of the diffusivities (with concentration $1 - p$) are zero:

$$P(D_i) = p\delta(D_i - D_0) + (1 - p)\delta(D_i) \tag{6.71}$$

From the CPA equation (6.69) we obtain for the DC diffusivity $D(0) = D$,

$$D(0) = \frac{pD_0}{1 + \frac{1}{3}\left(\frac{D_0 - D}{D}\right)} \tag{6.72}$$

where we have used relation (6.52) $\Lambda(0) = 1/D$. We can solve this equation for D to obtain

$$D = \frac{3}{2} D_0 \left(p - \frac{1}{3} \right) = \frac{3}{2} D_0 \left(p - p_c \right) \tag{6.73}$$

- We therefore identify the factor $\frac{1}{3}$ in the CPA equations (6.48), (6.69), or (6.70) as percolation threshold given by the CPA, and, from now on use p_c instead of $\frac{1}{3}$ in these equations.

  We now consider activated local diffusivities

$$D_i = D_0 e^{-E_i/k_B T} \tag{6.74}$$

  Then the CPA equation (6.69) for the DC diffusivity becomes (setting $E_i = E$)

$$D = \int_0^\infty dE P(E) \frac{D_0 e^{-E/k_B T}}{1 + p_c \left(\frac{D_0}{D} e^{-E/k_B T} - 1 \right)} \tag{6.75}$$

  Multiplying both sides with p_c/D we get

$$p_c = \int_0^\infty dE P(E) \frac{1}{(1 - p_c) \frac{D}{D_0} e^{E/k_B T} + 1} \tag{6.76}$$

  We now parametrize the DC diffusivity as

$$D = \frac{1}{1 - p_c} D_0 e^{-E_c/k_B T} \tag{6.77}$$

  and obtain for the CPA equation

$$p_c = \int_0^\infty dE P(E) \frac{1}{e^{[E - E_c]/k_B T} + 1} \tag{6.78}$$

  For temperatures much smaller than typical values of E the Fermi function in Eq. (6.78) becomes a step function and we get

$$p_c = \int_0^{E_c} dE P(E) \tag{6.79}$$

- This is a mathematical equivalent to the percolation construction: only the conductances with $E \leq E_c$ are relevant, and the DC diffusivity is of Arrhenius type independent of $P(E)$.

Figure 58: Albert Einstein and Peter Debye

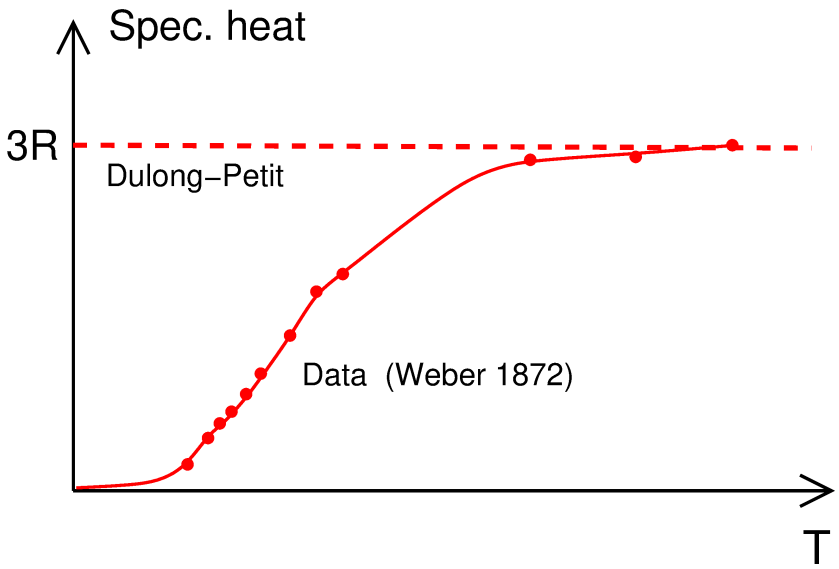

Figure 59: Specific heat of Diamond (Weber, 1872) [90].

7 Specific Heat and Phonons in solids

7.1 Historical introduction: Einstein and Debye model for the specific heat

Until Einstein's time at the turn of the previous centuries the only theory for the specific heat was the explanation of the law of Dulong and Petit in terms of the equipartition theorem

- Every degree of freedom, which appears quadratically in the Hamiltonian, contributes $\frac{1}{2}k_BT$ to the thermal energy density.

  This gives Dulong and Petit's value of $\frac{6}{2}R = 3R$ (where R is the gas constant) to the molar specific heat, where the number 6 comes from 3 displacement degrees of freedom and 3 momentum degrees of freedom.

In the second half of the 19th century it became clear that this law fails badly at low temperatures, see the measurement of Weber (1872) [90], Einstein's teacher in experimental physics at the ETH Zürich.

After the advent of Planck's quantum interpretation of the the law of black-body radiation, Einstein generalized the corresponding statistics to the now called Bose-Einstein statistics. He then imagined [91] a solid body as a collection of a large number individual,independent harmonic oscillators (now called Einstein oscillators) with essentially the same oscillator frequency ω. The thermal energy per oscillator is then

$$\frac{E}{N} = \frac{\hbar\omega}{e^{\hbar\omega/k_BT} - 1} \tag{7.1}$$

and the corresponding specific heat

$$C(T) = \frac{d}{dT}\frac{E}{N} = k_B \left(\frac{\hbar\omega}{k_BT}\right)^2 \frac{e^{\hbar\omega/k_BT}}{(e^{\hbar\omega/k_BT} - 1)^2} \tag{7.2}$$

- This function gave a rather nice overall fit of the data.
- This provided, in addition to Planck's explanation of the radiation law the second explanation of a previously not understood phenomenenon in terms of quantum theory.

Later it became clear that at very low temperatures Einstein's formula does not explain the specific heat data well. Instead of an exponential increase, as predicted by Eq. (7.2), a much less steep increase was experimentally observed.

- Debye (1912) [92] realized that the vibrations in a solid are not individual oscillations, but, instead, elastic waves, known from elasticity theory [92] realized that the vibrations in a solid are not individual oscillations, but, instead, elastic waves, known from elasticity theory
- These waves may be enumerated by their wave vector $\mathbf{k}_\nu$ and their three polarizations ν: 2 transverse and 1 longitudinal ones.

The corresponding energy density of a solid reads

$$\frac{E}{N} = \frac{1}{N}\sum_{\nu=1}^{3}\sum_{\mathbf{k}} \frac{\hbar\omega_{\mathbf{k}}^{\nu}}{e^{\hbar\omega_{\mathbf{k}}^{\nu}/k_BT} - 1} \tag{7.3}$$

with the longitudingal L and transverse T dispersions ($\nu = L, T$)

$$\omega_L = v_L k \qquad \omega_T = v_T k \tag{7.4}$$

with $k = |\mathbf{k}|$.

We can re-write this expression by means of the density of states $g(\omega)$

$$g(\omega) = \frac{1}{3N}\sum_{\nu=1}^{3}\sum_{\mathbf{k}} \delta(\omega - \omega_{\mathbf{k}}^{\nu}) = \frac{1}{3}\Big(g_L(\omega) + 2g_T(\omega)\Big) \tag{7.5}$$

$$\frac{E}{N} = \int_0^\infty d\omega\, g(\omega) \frac{\hbar\omega}{e^{\hbar\omega/k_BT} - 1} \tag{7.6}$$

$$C(T) = \frac{d}{dT}\frac{E}{N} = k_B \int_0^\infty d\omega\, g(\omega) \left(\frac{\hbar\omega}{k_BT}\right)^2 \frac{e^{\hbar\omega/k_BT}}{(e^{\hbar\omega/k_BT} - 1)^2} \tag{7.7}$$

In three dimensions the $\mathbf{k}$ sum can be converted to an integral by the formula

$$\sum_{\mathbf{k}} \to \frac{V}{(2\pi)^3} \int d^3\mathbf{k} = \frac{V}{2\pi^2} \int_0^{k_D} dk k^2 \tag{7.8}$$

Here the upper cutoff k_D (Debye cutoff) is fixed by the condition that the number of waves must be equal to the number N of molecules

$$N = \frac{V}{2\pi^2} \int_0^{k_D} dk k^2 = \frac{V}{6\pi^2} k_D^3 \;\Rightarrow\; k_D = \left[6\pi N/V\right]^{1/3}. \tag{7.9}$$

The density of states (in three dimensions) of one polarizatio ν is obtained as

$$g_\nu(\omega) = \frac{V}{2N\pi^2} \int_0^{k_D} dk k^2 \delta(\omega - v_\nu k) = \frac{3}{(v_\nu k_D)^2}\omega^2 \tag{7.10}$$

The total density of states is then, according to Eqs. (A.71) and (7.10) given by

$$g(\omega) = \frac{3}{\omega_D^3}\omega^2 \quad \text{for} \quad \omega \le \omega_D \tag{7.11}$$

where

$$\omega_D = \left[\frac{1}{3}\left(\frac{1}{v_L^3} + \frac{2}{v_T}^3\right)\right]^{-1/3} \tag{7.12}$$

Inserting this into Debye's expression for the specific heat we obtain for temperatures $T \ll \theta_D = \hbar\omega_D/k_B$ (Debye temperature)

$$C(T) \sim T^3 \tag{7.13}$$

For $T > \theta_D$ Debye's formula predicts – in agreement with experiments – a cross-over to the Dulong-Petit value $3k_B$.

- This behavior is observed in all crystalline solids.

7.2 Phonons in glasses: Quantum vs. classical description

7.2.1 Phonons in crystals: SiO_2

In Fig. 60 we show the phonon dispersions $\omega_\nu(\mathbf{k})$ of a SiO_2 crystal (quartz), as determined by Bosak et al. (2012) [93], who combined inelastic X-ray scattering with ab-initio simulations. Starting from the Γ point ($\mathbf{k} = 0$) we see the emerging

- transverse and longitudinal acoustic phonon branches.

  In the upper energy region there are the

- optical modes, which are due to the molecules and atoms against each other.
- In the middle panel the vibrational density of states (VDOS) is plotted.

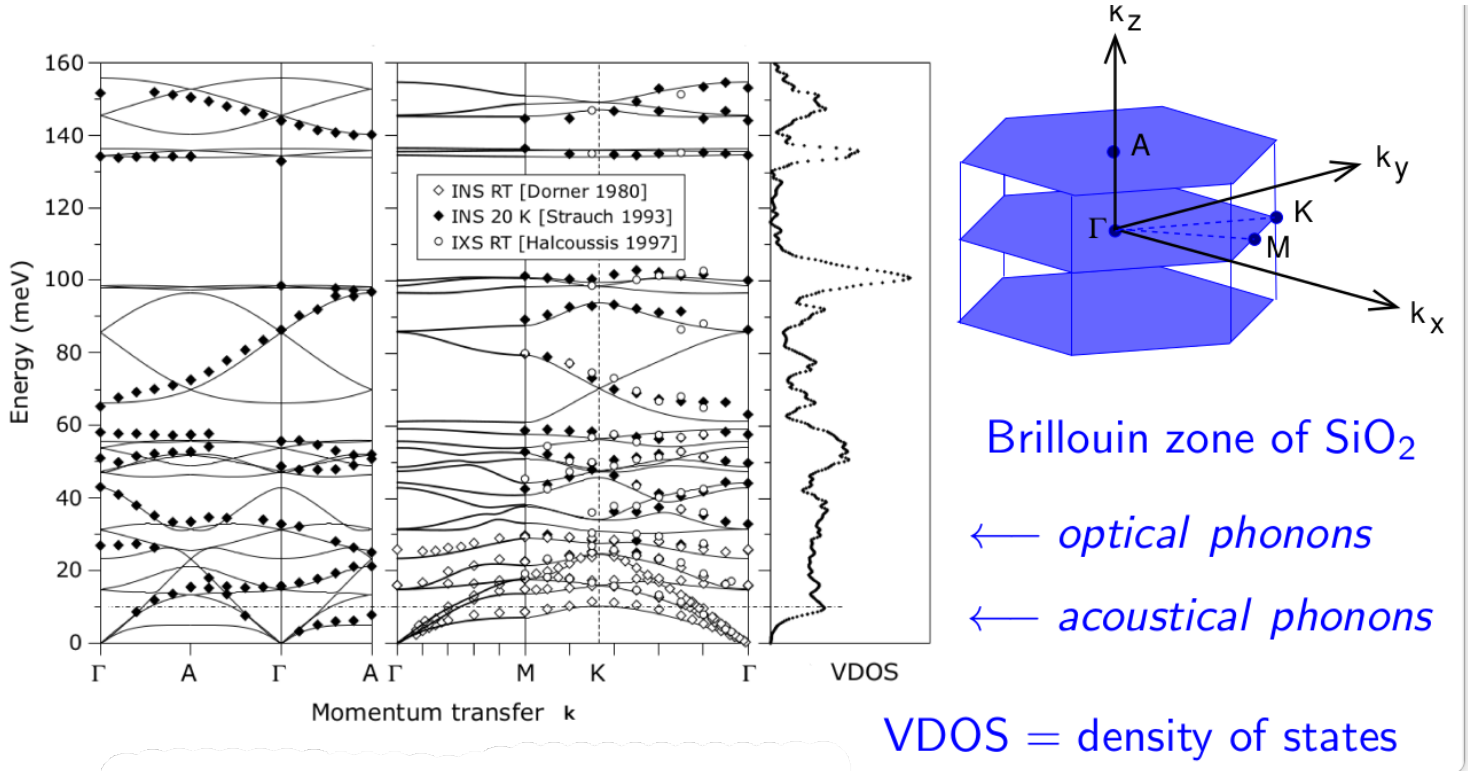

Figure 60: Left panel: Phonon dispersions $\omega_\nu(\mathbf{k})$ of crystalline SiO_2 (quartz), along different directions in the first Brillouin zone, which is depicted in the right panel [93]. Middle panel: vibrational density of states (VDOS).

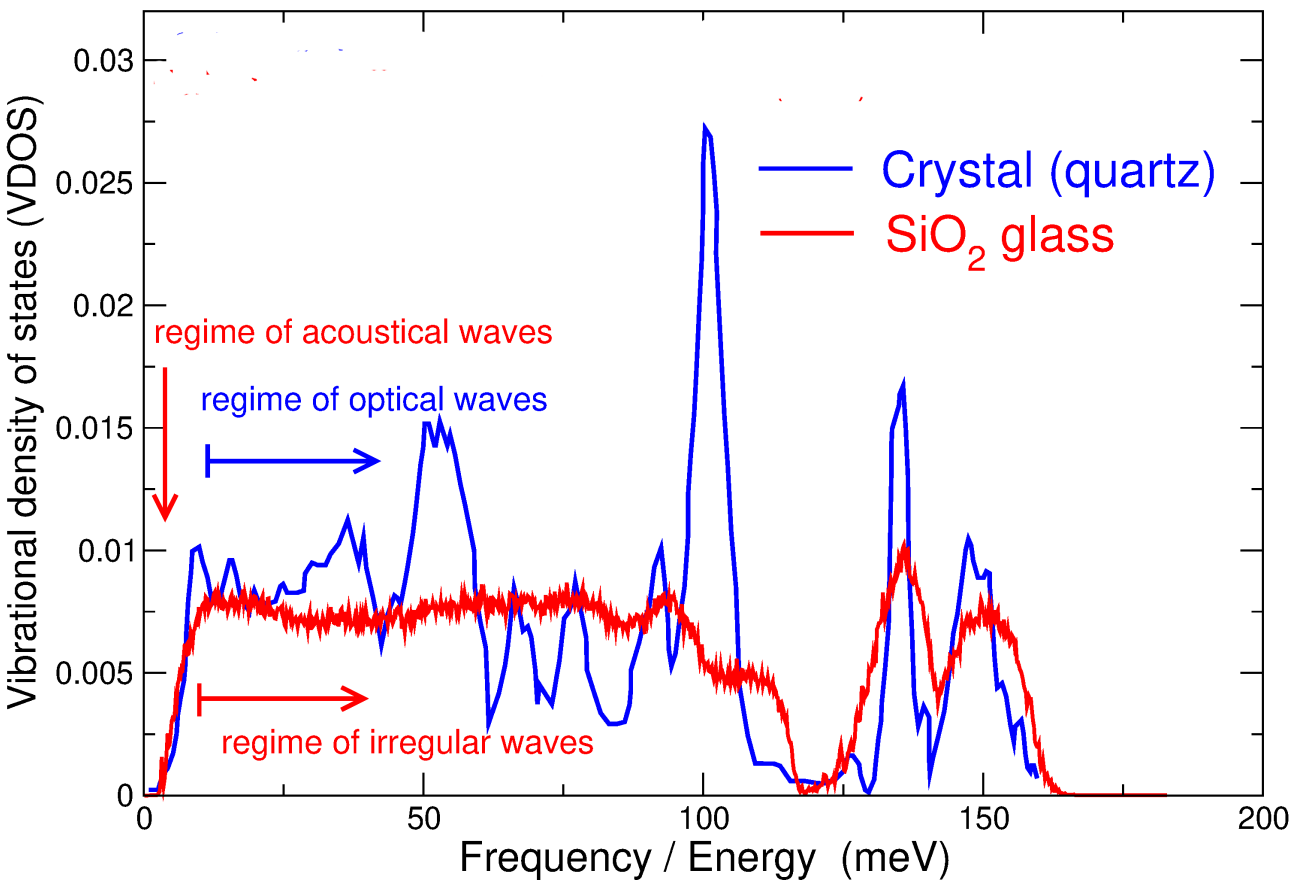

Figure 61: Density of states of crystalline [93] and glassy [94] SiO_2.

7.2.2 FAQ about phonons in glasses

- Do phonons exist in glasses?

  Yes! At low enough frequencies acoustical waves exist. Their quantized versions can be called phonons.

- Do optical phonons exist in glasses?

  No! Optical phonon dispersions appear in crystals with more than one atom in the unit cell. In glasses there is no lattice, no unit cell, etc.

- However, at high frequencies local vibrational modes do exist, e. g. stretching or bending modes of a molecule.

In Fig. 61 we show the density of states of crystalline and amorphous SiO_2. We see that the regime of acoustical waves is rather small. The spectrum of the crystal is dominated by the optical phonons.

- Understanding the frequency spectrum of the glass beyond the frequency regime of the acoustical waves will be done in the remainder of this lecture.

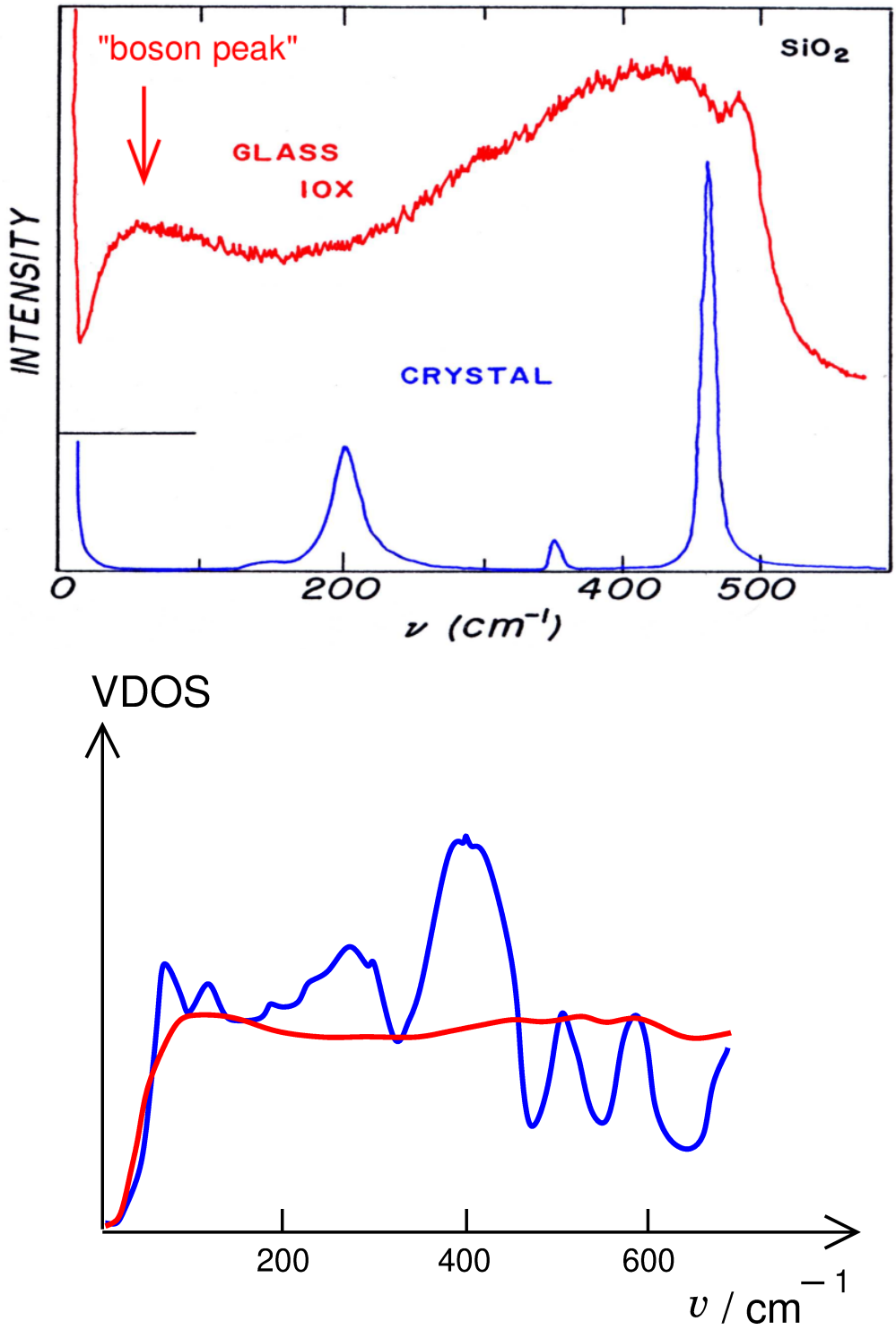

Figure 62: Top panel: Raman spectrum of crystalline (blue) and glassy (red) SiO_2. [95]. The arrow marks the boson peak.
Bottom panel: Low-frequency part of Fig. 61, using the Raman units ($\hbar\omega = h\nu$ =1 meV corresponds to $\nu/c = 80$ cm^{-1}).

8 Vibrational and Thermal anomalies in glasses

8.1 The boson peak

In Fig. 8.4 we compare the low-frequency part of the the density of states of Fig. 61 with the Raman intensity [95].

- The spectra differ appreciably!
- Obviously in the amorphous states the Raman selection rules are broken and all modes of the VDOS are visible. [96]
- The peak at ~ 50 cm^{-1} is called "boson peak". Why??
- Because the temperature dependence of the low-frequency spectrum can be represented as

$$I(\omega) = \big[n(\omega) + 1\big]\chi''(\omega) \tag{8.1}$$

where $\chi''(\omega)$ is a temperature-independent spectrum, and $n(\omega)$ is the boson occupation function

$$n(\omega) = \frac{1}{e^{\hbar\omega/k_BT} - 1} = \frac{1}{1 - e^{-\hbar\omega/k_BT}} - 1\,. \tag{8.2}$$

- The workers, who coined the name boson peak (named so first in the review paper of Jäckle, 1981 [97]), obviously were not familiar with Kubo's [50] quantum version of the fluctuation-dissipation theorem for the Fourier transform of a correlation function $C_{AA}(\omega)$ of a dynamical variable $A(t)$

$$C_{AA}(\omega) = \big[n(\omega) + 1\big]\chi''_{AA}(\omega) \tag{8.3}$$

where $\chi(\omega$ is the dynamical susceptibility corresponding to $A(t)$, and $\chi''(\omega)$ the corresponding spectral function.

Reasoning:

- The Raman spectrum is known [52] to be proportional to the correlation function of the electric permittivity $\epsilon(t)$, so the theorem applies.
- If the measured temperature dependence of the spectrum is given solely by the thermal factor $[n(\omega)+1]$, the spectrum $\chi''(\omega)$ must be temperature independent
- If the permittivity couples to the vibrational excitations, it must be harmonic vibrations, otherwise the spectrum would be temperature dependent.

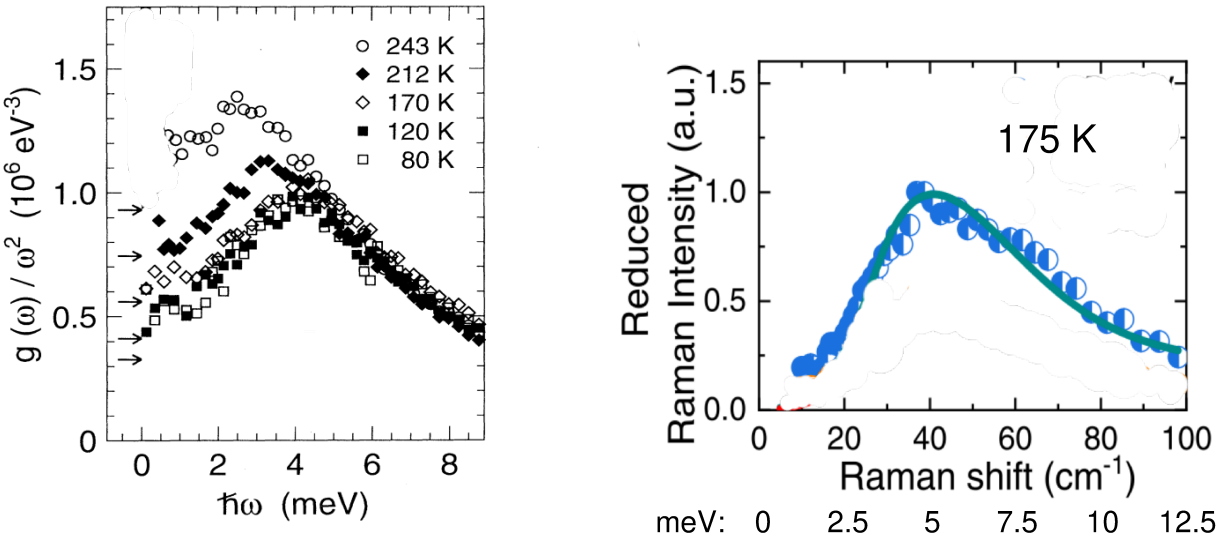

Figure 63: Left: Reduced density of states of glassy glycerol, $g(\omega)/\omega^2$, measured by inelastic neutron scattering by Wuttke et al. [98]. Right: Reduced Raman intensity $I(\omega)/[n(\omega)+1]\omega$, which, according to Shuker and Gammon's formula (8.4) should be equal to $g(\omega)/\omega^2$, measured by Uchino et al. [99], taken from Ref. [100].

8.1.1 Boson peak and the Debye VDOS

- Shuker and Gammon [96] advocated that the Raman susceptibility would be related to the VDOS $g(\omega)$ by

$$\chi''_{\text{Shuker}} \propto \frac{1}{\omega} g(\omega) \tag{8.4}$$

- Because at low frequencies $n(\omega)+1 = k_B T/\omega$, the Raman-intensity would then be given by

$$I_{\text{Shuker}}(\omega) \sim \frac{g(\omega)}{\omega^2} \tag{8.5}$$

- For a Debye VDOS $g(\omega) \propto \omega^2$ the intensity should not have a maximum, but be constant. This points to a deviation from Debye's frequency law for the VDOS.

This encouraged newtron scatterer to measure the density of states of a glass directly using inelastic neutron scattering. However, the dynamic scattering law $S(q,\omega)$ is not directly related to the VDOS. only for incoherent neutron scattering, the spectrum is related to the self van-Hove function [51]

$$S_{\text{self}}(q,\omega) = \frac{1}{N}\left\langle \int_{-\infty}^{\infty} dt \sum_{\ell} e^{i\mathbf{q}[\mathbf{r}_\ell(t)-\mathbf{r}_\ell(0)]} \right\rangle \sim [n(\omega)+1]\frac{g(\omega)}{\omega} \tag{8.6}$$

- The neutron scattering from protons is completely incoherent. Because glycerol is mainly composed by H atoms (together with three C and three O), neutron scattering from glycerol directly monitors the VDOS.

In Fig. 63 the reduced VDOS $g(\omega)/\omega^2$, extracted from the inelastic neutron-scattering data [98] is shown, which points to a deviation from Debye's ω^2 law, as anticipated by using Shuker and Gammon's formula (8.4).

- However, the VDOS extracted from the Raman data with the Shuker-Gammon formula 8.4 does not agree to the neutron data. Comparing the two panels of Fig. 63 with each other, we see that the Raman boson peak is situated at 5 meV, whereas the neutron-scattering boson peak is at 5 meV.

- This occurred in a large number of cases (see [101] for Refs.) Therefore one invented a phenomenological light-vibration coupling function

$$C(\omega) = \frac{I_{\text{Raman}}(\omega)}{I_{\text{neutron}}(\omega)}$$

and then evaluated the Raman intensity as

$$I_{\text{Raman}}(\omega) \sim C(\omega)\big[n(\omega)+1\big]\frac{1}{\omega}g(\omega) \tag{8.7}$$

We shall show below, how to formulate a consistent theory of Raman scattering in glasses without invoking $C(\omega)$.

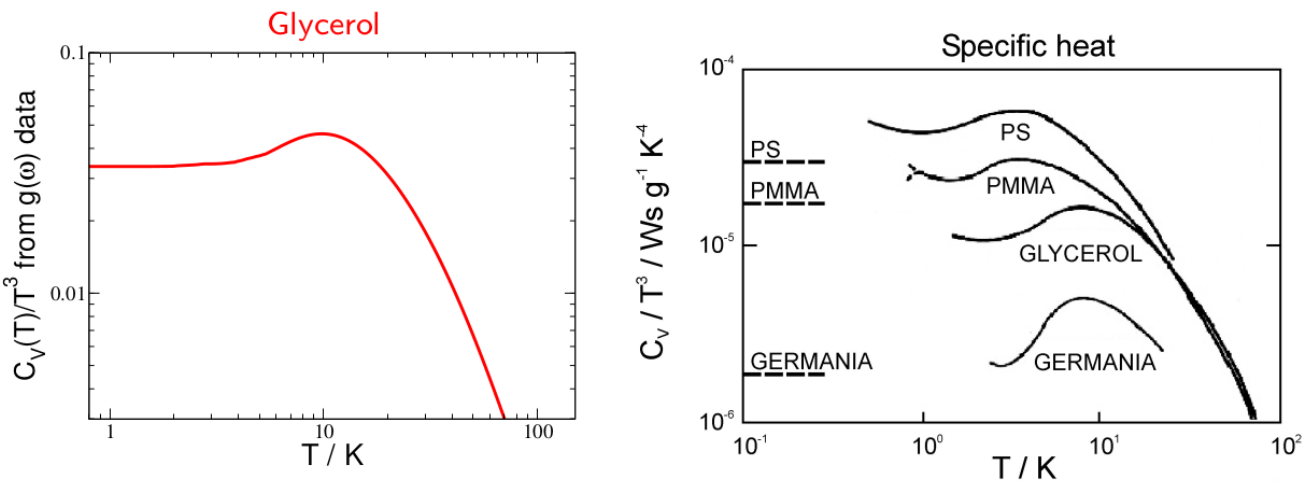

Figure 64: Left: reduced specific heat $C(T)/T^3$ calculated via

$$C(T) \sim \int_0^\infty d\omega\, g(\omega) \left(\frac{\hbar\omega}{k_B T}\right)^2 \frac{e^{\hbar\omega/k_B T}}{(e^{\hbar\omega/k_B T}-1)^2} \tag{7.7}$$

from the data of Wuttke et al. [98] Bottom right: Reduced-specific heat data for several glasses, including glycerol (Zeller, Pohl 1971) [102]. The dashed lines indicate the corresponding Debye prediction, calculated from the known sound velocities.

8.1.2 Specific heat boson peak and the shoulder of the thermal conductivity

In the left panel of Fig. 64 we show the calculation of the reduced specific heat $C(T)/T^3$ with the Debye formula (7.7) using the VDOS data of Wuttke et al. [98]. In the right panel $C(T)/T^3$ data [103] of some glass formers, including glycerol, are displayed. Clearly the calculated curve is very similar to the experimental one.

- The deviation from Debye's law for the specific heat, plotted as $C(T)/T^3$ mirrors the boson peak.

- In Fig. 65 we have added thermal conductivity data. They show a pronounced shoulder just, where $C(T)/T^3$ exhibits the boson peak. So it is obvious that the two features may be related [104].

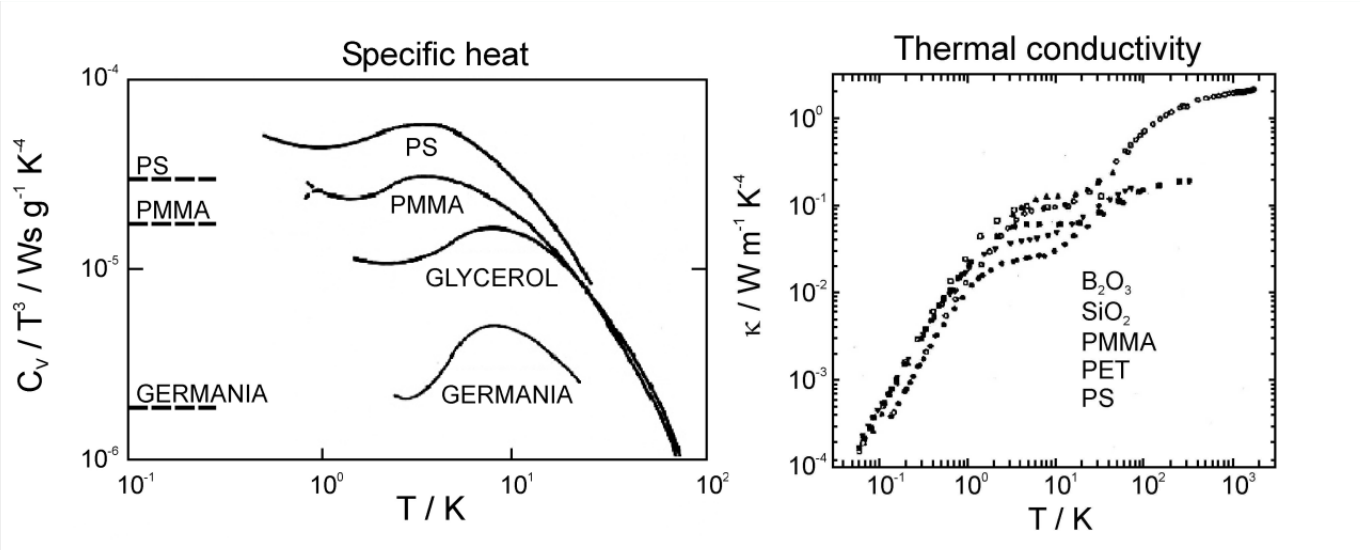

Figure 65: Left: reduced specific-heat data from Fig. 64. Right: Thermal conductivity data for several glasses [105].

8.1.3 Thermal anomalies at very low temperatures and the tunneling model

In Fig. 66 we show the original data of Zeller and Pohl (1971) [102], in which the temperature dependence of the specific heat and the thermal conductivity of crystalline and glassy SiO_2 are compared

- In the low-temperature regime the specific heat of the glass does not follow Debye's T^3 law, but

$$C(T) \sim T^x \quad \text{with} \quad x \gtrsim 1\,.$$

- The thermal conductivity near the boson peak (10 K) is 4 orders of maximum lower than that of the crystal.
- The thermal conductivity of the glass in the low-temperature regime follows a $\kappa \sim T^2$ law in contrast to the $\kappa \sim T^3$ behaviour of the crystal.

Explanation with the tunneling model:

- At these low temperature tunneling of the atomic configuration between adjacent potential-energy minima becomes possible.
- In quantum mechanics two potential wells, between tunneling is possible gives rise to two energy levels with separation ΔE. Assuming a flat distribution density of ΔE

$$P(\Delta E) = \text{const.}$$

one arrives at an energy density $\sim T^2$ and therefore a specific heat $C(T) \sim T$

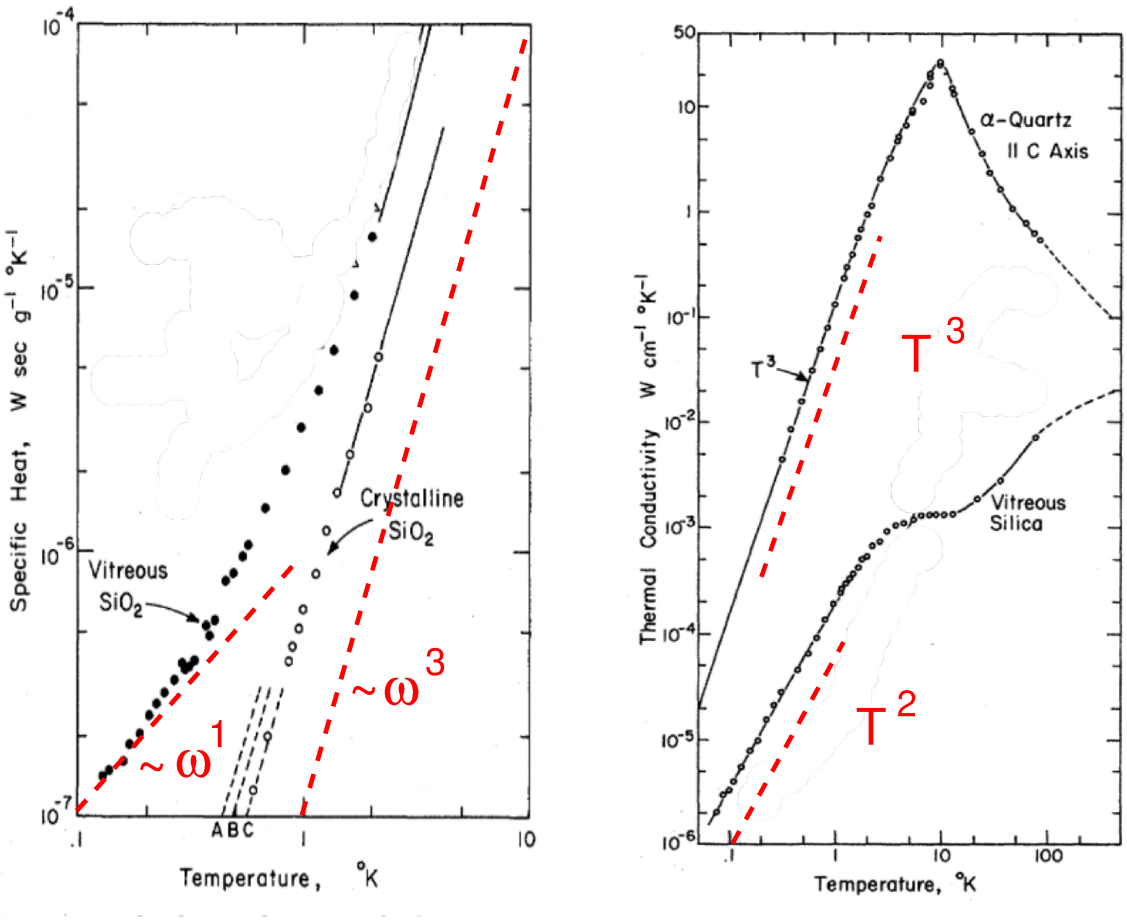

Figure 66: The low-temperature specific heat and thermal conductivity of crystalline, as well as glassy SiO_2 measured by Zeller and Pohl 1971 [102].

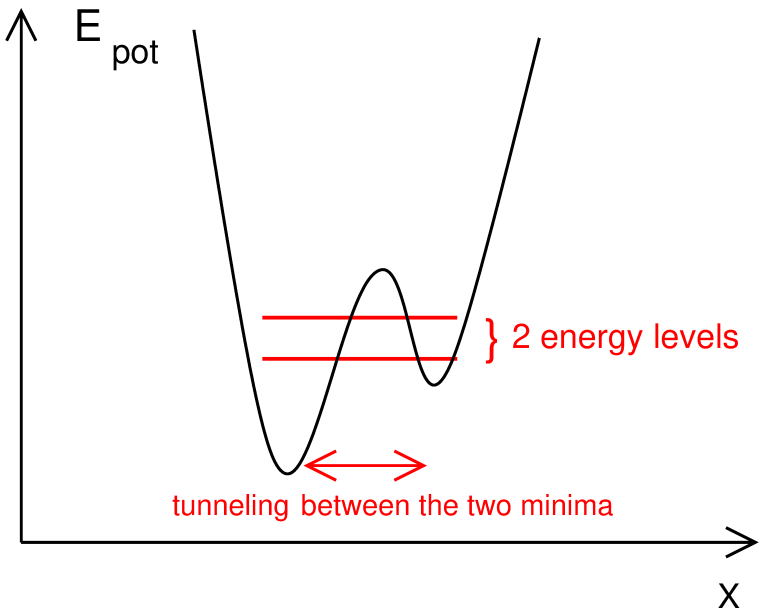

Figure 67: The tunneling model: A double-well potential, in which tunneling between the two wells is possible, gives rise to two separated energy levels [106, 107]

- Inelastic scattering of phonons between low-frequency waves from two-level systems produces a mean-free path of the phonons

$$\frac{1}{\ell} \sim \omega^2$$

Inserting this into the kinetic formula

$$\kappa(T) \sim \int_0^\infty d\omega\, \ell(\omega) g(\omega) \left(\frac{\hbar\omega}{k_B T}\right)^2 \frac{e^{\hbar\omega/k_B T}}{(e^{\hbar\omega/k_B T}-1)^2} \tag{8.8}$$

one obtains

$$\kappa(T) \sim T^2$$

.

9 Theory of vibrational anomalies in glasses

9.1 Scalar phonon model and the correspondence between anomalous diffusion and anomalous wave propagation

We consider the wave equation for a scalar displacement wave function $u(\mathbf{r})$ with a random spatial variation of an elastic constant $K(\mathbf{r})$

$$\frac{\partial^2}{\partial t^2} u(\mathbf{r},t) = \nabla \cdot \underbrace{\frac{1}{\rho_m} K(\mathbf{r})}_{v^2(\mathbf{r})} \cdot \nabla u(\mathbf{r},t) \tag{9.1}$$

Here ρ_m is the mass density, $K(\mathbf{r})$ the elastic (bulk) modulus and $v(\mathbf{r})$ the corresponding local sound velocity. We compare this with the diffusion equation in a disordered environment, which we have discussed above.

$$\frac{\partial}{\partial t} \rho(\mathbf{r},t) = \nabla \cdot D(\mathbf{r}) \cdot \nabla \rho(\mathbf{r},t) \tag{9.2}$$

A Fourier transform with respect to time of Eqs. (9.1) and (9.1) gives

$$-\omega^2\, u(\mathbf{r},\omega) = \nabla \cdot v^2(\mathbf{r}) \cdot \nabla u(\mathbf{r},\omega) \tag{9.3}$$

$$-i\omega \rho(\mathbf{r},\omega) = \nabla \cdot D(\mathbf{r}) \cdot \nabla \rho(\mathbf{r},\omega) \tag{9.4}$$

- The "only" difference between the two equations is the order of the time derivative.
- in frequency space we can go from the diffusion model to the wave model just by replacing $-i\omega$ by $-\omega^2$
- we observe that Eq. (9.3) can be put into the form of an eigenvalue equation

$$\underbrace{\omega^2}_{\lambda}\, u(\mathbf{r},\omega) = -\nabla \cdot v^2(\mathbf{r}) \cdot \nabla u(\mathbf{r},\omega) \tag{9.5}$$

where $\lambda = \omega^2$ is the eigenvalue.

In the effective medium the two Equations (9.3 and (9.4 read

$$-\omega^2\, u(\mathbf{r},\omega) = \nabla \cdot v^2(\omega) \cdot \nabla u(\mathbf{r},\omega) \tag{9.6}$$

$$-i\omega \rho(\mathbf{r},\omega) = \nabla \cdot D(\omega) \cdot \nabla \rho(\mathbf{r},\omega) \tag{9.7}$$

And we can use the same CPA, which we used for $D(\omega)$ for calculating $v^2(\omega)$ The Green's function of the effective medium, given by Eq. (6.47) takes the form

$$G(\mathbf{q}, z) = \frac{1}{z + q^2 v^2(z)} \tag{9.8}$$

where $z = -\omega^2 - i\epsilon$. So the Laplace parameter has just been rotated by 90° from the vicinity of the imaginary axis ($s = -i\omega + \epsilon$) to the vicinity of the real axis.

- However, the function $v^2(z)$ is the same analytical function as $D(s)$, if calculated with the same distribution of $D_i \equiv v_i^2$, $P(D_i)$.

$$0 = \int dD_i P(D_i) \frac{D_i - D(s)}{1 + \frac{1}{3}[D_i - D(s)]\Lambda(s)} \tag{9.9}$$

or, *mutatis mutandis*

$$0 = \int dv_i^2 P(v_i^2) \frac{v_i^2 - v^2(z)}{1 + \frac{1}{3}[v_i^2 - v^2(z)]\Lambda(z)} \tag{9.10}$$

The density of states of the wave model can be calculated from the $\mathbf{q}$ sum over the Green's function as

$$g(\omega) = \frac{2\omega}{\pi} \mathrm{Im}\{G(z)\} \tag{9.11}$$

with the $\mathbf{q}$ summed Green's function

$$G(z) = \frac{1}{N} \sum_{\mathbf{q}} G(\mathbf{q}, z) = \frac{3}{k_D^3} \int_0^{k_D} dq q^2 \frac{1}{z + q^2 v^2(z)} \tag{9.12}$$

In Fig. 68 we compare the CPA calculation of the AC conductivity of Fig. 57 with the reduced density of states

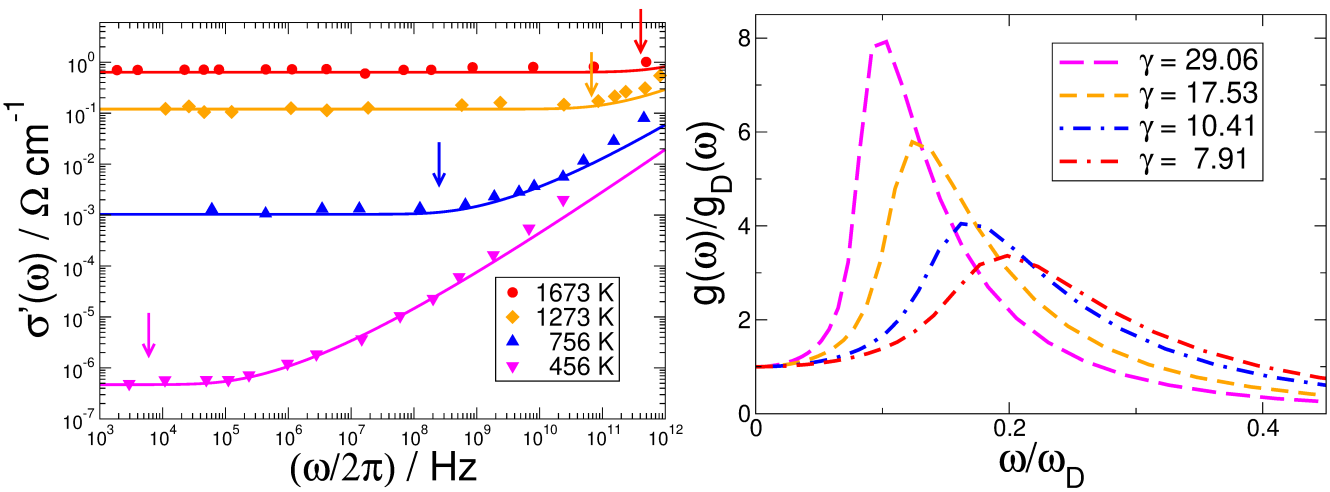

Figure 68: Left: (same as Fig. 57) CPA calculation of the AC conductivity using a constant activation energy distribution $P(E)$, compared with data on Sodium-Trisilicate glass [75] The arrows mark the cross-over from DC to AC behaviour.
Right: Calculation of the reduced density of states $g(\omega)/g_D(\omega)$ with the same distribution density $P(D_i) \equiv P(v_i^2)$. The boson peaks at $\tilde{\omega}^*$ appear just at the frequencies $\omega^* = \sqrt{\tilde{\omega}^*}$ marked in the left panel, i.e. the DC-AC crossover.

$$\frac{g(\omega)}{g_D(\omega)} = \frac{g(\omega)\omega_D^3}{3\omega^2} \tag{9.13}$$

The Debye frequency is given by

$$\omega_D = v(z=0)k_D \quad \text{with} \quad k_D = \left[6\pi^2 \frac{N}{V}\right]^{1/3} \tag{9.14}$$

We converted the constant distribution density of activation energies

$$P(E_i) = \frac{1}{E_0} \quad \text{for} \quad E \leq E_0 \tag{9.15}$$

of $D_i = D_0 e^{-E_i/k_B T}$ to a distribution of diffusivities D_i viz. squared velocities v_i^2

$$P(D_i) = P(v_i^2) = \frac{1}{\mu/D_i}\frac{1}{D_i} \quad \mu \leq D_i \leq D_0 \tag{9.16}$$

with $\mu = D_0 e^{-E_0/k_B T}$. The relative variance (disorder parameter) of this distribution is given by [84]

$$\gamma = \frac{1}{\langle D_i \rangle^2}\left\langle \left(D_i - \langle D_i \rangle\right)^2 \right\rangle = \frac{E_0}{2k_B T} \tag{9.17}$$

Important result:

- The boson peak corresponds to the DC-AC crossover of the analogous diffusion problem!

Let us call the DC-AC crossover frequency ω^* corresponding to $\sqrt{\tilde{\omega}^*}$ for the waves. Then we have the following correspondences

	Diffusion	Vibrations
below $\omega^* = \sqrt{\tilde{\omega}^*}$	normal diffusion	wave propagation
	D frequency independent	v^2 frequency independent
wave function	Gaussian	plane wave
above $\omega^* = \sqrt{\tilde{\omega}^*}$	$D(s)$ frequency dependent	$v^2(z)$ frequency dependent
wave function	irregular	random-matrix like

9.2 The paradigm of Ioffe and Regel

In a frequently cited paper on disordered semiconductors Ioffe and Regel (1960) [108] pointed out:

> "It appears that for all semiconductors with mobility $\mu < 100$ cm^{2}V^{-1}sec^{-1}
>
> $$L < \lambda\,.$$
>
> (L = mean-free path, λ = wavelength of the electron, WS.)
> However, the free forward motion with a mean velocity v occurs only over distances L. It is clear, therefore, that for all semiconductors with mobility less than 100 cm^{2}V^{-1}sec^{-1} the concept of velocity of the charge carriers loses its meaning".

Obviously the authors were critizing earlier literature, in which conductivity data of disordered semiconductors were discussed in terms of the kinetic free-electron theory of Drude and Sommerfeld [109], which based on the assumption of nearly-free electron motion with occasional collisions. Sir Nevill Mott [110, 111] repeatedly quoted this paper, emphasizing its importance. He conjectured that in a disordered material, in which the disorder-induced mean-free path becomes smaller than the electron's de-Broglie wavelength, the electrons become Anderson-localized. In his seminal paper of 1958 [112] Anderson had postulated that, if the disorder in a disordered electronic conductor is strong enough, the wavefunction of the electron extends only over a finite extent (localization length).

In the mit 80's, when the discussion about the boson peak started, it was noted [113, 114] that the boson peak just occurs near the frequency, where the mean-freee path of the acoustic waves, as estimated from the high-frequency sound attenuation, is approximately equal to the wavelength of the transverse acoustic waves. This was confirmed later by computer simulations [115, 116]. The authors of [113, 114] postulated that beyond the boson peak, i.e. beyond the Ioffe-Regel limit the vibrational states are localized and therefore cause the boson peak. However, it was shown later with simulations [117] and model calculations [118] that the boson peak position does not co-incide with the Anderson-localization frequency, which occurs just below the Debye frequency, i.e much higher than the boson peak.

We may note:

- The boson peak, which marks the cross-over between waves and non-waves occurs just at Ioffe and Regel's frequency, where the wavelength of the lowest excitations, i.e. the transverse waves becomes comparable to the mean-free path.

9.3 Heterogeneous-elatsticity theory (HET)

9.3.1 Equations of motion of elasticity theory

The equation of motion for the displacements $\mathbf{u}(\mathbf{r},t)$ of an elastic body with bulk modulus K and shear modulus G are [119]

$$\rho_m \frac{\partial^2}{\partial t^2}\mathbf{u}(\mathbf{r},t) = \Big(\underbrace{K + \frac{4}{3}G}_{M}\Big)\nabla\nabla\cdot\mathbf{u}(\mathbf{r},t) - G\,\nabla\times\nabla\times\mathbf{u}(\mathbf{r},t) \tag{9.18}$$

M is the longitudinal modulus. We can seprate Eq. (9.18) into a longitudinal and a transverse equation of motion by introducing longitudinal and transverse wave functions $\mathbf{u}_L(\mathbf{r},t)$ and $\mathbf{u}_T(\mathbf{r},t)$ with

$$\nabla\times\mathbf{u}_L(\mathbf{r},t) = 0 \qquad \nabla\cdot\mathbf{u}_T(\mathbf{r},t) = 0 \tag{9.19}$$

If we apply this to plane waves $\mathbf{u}_{L,T} \sim e^{i\mathbf{kr}}$ we obtain

$$\mathbf{k}\times\mathbf{u}_L(\mathbf{r},t) = 0 \qquad \mathbf{k}\cdot\mathbf{u}_T(\mathbf{r},t) = 0\,, \tag{9.20}$$

from which follows

$$\mathbf{k} \parallel \mathbf{u}_L(\mathbf{r},t) \qquad \mathbf{k} \perp \mathbf{u}_T(\mathbf{r},t) \tag{9.21}$$

It is important to note that for a given $\mathbf{k}$ vector there are two linearly independent transverse waves, which are rectangular to one longitudinal wave.

Eq. (9.18) applied to the longitudinal and transverse waves leads to

$$\frac{\partial^2}{\partial t^2}\mathbf{u}_L(\mathbf{r},t) = v_L^2\,\nabla\nabla\cdot\mathbf{u}_L(\mathbf{r},t) \tag{9.22a}$$

$$\frac{\partial^2}{\partial t^2}\mathbf{u}_T(\mathbf{r},t) = v_T^2\,\nabla^2\mathbf{u}_T(\mathbf{r},t) \tag{9.22b}$$

where we have used the identity

$$\nabla\times\nabla\times\mathbf{u} = \nabla(\nabla\cdot\mathbf{u}) - \nabla^2\mathbf{u}$$

$v_{L,T}$ are the longitudinal and the transverse sound velocities given by

$$M = K + \frac{4}{3}G = \rho_m\,v_L^2 \tag{9.23a}$$

$$G = \rho_m\,v_T^2 \tag{9.23b}$$

Inserting the wave ansatz

$$\mathbf{u}_{L,T} = \mathbf{u}_{L,T}^{(0)} e^{i[\mathbf{kr}-\omega_{L,T}t]} \tag{9.24}$$

into Eqs. (9.22) we obtain

$$\omega_L(k) = v_L\,k \qquad \omega_T(k) = v_T\,k \tag{9.25}$$

The Green's functions are

$$G_{L,T}(k,z) = \frac{1}{z + k^2 v_{L,T}^2} \qquad z = -\omega^2 - i\epsilon \tag{9.26}$$

and the Debye density of states is given by

$$
\begin{aligned}
g_D(\omega) &= \frac{2\omega}{\pi}\frac{1}{3N}\mathrm{Tr}\{\overset{\leftrightarrow}{\mathrm{G}}(\mathrm{z})\} = \frac{2\omega}{\pi}\frac{1}{3\mathrm{N}}\sum_{\nu}\sum_{\mathbf{k}}\mathrm{G}_{\nu}(\mathbf{k},\mathrm{z}) \\
&= \frac{2\omega}{\pi}\frac{1}{3}\frac{3}{k_D^3}\int_0^{k_D} dk k^2\Big[G_L(k,z)+2G_T(k,z)\Big]\Big] \\
&= \omega^2\left(\frac{1}{(v_L k_D)^3}+2\frac{1}{(v_T k_D)^3}\right) = \frac{3\omega^2}{\omega_D^3}
\end{aligned}
\tag{9.27}
$$

9.3.2 Spatially fluctuating shear modulus

and SCBA We now assume that the shear modulus G fluctuates in space. We obtain the equations of motion

$$
\rho_m\frac{\partial^2}{\partial t^2}\mathbf{u}(\mathbf{r},t) = \nabla\Big(\underbrace{K+\frac{4}{3}G(\mathbf{r})}_{M(\mathbf{r})}\Big)\nabla\cdot\mathbf{u}(\mathbf{r},t) - \nabla\times G(\mathbf{r})\,\nabla\times\mathbf{u}(\mathbf{r},t) \tag{9.28}
$$

We now introduce, as before an effective medium, in which the shear modulus $G(s)$ is frequency dependent. The Green's functions of the effectve medium are

$$
G_{L,T}^{\mathrm{med}}(k,z) = \frac{1}{z+k^2 v_{L,T}^2(z)} \tag{9.29}
$$

with

$$
v_T^2(z) = \big[\tilde{G}_0 - \Sigma(z)\big] = \tilde{G}(z) \tag{9.30a}
$$

$$
v_L^2(z) = \tilde{K}_0 + \frac{4}{3}\big[\tilde{G}_0 - \Sigma(z)\big] = \tilde{K}_0 + \frac{4}{3}\tilde{G}(z) \tag{9.30b}
$$

and we introduce the Green matrix

$$
\overset{\leftrightarrow}{G}^{\mathrm{med}}(\mathbf{k}.z) = \begin{pmatrix} G_L^{\mathrm{med}}(k,z) & 0 & 0 \\ 0 & G_T^{\mathrm{med}}(k,z) & 0 \\ 0 & 0 & G_T^{\mathrm{med}}(k,z) \end{pmatrix}
$$

The effective-medium free energy involves a $\mathbf{k}$ sum and a sum over the cartesial directions:

$$
\beta\mathcal{F}\{\Sigma(z)\}_{\mathrm{med}} = -\mathrm{Tr}\Big\{\ln\{\overset{\leftrightarrow}{\mathrm{G}}_{\mathrm{med}}(\mathbf{q},\mathrm{s})^{-1}\}\Big\} \tag{9.31}
$$

$$
= -\sum_{\mathbf{k}}\left(\ln\left\{z+q^2\big(\tilde{K}_0+\frac{4}{3}\big[\tilde{G}_0-\Sigma(z)\big]\right\} + 2\ln\{z+q^2\big[\tilde{G}_0-\Sigma(z)\big]\}\right)
$$

The SCBA free energy is, as before (we set $G(\mathbf{r})/\rho_m = \tilde{G}(\mathbf{r}) = \tilde{G}_0 + \Delta\tilde{G}(\mathbf{r})$)

$$
\beta\mathcal{F}_{\mathrm{SCBA}} = -\Lambda(z)\Sigma(z) + \frac{1}{2}p_c\Lambda(z)^2\langle(\Delta\tilde{G})^2(\mathbf{r})\rangle\,. \tag{9.32}
$$

which, as before, by varying $\Lambda(z)$, leads to

$$
\Sigma(z) = p_c\langle(\Delta\tilde{G})^2\rangle\Lambda(z) \tag{9.33}
$$

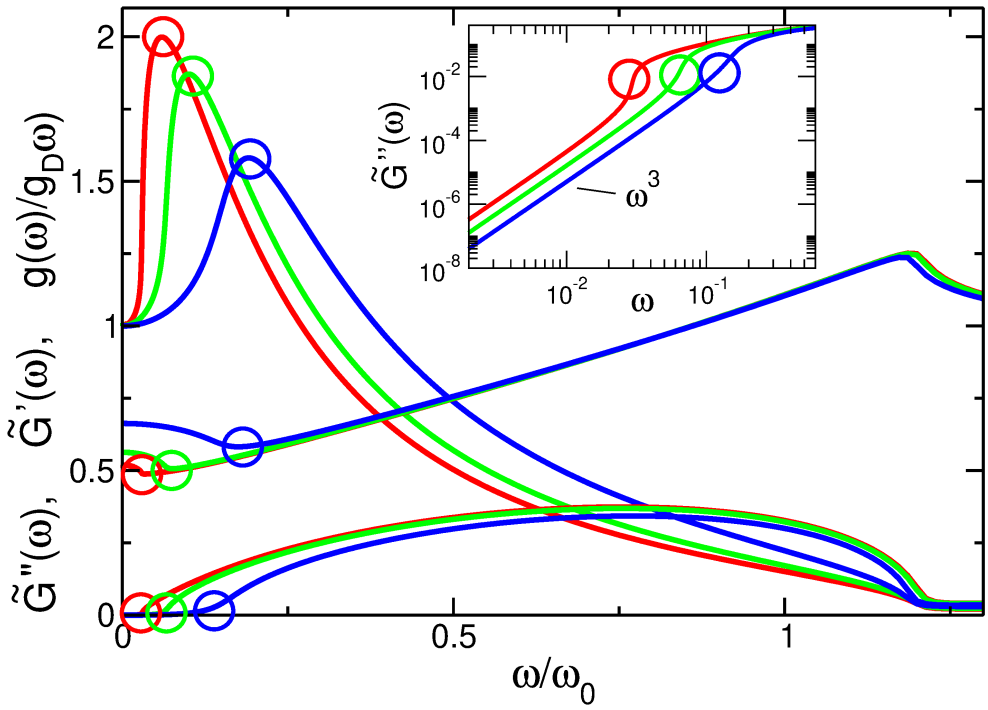

Figure 69: Reduced density of states as calculated in SCBA for three different values of γ together with the real and the imaginary part of the frequency dependent shear modulus $G'(\omega)$ and $G''(\omega)$. The circles indicate the boson-peak related anomalies.
The inset is a double-logarithmic blow-up of $G''(\omega)$.

Varying now $\beta\mathcal{F}\{\Sigma(z)\}_{\text{med}} + \beta\mathcal{F}_{\text{SCBA}}$ with respect to $\Sigma(z)$ we get

$$\Lambda(z) = \sum_{\mathbf{k}} \left(\frac{4}{3} \frac{k^2}{z + k^2(K_0 + \frac{4}{4}\left[\tilde{G}_0 - \Sigma(z)\right])} + 2 \frac{k^2}{z + k^2\left[\tilde{G}_0 - \Sigma(z)\right]} \right) \tag{9.34}$$

and finally

$$\Sigma(z) = \gamma \tilde{G}_0^2 \sum_{\mathbf{k}} k^2 \left(\frac{2}{3} G_L^{\text{med}}(k,z) + G_T^{\text{med}}(k,z) \right) \tag{9.35}$$

with the disorder parameter

$$\gamma = \frac{2p_c}{\tilde{G}_0} \langle (\Delta \tilde{G})^2 \rangle \tag{9.36}$$

9.3.3 The three boson-peak-related vibrational anomalies

In Fig. 70 we show the reduced density $g(\omega)/\omega^2$ together with the real and imaginary part of the complex, frequency dependent shear modulus

$$\tilde{G}(z) = Q(z) = \tilde{G}_0 - \Sigma(z) = \tilde{G}'(\omega) - i\tilde{G}''(\omega) \tag{9.37}$$

- The three boson-peak related vibrational anomalies are
  - The boson peak itself: peak in the reduced VDOS $g(\omega)/\omega^2$;
  - a pronounced dip in $\tilde{G}'(\omega) = \text{Re}\{v(z)^2\}$

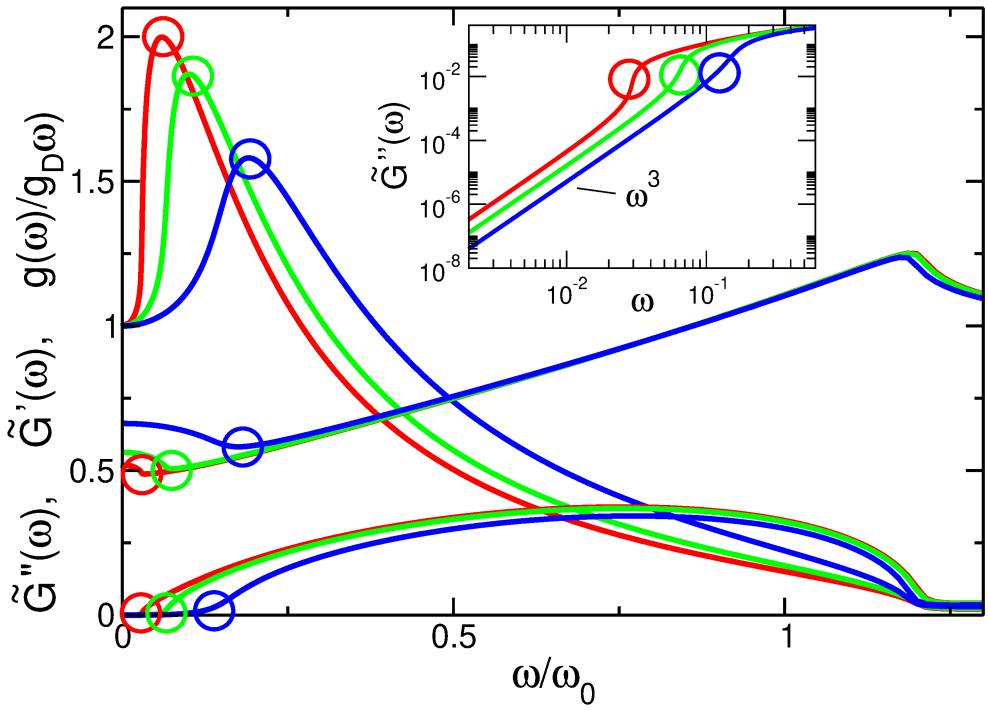

Figure 70: Reduced density of states as calculated in SCBA for three different values of γ together with the real and the imaginary part of the frequency dependent shear modulus $G'(\omega)$ and $G''(\omega)$. The circles indicate the boson-peak related anomalies.
The inset is a double-logarithmic blow-up of $G''(\omega)$.

$\rightarrow$ The dip in $\tilde{G}$ is related to a dip in $v'(\omega) = \mathrm{Re}\{v(z)\}$ via

$$\begin{aligned} G(z) &= G(0) + \Delta G(z) \\ v(z) &= [G(0) + \Delta G(z)]^{1/2} = [G(0)]^{1/2}[1 + \frac{\Delta G(z)}{G(0)}]^{1/2} \\ &\approx [G(0)]^{1/2}[1 + \frac{1}{2}\frac{\Delta G(z)}{G(0)}] \end{aligned}$$

- a strong increase of $\tilde{G}''(\omega)$, which then becomes comparable to $\tilde{G}'(\omega)$.

- Below the boson peak (Debye regime or allowed Ioffe-Regel regime) we have
  - Constant reduced VDOS
  - Constant $\tilde{G}'(\omega) = \tilde{G}_0$
  - Rayleigh scattering

$$\Gamma(\omega) \sim \omega G''(\omega) \sim \omega^4 \tag{9.38}$$

In Fig. 71 we show the results for the three boson-peak related anomalies, extracted from the resut of a molecular-dynamics simulation of a system of 10 million particles, ineracting via a so-called soft-sphere potential ($r_{ij} = |\mathbf{r}_i - \mathbf{r}_j|$)

$$\phi(r_{ij}) \sim \frac{1}{r_{ij}^{12}} \tag{9.39}$$

The system has been quenched towards three different temperatures below the glass transition. The complex moduli $\tilde{G}(z)$ and the longitudinal modulus

$$\tilde{M}(z) = \tilde{K}_0 + \frac{4}{3}\tilde{G}(z) \tag{9.40}$$

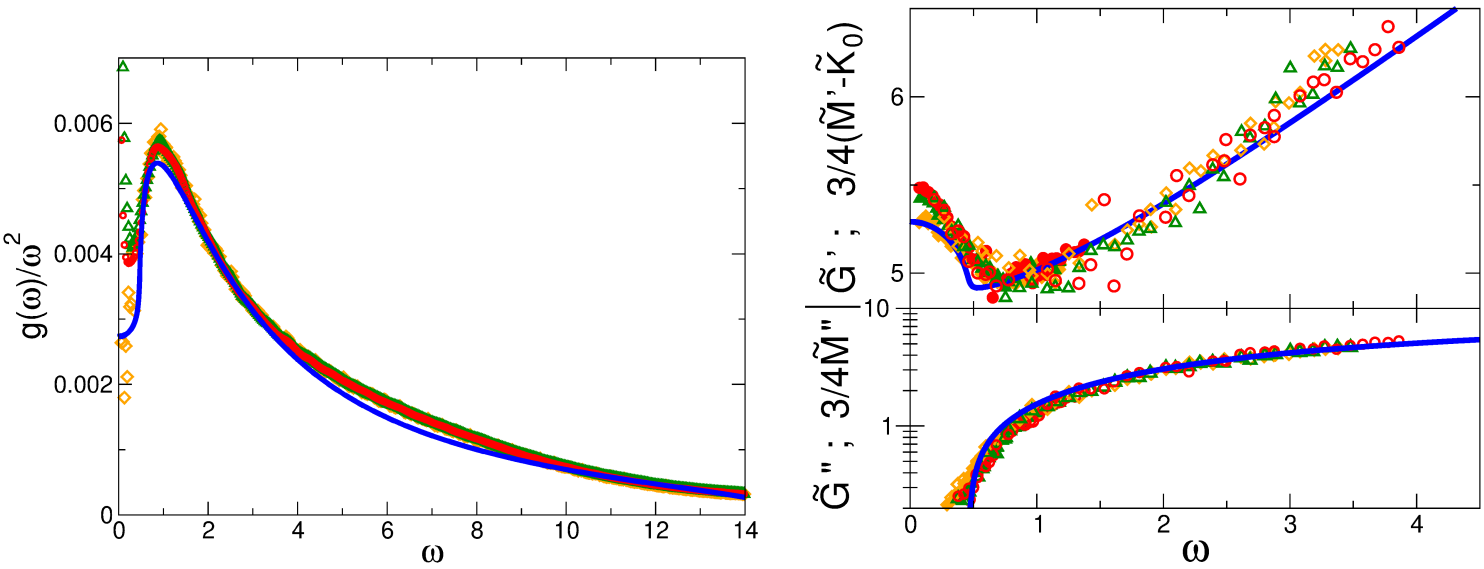

Figure 71: Reduced DOS and the real and imaginary parts of the shear modulus together with those of the quantity $\frac{3}{4}[M(z)-K_0]$. Symbols: Results of a soft-sphere molecular-dynamics simulation with 10^7 particles with four different temperatures below the glass transition. Full line: SCBA calculation [116].

have been extracted from a calculation of the longitudinal and transverse current correlation functions (see the Appendix A3 and [116].

- All three anomalies show up in the simulation;
- the HET theory (blue line) agrees satisfactorily to the data
- the quantities
$$\frac{3}{4}\left[\tilde{M}'(\omega)-\tilde{K}_0\right] \quad \text{and} \quad \frac{3}{4}\tilde{M}''(\omega)$$
ly on top of $\tilde{G}'(\omega)$ and $\tilde{G}''(\omega)$, which proves that there is no frequency dependence of the bulk modulus.

In Fig. 72 we show The vibrational anomalies extracted from inelastic X-ray scattering experiments on glassy glycerol [120] and SiO_2 [121]. The data show the boson peak together with the dispersion of the longitudinal sound velocity $v_L(q)$ as well as the q dependent line width (acoustic attenuation) $\Gamma(q)$.

- The wavenumbers q can be converted to frequencies via $\omega = v_L(0)q$
  - For glycerol the boson peak is at $\omega_B = 4\,\text{meV} \hat{=} 6\,\text{ps}^{-1}$. With $v_L(0) = 3.5$ km s^{-1} this gives $q_B = 1.7$ nm^{-1}.
  - For SiO_2 the boson peaks are at $\omega_B = 4\,\text{meV}(\text{T} = 300\text{ K})$ and at $\omega_B = 4\,\text{meV}(\text{T} = 1620\text{ K}) \hat{=} 6$ and 9 ps^{-1}. With $v_L(0) \sim 6$ km s^{-1} this gives $q_B = 1.0$ and 1.5 nm^{-1}.
- In both cases this gives the q range of the observed anomalies
- In both cases the predicted Rayleigh scattering law
$$\Gamma(\omega) \sim \omega^4$$
is observed.

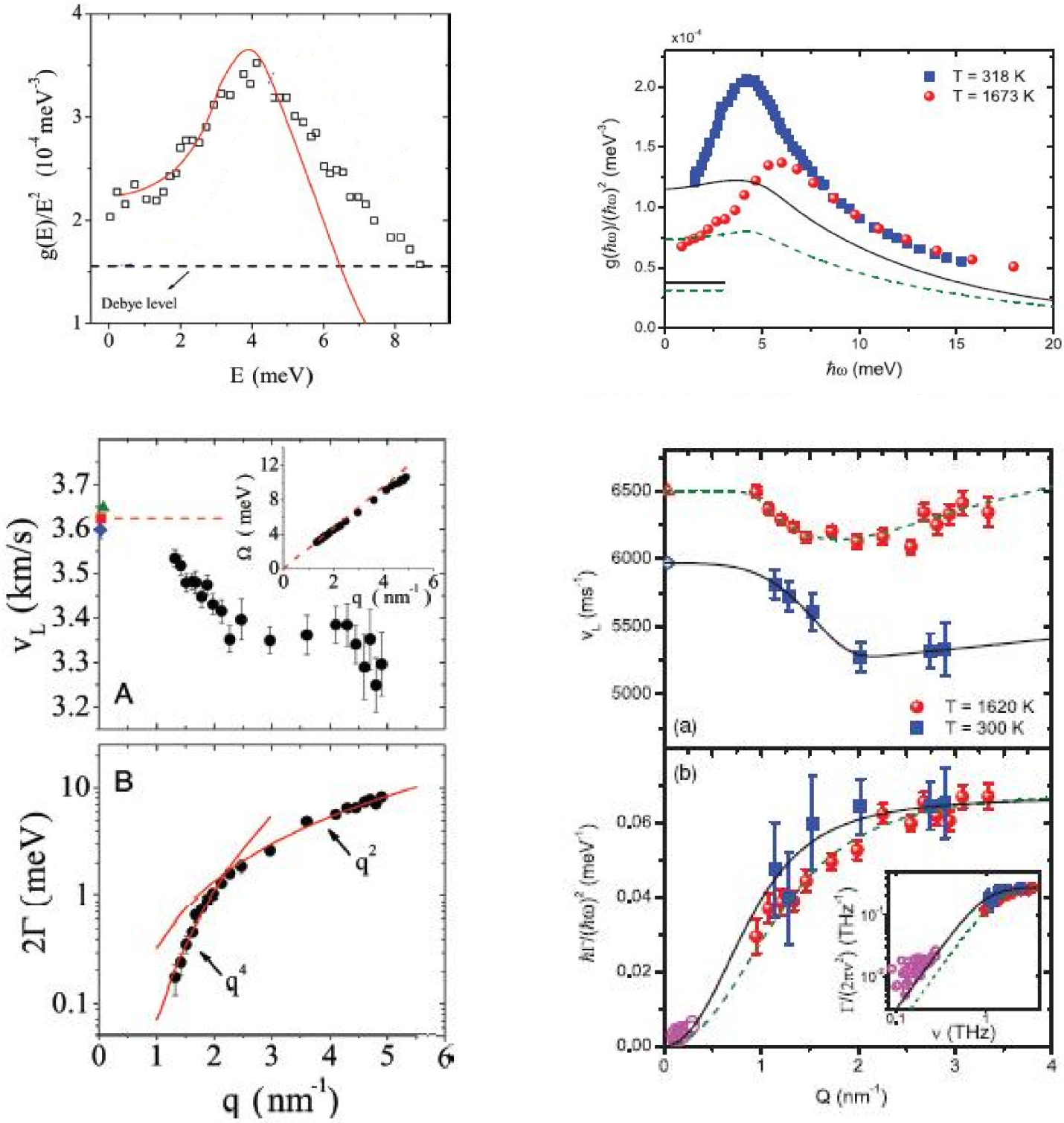

Figure 72: Results from inelastic X-ray scattering experiments on glassy glyserol (left, [120]) and glassy SiO_2 (right, [121]). The top curves show the reduced VDOS with the boson peak, the bottom curves show the q dependence of the sound velocity and the sound attenuation coefficient $\Gamma(q)$.

9.3.4 CPA for heterogeneous-elasticity theory (HET) and disorder descriptors for glasses

For the HET-CPA we have to miniminize

$$\beta\mathcal{F}\{Q(z),\Lambda(z)\} = \mathcal{F}_{\text{med}}\{Q(z)\} + \mathcal{F}_{\text{CPA}}\{Q(z),\Lambda(z)\} \tag{9.41}$$

Here $\mathcal{F}_{\rm med}$ is the same as given in (**??**), but now using $Q(z) = \tilde{G}_0 - \Sigma(z)$, which gives

$$\beta\mathcal{F}\{Q(z)\}_{\rm med} = -{\rm Tr}\Big\{ \ln\{\overleftrightarrow{\rm G}_{\rm med}\,(\mathbf{q},{\rm s})^{-1}\}\Big\} \tag{9.42}$$
$$= -\sum_{\mathbf{k}}\left(\ln\left\{z + q^2\big(\tilde{K}_0 + \frac{4}{3}Q(z)\right\} + 2\ln\left\{z + q^2 Q(z)\right\}\right)$$

The CPA free energy is given, as before (replacing D_i by $\tilde{G}_i$)

$$\beta\mathcal{F}\{Q(s),\Lambda(s)\}_{\rm CPA} = -\frac{1}{p_c}\Big\langle \ln\{1 + p_c\Lambda(s)[\tilde{G}_i - Q(s)]\}\Big\rangle \tag{9.43}$$

from which follows the CPA equation

$$\frac{d}{d\Lambda(s)}\beta\mathcal{F} = 0 = -\left\langle \frac{\tilde{G}_i - Q(s)}{1 + p_c\Lambda(s)[\tilde{G}_i - Q(s)]}\right\rangle_{P(\tilde{G}_i)} \tag{9.44}$$

Minimizing the full $\beta\mathcal{F}$ with respect to $Q(s)$ gives, as in the SCBA case

$$\begin{aligned}\Lambda(z,q_\xi) &= \sum_{\mathbf{k}}\left(\frac{4}{3}\frac{k^2}{z + k^2(K_0 + \frac{4}{4}\big[\tilde{G}_0 - \Sigma(z)\big])} + 2\frac{k^2}{z + k^2\big[\tilde{G}_0 - \Sigma(z)\big]}\right)\\ &= \frac{3}{q_\xi^3}\int_0^{q_\xi} dk\left(\frac{4}{3}\frac{k^2}{z + k^2(K_0 + \frac{4}{4}\big[\tilde{G}_0 - \Sigma(z)\big])} + 2\frac{k^2}{z + k^2\big[\tilde{G}_0 - \Sigma(z)\big]}\right)\end{aligned} \tag{9.45}$$

The imaginary part of this function turns out to be related to the depolarized Raman intensity via (Appendix 3)

$$I_{VH}(\omega) = \big[n(\omega) + 1\big]\Lambda''(\omega) \tag{9.46}$$

We now introduce the log-normal distribution density

$$P(\tilde{G}_i,\tilde{G}_0,\sigma) = \frac{1}{\sigma\sqrt{2\pi}}\frac{1}{\tilde{G}_i}\exp\left\{-\frac{1}{2\sigma^2}[\ln(\tilde{G}_i/\tilde{G}_0)]^2\right\} \tag{9.47}$$

- This distribution is restricted to positive values of G_i.
- It reduces to a Gaussian for small disorder.

Here $\tilde{G}_0$ is the geometric mean, and the width parameter σ^2 is related to the relative variance by

$$\gamma = \frac{1}{\langle\tilde{G}_i\rangle^2}\mathsf{Var}[\tilde{G}_i] = e^{\sigma^2} - 1 \tag{9.48}$$

G_0 is the geometric average

Within the CPA the parameters σ and $\tilde{G}_0$ are related by [100]

$$\frac{1}{4}\sigma^2 = 1 - \frac{\tilde{G}(0)}{\tilde{G}_0} = 1 - \frac{v_T^2}{v_0^2} \equiv n\,, \tag{9.49}$$

where v_T is the (experimental measurable) transverse sound velocity, and $v_0 = \sqrt{\tilde{G}_0}$.

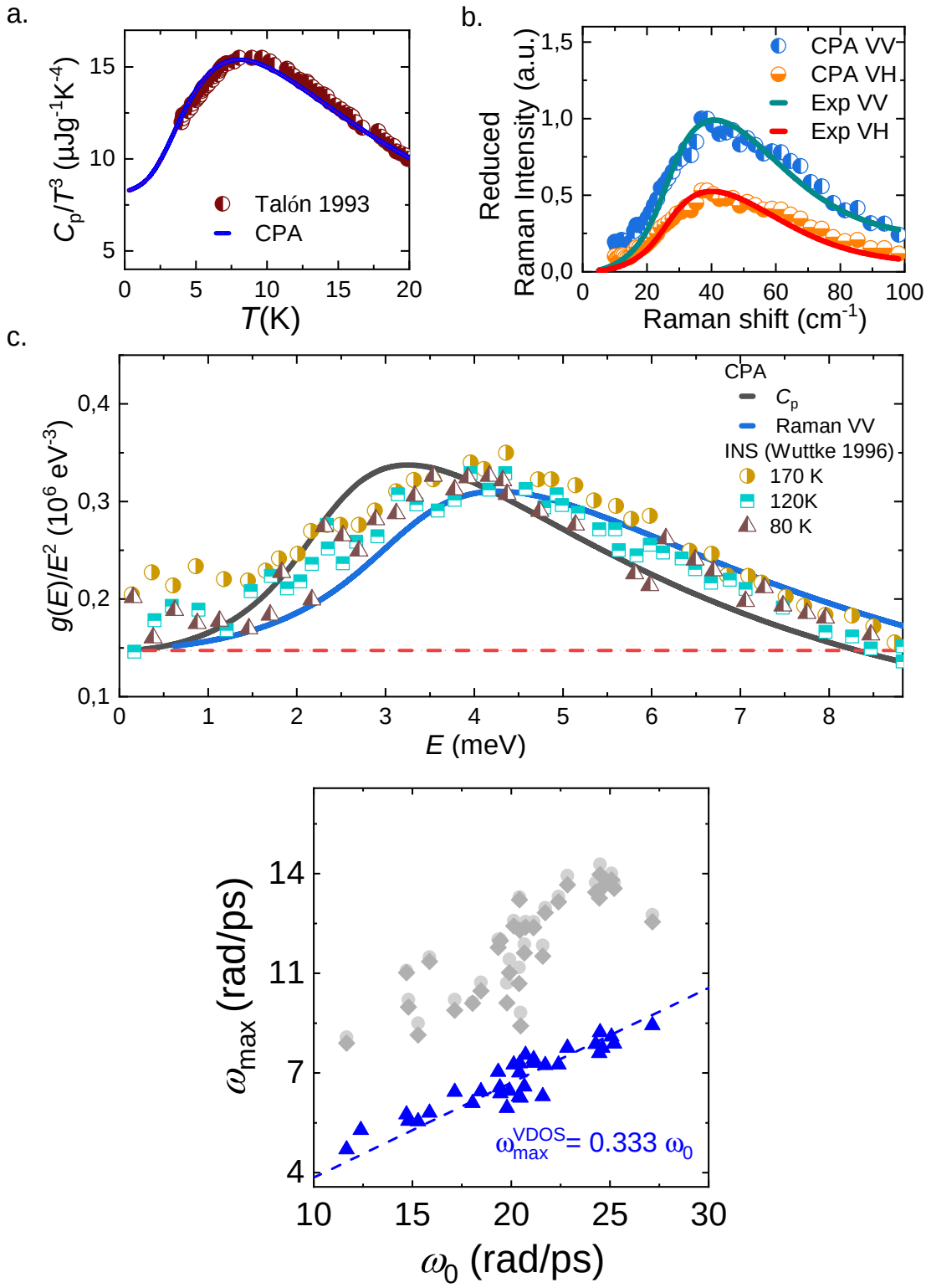

Figure 73: Top left: Reduced specific heat $C(T)/T^3$, measured by Talon et al. [122] together with a HET-CPA fit [100].
Top right: Raman spectra together with HET-CPA fits [100].
Middle: Reduced VDOS measured by inelastic neutron scattering [49] together with the VDOS curves using the fit parameters for the specific heat and Raman data [100].
Bottom panel: Boson-peak frequency vs. $\omega_0 = v_0 q_\xi$ (blue triangles) and frequencies of the Raman maximum (grey circles).

- n is called non-affine parameter. It describes the deviation of the disordered elasticity from affine elasticity, for which we expect

$$\tilde{G}_0 = \langle \tilde{G}_i \rangle = \tilde{G}(0) = v_T^2.$$

- Within HET-CPA and the log-normal distribution we can describe the glas with two descriptors
$$(\sigma^2, q_\xi) \quad \text{or} \quad (v_0, q_\xi).$$

In Ref. [100] 50 technically relevant glasses, including glycerol and SiO_2 have been fitted either to the temperature dependence of the specific heat (in the case of metallic glasses or the Raman spectra.

- Using this version of the HET-CPA, characterized by two parameters ("descriptors") we can
  - give good descriptions of the anomalous spectra of glass;
  - extract and predict a density of states (VDOS);
  - establish trends and phenomenological relations between physical quantities and the descriptors.

In Fig. 73 we show a HET-CPA fit to both specific heat data and Raman data of glycerol (top panels). We then compare the measured VDOS of glycerol with the VDOS predicted by the fits of the top panels. We see that this procedure is quite reliable..

- In the bottom left panel we plot the boson peak frequency ω_B against the disorder-related frequency
$$\omega_0 = q_\xi v_0 \sim \frac{v_0}{\xi},$$
which gives the relation
$$\omega_B = 0.333\omega_0 \sim \frac{1}{\sqrt{1-n}}\frac{v_T}{\xi} \tag{9.50}$$

- A similar relation has been suggested previously [123, 124]. Without the non-affine correction the correlation is less perfect.

- The argument is similar to the Ioffe-Regel-related argumentation: If the wavelength $\lambda = 2\pi v_T/\omega$ becomes comparable with the correlation length of the elasticity fluctuations the homogeneity of the glass breaks down.

  In the figure also the maxima of the Raman spectra ("Raman boson peaks") are shown for comparison. The correlation is less convincing.

A Appendix

A.1 Laplace transform

A.1.1 Definition

A Laplace transform is defined as follows

$$\mathcal{L}_s\{f(t)\} = \int_0^\infty dt e^{-st} f(t) = f(s)\,, \tag{A.1}$$

where s is a complex number with real part > 0. If we associate this number to be composed of an infinitely small real part and a large imaginary part, corresponding to an oscillation frequency $s = \epsilon - i\omega$, we obtain a relation between the Laplace and Fourlier transform (see the Appendix)

$$f(\omega) = \frac{1}{2}\mathrm{Re}\Big\{\mathcal{L}_{\epsilon - i\omega}\{f(t)\}\Big\} \tag{A.2}$$

We may apply the Laplace transform to a constant function $f(t) = c$

$$\mathcal{L}_s\{c\} = c\int_0^\infty dt e^{-st} = \frac{c}{s} \tag{A.3}$$

or to an exponental function $f(t) = e^{s_0 t}$

$$\mathcal{L}_s\{e^{s_0 t}\} = \int_0^\infty dt e^{-[s-s_0]t} = \mathcal{L}_{s-s_0}\{1\} = \frac{1}{s-s_0} \tag{A.4}$$

We may also calculate the Laplace transform of the derivative $\dot{f}(t)$ by an integration by part:

$$\mathcal{L}_s\{\dot{f}(t)\} = \int_0^\infty dt e^{-st}\dot{f}(t) = -f(t{=}0) + s\int_0^\infty dt e^{-st} f(t) \tag{A.5}$$

And, iterating Eq. (A.5)

$$\mathcal{L}_s\{\ddot{f}(T)\} = -\dot{f}(t{=}0) + s\mathcal{L}\{\dot{f}(t)\} = -\dot{f}(t{=}0) + s\Big(-f(t{=}0) + sf(s)\Big) \tag{A.6}$$

A.1.2 Damped harmonic oscillator

Let's now consider the well-known undergraduate problem of a damped harmonic oscillator:

$$\ddot{x}(t) + \gamma\dot{x}(t) + \omega_0^2 x(t) = 0 \tag{A.7}$$

Laplace transformed we get

$$-\dot{x}(t{=}0) + s\Big(-x(t{=}0) + sx(s)\Big) + \gamma\Big(-x(t{=}0) + sx(s)\Big) + \omega_0^2 x(s) \tag{A.8}$$

which can be solved for $x(s)$

$$\begin{aligned} x(s) &= \frac{\dot{x}(t{=}0) + (\gamma + s)x(t{=}0)}{s^2 + \gamma s + \omega_0^2} \\ &= \frac{\dot{x}(t{=}0) + (\gamma + s)x(t{=}0)}{(s - s_1)(s - s_2)}\,, \end{aligned} \tag{A.9}$$

where $s_{1,2}$ are the roots of the denominator set =0:

$$s_{1,2} = -\frac{\gamma}{2} \pm i\,\underbrace{\sqrt{\omega_0^2 - \gamma^2/4}}_{\omega_1} \tag{A.10}$$

and we have assumed $\omega_0 > \gamma/2$. Let's for simplicity assume $\dot{x}(t{=}0) = 0$, then Eq. (A.9) decomposes as

$$x(s) = x(t{=}0)\left(\frac{A}{s - s_1} + \frac{B}{s - s_2}\right) \text{ with } \quad A = \frac{\gamma + s_1}{s_1 - s_2}\,, \quad B = \frac{\gamma + s_2}{s_2 - s_1} \tag{A.11}$$

and we get from (A.4)

$$x(t) = x(t{=}0)e^{-\frac{1}{2}\gamma t}\left(A\,e^{i\omega_1 t} + B\,e^{-i\omega_1 t}\right) \tag{A.12}$$

A.1.3 Relation to Fourier transform

We may insert for $f(t)$ its Fourier-transformed version

$$f(t) = \frac{1}{2\pi}\int_{-\infty}^{\infty} d\omega e^{-i\omega t} f(\omega) \tag{A.13}$$

into the Laplace transform:

$$\begin{aligned} \mathcal{L}_s\{f(t)\} &= \int_0^{\infty} e^{-st} f(t) = \frac{1}{2\pi}\int_{-\infty}^{\infty} d\omega f(\omega)\int_0^{\infty} dt e^{-[s-i\omega]t} \\ &= \frac{1}{2\pi}\int_{-\infty}^{\infty} d\omega \frac{f(\omega)}{s + i\omega} \end{aligned} \tag{A.14}$$

We remember that s must have a positive real part in order that the integral converges. So we just take an infinitesimally small real part

$$s = \epsilon - i\tilde{\omega} \tag{A.15}$$

We decompose the denominator as

$$\frac{1}{s + i\omega} = \frac{\epsilon + i[\omega - \tilde{\omega}]}{\epsilon^2 + [\omega - \tilde{\omega}]^2} \xrightarrow{\epsilon \to 0} \pi\delta(\omega - \tilde{\omega}) - i\frac{1}{\omega - \tilde{\omega}}\theta(\epsilon^2 - [\omega - \tilde{\omega}]^2) \tag{A.16}$$

which is called Sokhotski-Plemelj identity. The θ function[7] is zero for $|\omega - \tilde{\omega}| < \epsilon$ and one otherwise. We get for the Laplace transform

$$f(s) = \mathcal{L}_s\{f(t)\} = \frac{1}{2}f(\tilde{\omega}) - i\frac{1}{2\pi}P\int_{-\infty}^{\infty} d\omega \frac{1}{\omega - \tilde{\omega}} f(\omega) \tag{A.17}$$

where P denotes the principle-part integral, in which the ϵ interval around $\omega = \tilde{\omega}$ is omitted. If we take the real part, we get

$$\mathrm{Re}\{f(s)\} = \frac{1}{2}f(\tilde{\omega})\,. \tag{A.18}$$

[7] $\theta(x) = 0$ for $x < 0$, and 1 for $x \geq 0$.

A.1.4 Convolution theorem

Let us define two one-sided functions

$$\hat{f}(t) = \theta(t)f(t) \qquad \hat{g}(t) = \theta(t)g(t) \tag{A.19}$$

then the convolution between them is

$$\hat{h}(t)\hat{f} \circ \hat{g} = \begin{cases} \int_0^t d\tilde{t} f(\tilde{t})g(t-\tilde{t}) \text{for} t > 0 \\ 0 \qquad \text{else} \end{cases} \tag{A.20}$$

We may easily check the relation

$$\hat{f}(\omega) = \mathcal{L}_{-i\omega+\epsilon}\{f(t)\} = f(s) \tag{A.21}$$

from which we get the convolution theorem for Laplace transforms

$$f(s)g(s) = \mathcal{L}_s\{h(t)\} \tag{A.22}$$

A.2 CPA on a cubic lattice

The lattice CPA for a system with fluctuating nearest-neighbour hopping was derived independently in Refs. [83, 81, 82]. We consider a random walk on a cubic lattice with spatially fluctuating transition rates W_{ij} between nearest-neighbour sites i, j: The equation of motion is

$$\begin{aligned} \frac{d}{dt}G_{i\ell}(t) &= -\sum_{\substack{j \\ n.N.}} W_{ij}\left[G_{i\ell}(t) - G_{ij}(t)\right] - \delta(t)\delta_{ij} \\ &= \sum_j H_{ij}G_{ij}(t) - \delta(t)\delta_{ij} \end{aligned} \tag{A.23}$$

with

$$\begin{aligned} H_{ii} &= \sum_\ell W_{i\ell} \\ H_{ij} &= -W_{ij} \quad i \neq j \end{aligned} \tag{A.24}$$

Performing the Laplace transform we get

$$\begin{aligned} sG_{i\ell}(t) &= -\sum_{\substack{j \\ n.N.}} W_{ij}\left[G_{i\ell}(s) - G_{ij}(s)\right] - \delta_{ij} \\ &= -\sum_j H_{ij}G_{ij}(s) - \delta_{ij} \end{aligned} \tag{A.25}$$

The lattice Green's matrix is given by

$$G_{ij}(s) = \left[[s-H]^{-1}\right]_{ij} \tag{A.26}$$

with $s = \epsilon - i\omega$. In the effective medium the W_{ij} are replaced by a non-fluctuating frequency-dependent force constant $Q(s)$. The lattice Green's matrix $G_{ij}(s)$ of the effective medium obeys the equation

$$\begin{aligned} & sG_{i\ell}(s) + Q(s)\sum_{\substack{j \\ n.N.}}\big[G_{i\ell}(s) - G_{j\ell}(s)\big] \\ &= sG_{i\ell}(s) + Z\,Q(s)\big[G_{i\ell}(s) - G_{j\ell}(s)\big] \\ &= \delta_{i\ell} \end{aligned} \tag{A.27}$$

where $Z = 6$ is the number of nearest neighbors. In reciprocal space we obtain

$$\begin{aligned} G(\mathbf{k}, s) &= \sum_{i\ell} e^{i\mathbf{k}(\mathbf{r}_i - \mathbf{r}_\ell)} G_{ij}(s) \\ &= \frac{1}{s + Q(s)f(\mathbf{k})} = \frac{1}{Q(s)} G_0(\mathbf{k}, \frac{s}{Q(s)}) \end{aligned} \tag{A.28}$$

with the geometrical dispersion of the simple cubic lattice

$$f(\mathbf{k}) = 6 - 2\cos(k_x a) - 2\cos(k_y a) - 2\cos(k_z a) \tag{A.29}$$

and $G_0(\mathbf{k}, s)$ is the bare Green's function of the lattice

$$G_0(\mathbf{k}, s) = \frac{1}{s + f(\mathbf{k})} \tag{A.30}$$

We now pick a pair of sites (i_0, j_0) and replace the effective-medium force constant $Q(s)$ by the true, fluctuating W_{i_0,j_0}. The corresponding perturbation matrix is two-dimensional and has the form

$$\overset{\leftrightarrow}{V} = v(s) \begin{pmatrix} 1 & -1 \\ -1 & 1 \end{pmatrix} \tag{A.31}$$

with

$$v(s) = Q(s) - W_{ij}\,. \tag{A.32}$$

We call the Green matrix elements of the unperturbed effective medium, which correspond to the sites i_0, j_0

$$G_{i_0 i_0}(s) = G_{j_0 j_0}(s) \equiv G_1(s)$$

,

$$G_{i_0 j_0}(s) = G_{j_0 i_0}(s) \equiv G_2(s)$$

. Their difference is called

$$G_1(s) - G_2(s) = \Delta G(s)$$

.

In the (i_0, j_0) subspace the unperturbed Green matrix is

$$\overset{\leftrightarrow}{G}_0\,(s) \equiv \begin{pmatrix} G_1 & G_2 \\ G_2 & G_1 \end{pmatrix} \tag{A.33}$$

The full Green matrix is given by

$$\begin{aligned}\overleftrightarrow{G}_v &= \frac{1}{\underbrace{s-H_0}_{\overleftrightarrow{G}_0^{-1}}-\overleftrightarrow{V}}\overleftrightarrow{G}_v=\frac{1}{\underbrace{s-H_0}_{\overleftrightarrow{G}_0^{-1}}}\left(1+\frac{\overleftrightarrow{V}}{\underbrace{s-H_0}_{\overleftrightarrow{G}_0^{-1}}-\overleftrightarrow{V}}\right)\\ &= \overleftrightarrow{G}_0+\overleftrightarrow{V}\overleftrightarrow{G}_V \end{aligned} \tag{A.34}$$

Here we mean by 1 the 2×2 matrix

$$1=\begin{pmatrix}1 & 0\\ 0 & 1\end{pmatrix}$$

Iterating this equation, we obtain

$$\begin{aligned}\overleftrightarrow{G}_v &= \overleftrightarrow{G}_0+\overleftrightarrow{G}_0\overleftrightarrow{V}\overleftrightarrow{G}_0+\overleftrightarrow{G}_0\overleftrightarrow{V}\overleftrightarrow{G}_0\overleftrightarrow{V}\overleftrightarrow{G}_0+\overleftrightarrow{G}_0\overleftrightarrow{V}\overleftrightarrow{G}_0\overleftrightarrow{V}\overleftrightarrow{G}_0\overleftrightarrow{V}\overleftrightarrow{G}_0+\dots\\ &= \overleftrightarrow{G}_0+\overleftrightarrow{G}_0\overleftrightarrow{V}\left[1-\overleftrightarrow{V}\overleftrightarrow{G}_0\right]^{-1}\overleftrightarrow{G}_0\\ &= \overleftrightarrow{G}_0+\overleftrightarrow{G}_0\overleftrightarrow{T}\overleftrightarrow{G}_0 \end{aligned} \tag{A.35}$$

The T matrix is explicitly given by

$$\overleftrightarrow{T}=\frac{1}{Det[1-\overleftrightarrow{G}\overleftrightarrow{V}]}\overleftrightarrow{V}=\frac{1}{1-2v(s)\Delta G}\overleftrightarrow{V} \tag{A.36}$$

From (A.27), setting $i=j$ we get (inserting the lattice coordination number $Z=6$:

$$\Delta G=\frac{1}{6\,Q(s)}\left[1-sG_1\right]\equiv\frac{1}{6}\Lambda(s) \tag{A.37}$$

In the CPA one requires that the perturbed Green matrix *on the average* be the same as that of the effective medium, i.e.

$$\overleftrightarrow{G}_0\,(s)=\langle\overleftrightarrow{G}_v\,(s)\rangle \quad\Leftrightarrow\quad \langle\overleftrightarrow{T}\rangle=0 \tag{A.38}$$

From all the 4 entries of the matrices we obtain

$$\left\langle\frac{Q(s)-W}{1-\left[Q(s)-W\right]\frac{1}{3}\Lambda(s)}\right\rangle_{P(W)} \tag{A.39}$$

or in the previously used form

$$\left\langle\frac{W-Q(s)}{1+\left[W-Q(s)\right]\frac{1}{3}\Lambda(s)}\right\rangle_{P(W)} \tag{A.40}$$

with $W=W_{i_0j_0}$ and

$$\Lambda(s)=\frac{1}{Q(s)}\left[1-sG_1(s)\right] \tag{A.41}$$

Here $\langle\dots\rangle_{P(W)}$ is an average over the distribution of force constants $P(W)$. Explicitly we have

$$G_1(s)=\frac{1}{Q(s)}G_0\left(\frac{s}{Q(s)}\right)=\sum_{BZ}\frac{1}{s+Q(s)f(\mathbf{k})} \tag{A.42}$$

where

$$G_0(s) = \sum_{BZ} \frac{1}{s + f(\mathbf{k})} \tag{A.43}$$

is the reference local Green's function of the effective medium, here that of a single-cubic lattice.
The susceptibility function is given by

$$\begin{aligned} \Lambda(s) &= 6\Delta G(s) = 6\big[G_1(s) - G_2(s)\big] \\ &= \sum_{BZ} \frac{f(\mathbf{k})}{s + Q(s) f(k)} \end{aligned} \tag{A.44}$$

Here $\sum_{BZ}$ is a $\mathbf{k}$ sum over the 1st Brillouin zone with $\sum_{BZ} 1 = 1$.

A.2.1 Derivation of the lattice CPA from the variatonal principle

Let us consider the mean-field free energy of the form ($\beta = 1/k_B T$)

$$\beta\mathcal{F}\{Q(s), \Lambda(s)\} = \beta\mathcal{F}\{Q(s)\}_{\text{med}} + \beta\mathcal{F}\{Q(s), \Lambda(s)\}_{\text{CPA}} \tag{A.45}$$

with [125, 80]

$$\beta\mathcal{F}\{Q(s)\}_{\text{med}} = -\text{Tr}\Big\{ \ln\{\text{G}_{\text{med}}(\mathbf{q}, \text{s})^{-1}\} \Big\} = -\sum_{\mathbf{q}\in\text{BZ}} \ln\{\text{s} + \text{f}(\mathbf{q})\text{Q}(\text{s})\} \tag{A.46}$$

and

$$\beta\mathcal{F}\{Q(s), \Lambda(s)\}_{\text{CPA}} = -\frac{1}{p_c}\Big\langle \ln\{1 + p_c\Lambda(s)[W - Q(s)]\} \Big\rangle \tag{A.47}$$

$$\frac{d}{d\Lambda(s)}\beta\mathcal{F} = 0 = -\left\langle \frac{W - Q(s)}{1 + p_c\Lambda(s)[W - Q(s)]} \right\rangle \tag{A.48}$$

According to (6.70) this is equivalent to

$$1 = \left\langle \frac{1}{1 + p_c\Lambda(s)[W - Q(s)]} \right\rangle \tag{A.49}$$

Varying $\beta\mathcal{F}$ with $Q(s)$ gives

$$\frac{d}{dQ(s)}\beta\mathcal{F} = 0 = -\sum_{\mathbf{q}\in\text{BZ}} \frac{f(q)}{s + f(\mathbf{q})Q(s)} + \Lambda(s) \underbrace{\left\langle \frac{1}{1 + p_c\Lambda(s)[W - Q(s)]} \right\rangle}_{=1} \tag{A.50}$$

$\Rightarrow$

$$\Lambda(s) = \sum_{\mathbf{q}\in\text{BZ}} \frac{f(q)}{s + f(\mathbf{q})Q(s)} = \frac{1}{Q(s)} \left[1 - s \sum_{\mathbf{q}\in\text{BZ}} \frac{1}{s + f(\mathbf{q})Q(s)} \right] \tag{A.51}$$

<u>Continuum limit</u>

For obtaining the continuum limit we make the small q expansion

$$f(\mathbf{q}) = 6 - 2\cos(q_x a) - 2\cos(q_y a) - 2\cos(q_z a) \approx q^2 a^2 \tag{A.52}$$

and replace the fluctuating hopping rates by locally fluctuating diffusivities

$$D_i = W_{ij} a^2 \tag{A.53}$$

and define an effective-medium diffusivity by

$$D(s) = Q(s) a^2 \tag{A.54}$$

The trace operation is now no more a sum over the Brillouin zone, but a $\mathbf{q}$ sum up to an ultraviolet cutoff q_ξ.

The effective-medium Green's function is then

$$G_{\text{med}}(\mathbf{q}, s) = G_{\text{med}}(q, s) = \frac{1}{s + q^2 D(s)}\,, \tag{A.55}$$

The free energy is now given by

$$\beta\mathcal{F}\{D(s), \Lambda(s)\} = -\mathrm{Tr}\left\{ \ln\{\mathrm{G_{med}}(\mathbf{q}, \mathrm{s})^{-1}\} \right\} - \frac{1}{\mathrm{p_c}} \left\langle \ln\{1 + \mathrm{p_c}\Lambda(\mathrm{s})[\mathrm{D_i} - \mathrm{D}(\mathrm{s})]\} \right\rangle \tag{A.56}$$

The trace operation is now given by a $\mathbf{q}$ integration up to the cutoff q_ξ, and we get the CPA equations written down previously, Eqs. (6.48)

$$\left\langle \frac{D_i - D(s)}{1 + \frac{1}{3}[D_i - D(s)]\Lambda(s)} \right\rangle = 0$$

and (6.49)

$$\Lambda(s) = \nu \int_{|\mathbf{q}| \le q_\xi} d^3\mathbf{q} \frac{q^2}{s + q^2 D(s)} = \frac{3}{q_\xi^3} \int_0^{q_\xi} q^2 \frac{q^2}{s + q^2 D(s)}$$

A.3 Spectral properties of glasses

A.3.1 Correlation functions and frequency-dependent elastic moduli

This overview is taken from [126]. The correlation function, which is proportional to the scattering cross-section of inelastic X-ray and neutron scattering is the one-phonon dynamical structure factor $S(k, \omega)$. It is related to the longitudinal dynamical susceptibility by the fluctuation-dissipation theorem [50]:

$$S(k, \omega) = \frac{\hbar}{\pi m}[n(\omega) + 1]\chi_L''(k, \omega) \qquad \omega \neq 0 \tag{A.57}$$

Here m is the ratio of the mass density ρ_m and the number density N/V of the material. In the classical $\hbar\omega/k_B T \to 0$ limit we have

$$S(k, \omega) = \frac{k_B T}{\pi m \omega}\chi_L''(k, \omega) \qquad \omega \neq 0 \tag{A.58}$$

In a glass the longitudinal dynamical susceptibility $\chi_L(k,z) = \chi'_L(k,\omega) + i\chi''_L(k,\omega)$ $(z = \omega + i\epsilon, \epsilon \to +0)$ can be represented as [127, 116]

$$\chi_L(k,z) = \frac{k^2}{-z^2 + k^2 v_L^2(z)} = k^2 \mathcal{G}_L(k,z) \tag{A.59}$$

where the longitudinal frequency-dependent sound velocity $v_L(z)$ is related to the frequency-dependent longitudinal modulus $M(z)$ by

$$M(z) = \rho_m v_L(z)^2 = M'(\omega) - iM''(\omega) \tag{A.60}$$

$\mathcal{G}_L(k,z)$ is the longitudinal (disorder-averaged) Green's function[8] corresponding to the longitudinal wave equation (see next section). The sound attenuation coefficient can be defined as [116]

$$\Gamma_L(\omega) = \omega M''(\omega)/M'(\omega) \tag{A.61}$$

Taking Eqs. (A.58), (A.59) and (A.61) together and defining the resonance frequency $\Omega_L(\omega) = \sqrt{M'(\omega)}k = v'_L(\omega)k$ we obtain

$$S(k,\omega) = \frac{k_B T}{m\omega} k^2 \frac{1}{\pi} \frac{\Omega_L^2 \Gamma_L(\omega)/\omega}{(\Omega_L^2 - \omega^2)^2 + \left(\Omega_L^2 \Gamma_L(\omega)/\omega\right)^2} \tag{A.62}$$

Near resonance $\omega = \Omega_L$ we obtain the "damped-harmonic-oscillator" (DHO) function, with which many Brillouin-scattering spectra have been fitted:

$$\begin{aligned} S(k,\omega) &= \frac{k_B T}{m\omega} k^2 \frac{1}{\pi} \frac{\omega \Gamma_L(\omega)}{(\Omega_L^2 - \omega^2)^2 + \omega^2 \Gamma_L(\omega)^2} \\ &\overset{\Gamma_l \to 0}{=} \frac{k_B T}{m\Omega_L^2} k^2 \frac{1}{2} \Big[\delta(\omega - \Omega_L) + \delta(\omega + \Omega_L) \Big] \end{aligned} \tag{A.63}$$

In this context it is important to remark that the inverse line width Γ in a disordered system is *not* equivalent to a "life time" of an excitation. In fact, in a disordered *harmonic* system there is no damping. This means that all oscillatory degrees of freedoms, if excited, live forever. They can only dy out by an anharmonic mechanism. A finite Γ is just due to the disorder and describes static scattering. Similar to electrons in impure metals [128]. $\tau = \Gamma^{-1}$ is proportional to the elastic mean-free path, divided by the wave velocity, which involves no dissipation.

On the other hand, at frequencies much below the BP there is evidence for an anharmonic origin of sound attenuation [129, 130, 131, 132]. In this case the corresponding inverse sound attenuation frequency is a true decay time.

The scattering law $S(k,\omega)$ is connected via the equation of continuity to the longitudinal current-correlation function

$$C_L(k,\omega) = \frac{\omega^2}{k^2} S(k,\omega) = \frac{k_B T \omega}{\pi m} \mathcal{G}''_L(k,\omega) \tag{A.64}$$

[8] Here, we use $\mathcal{G}$ for the Green's function and G for the shear modulus.

In a similar way, one can define transverse correlation functions as [115]

$$C_T(k,\omega) = \frac{\omega^2}{k^2} S_T(k,\omega) = \frac{k_B T \omega}{\pi m} \mathcal{G}''_T(k,\omega) \tag{A.65}$$

with the transverse Greens function

$$\mathcal{G}_T(k,z) = \frac{1}{k^2}\chi_T(k,z) = \frac{1}{-z^2 + k^2 v_T(z)^2} \tag{A.66}$$

The frequency-dependent transverse sound velocity is related to the frequency-dependent shear modulus by

$$\rho_m v_T(z)^2 = G(z) = G'(\omega) + iG''(\omega) \tag{A.67}$$

$G(z)$ is related to $M(z)$ by

$$M(z) = K(z) + \frac{4}{3}G(z) \tag{A.68}$$

where $K(z)$ is the macroscopic (frequency-dependent) bulk modulus. One can define a transverse acoustic attenuation coefficient as

$$\Gamma_T(\omega) = \omega G''(\omega)/G'(\omega) \tag{A.69}$$

One can relate the longitudinal and the transverse sound attenuation functions with an elastic, disorder-induced mean free path:

$$\frac{1}{\ell_{L,T}(\omega)} = \frac{\Gamma_{L,T}(\omega)}{2v_{L,T}(0)} \tag{A.70}$$

The Ioffe-Regel (IR) limit is reached when this length becomes equal to the wavelength $\lambda_{L,T} = \omega/2\pi v_{L,T}(0)$, i.e. for $\omega^{IR}_{L,T} = \pi\Gamma_{L,T}(\omega)$. In molecular-like model glasses the *transverse* IR limit is reached near the BP [115, 133, 116], whereas in network glasses, where these frequencies are nearer to each other, both limits appear to be reached near the [134].

A.3.2 Wavenumber-independent spectra

Within a generalized Debye model, which is described by the Green's functions $\mathcal{G}_{L,T}$ defined in Eqs. (A.59) and (A.66) the vibrational density of states (DOS) is given by

$$\begin{aligned} g(\omega) &= \frac{2\omega}{3\pi}\frac{1}{N}\sum_{|\mathbf{k}|<k_D}\Big(\mathcal{G}''_L(k,\omega) + 2\mathcal{G}''_T(k,\omega)\Big) \\ &= \frac{2\omega}{3\pi}\frac{3}{k_D^3}\int_0^{k_D} dk k^2 \Big(\mathcal{G}''_L(k,\omega) + 2\mathcal{G}''_T(k,\omega)\Big) \end{aligned} \tag{A.71}$$

where $k_D = \sqrt[3]{6\pi^2 N/V}$is the Debye cutoff wavenumber, V being the total volume of the sample and N the total number of atoms or molecular units.

We now define the local velocity correlation function as

$$Z(\omega) = \frac{1}{< v^2 >} \frac{1}{N} \sum_{|\mathbf{k}|<k_D} \left(C_L''(k,\omega) + 2C_T''(k,\omega) \right) \tag{A.72}$$

with $< v^2 >= \frac{3}{2} k_B T/m$. Inserting (A.65) and (A.64) into (A.72) we find by comparing with (A.71) [135]

$$g(\omega) = Z(\omega) \tag{A.73}$$

For the following it will be useful to define longitudinal and transverse susceptibility integrated up to a certain wavenumber cutoff k_ξ

$$\chi_{L,T}^{\xi}(z) = \frac{3}{{k_\xi}^3} \int_0^{k_\xi} dk k^2 \chi_{L,T}(k,z) \tag{A.74}$$

k_ξ can be related to the correlation length ξ of the spatially fluctuating density ρ, the elastic constants K, G or the Pockels (light-elastic) coupling constants α by $k_\xi = \nu/\xi$, where ν is a constant of order unity. For Raman scattering [136, 101] these functions (with ξ referring to the Pockels constant fluctuations) enter as follows into the observed intensities

$$I_{VV}(\omega) = A f_1 [n(\omega)+1][\chi_L^{\xi_\alpha}(\omega)]'' + \frac{4}{3} I_{VH}(\omega) \tag{A.75}$$

$$I_{VH}(\omega) = A[n(\omega)+1] f_2 \frac{1}{30} \left(2[\chi_L^{\xi_\alpha}(\omega)]'' + 3[\chi_T^{\xi_\alpha}(\omega)]'' \right) \tag{A.76}$$

where A is a proportionality constant and $f_{1,2}$ are the longitudinal and transverse mean-square Pockels constant fluctuations. As pointed out in [136, 101] the correlation length ξ in these expressions refer to the correlation functions of the spatially fluctuating light-vibration (Pockels) constants.
For *incoherent neutron scattering* the observed intensity is proportional to the density of states:

$$S(k,\omega)_{\text{incoh}} \propto [n(\omega)+1] \frac{g(\omega)}{\omega} \tag{A.77}$$

In materials, which scatter predominantly incoherently this is a way to obtain the DOS directly [98]. Similarly is the *inelastic nuclear scattering* (INS) a direct way to obtain the DOS of glasses [137].
In many materials, which have been investigated by inelastic neutron scattering, the scattering is *coherent*, which precludes the usage of Eq. (A.77). However, it is known [138, 139, 140] that in the limit $k \to \infty$ all coherence is lost, i.e. $S(k,\omega) \to S_{\text{incoh}}(k,\omega)$.This limit is expected to hold for k values at which the static structure factor $S(k)$ becomes equal to its coherent counterpart $S(k)_{\text{incoh}} = 1$. Typical values for inelastic coherent neutron scattering, however, range around and somewhat beyond the central peak of $S(k)$. In the *incoherent approximation* [138, 141, 142, 143], the coherent dynamical structure factor is replaced by the expression (A.77). In order to make the data more incoherent (and to gain statistics) it has become use [138, 141, 142, 143],

to average the data over the k range accessible by the kinetic window of the neutrons and write

$$\begin{aligned} \langle S(k,\omega)\rangle &= \frac{1}{k_{\max}-k_{\min}}\int_{k_{\min}}^{k_{\max}} dk S(k,\omega) \\ &\propto [n(\omega)+1]\frac{g_{\text{neutron}}(\omega)}{\omega} \end{aligned} \tag{A.78}$$

The error made by this approximation has been discussed in detail in [142, 143]

A.3.3 Thermal properties

The specific heat can be calculated from the DOS by the usual formula

$$C(T) \propto \int_0 \infty d\omega g(\omega)(\omega/T)^2 \frac{e^{\hbar\omega/k_B T}}{[e^{\hbar\omega/k_B T}-1]^2} \tag{A.79}$$

In terms of the *transport* mean-free path $\ell_{\text{tr}}(\omega)$ the thermal conductivity is given by

$$\kappa(T) \propto \int_0 \infty d\omega \ell_{\text{tr}}(\omega) g(\omega)(\omega/T)^2 \frac{e^{\hbar\omega/k_B T}}{[e^{\hbar\omega/k_B T}-1]^2} \tag{A.80}$$

As shown in [104] by an analysis of the Gaussian contributions beyond the SCBA saddlepoint (which are important for transport properties [144, 145]) the transport mean-free path $\ell_{\text{tr}}(\omega)$ to be inserted into (A.80) is not the one-particle mean-free path $\ell(\omega)$ calculated from the sound attenuation, but has to be multiplied with the inverse reduced DOS:

$$\ell_{\text{tr}}(\omega) \propto \frac{\omega^2}{g(\omega)}\ell(\omega) \tag{A.81}$$

where $\ell(\omega) \propto \ell_T(\omega)$ if the disorder scattering is due to the transverse shear fluctuations.

References

[1] P. Richet, Ed. *Encyclopedia of glass science, technology,history and culture*, volume I,II. Wiley, Hoboken, NJ, 2021.

[2] W. Schirmacher. *Theory of liquids and other disordered media*, volume 887 of *Lecture Notes in Physics*. Springer, Heidelberg, 2015.

[3] J. E. Enderby. Liquid state physics - or is it chemistry? *J. Phys. C. Sodid State Phys.*, 15:4609, 1982.

[4] W. Kob and Hans C. Andersen. Testing mode-coupling theory for a supercooled binary lennard-jones mixture. ii. intermediate scattering function and dynamic susceptibility. *Phys. Rev. E*, 52:4134, 1995.

[5] Ludovic Berthier and Giulio Biroli. Theoretical perspective on the glass transition and amorphous materials. *Rev. Mod. Phys.*, 83:587, 2011.

[6] D. L. Morse. Welcome to the glass age. *Int. J. Appl. Glass Sc.*, 7:409, 2016.

[7] P. Richet, Ref. [1]. General introduction. page 1, 2021.

[8] Section X. of Ref. [1]. History. page 1231, 2021.

[9] R. Conradt, Ref. [1]. Glass production: An overview. page 25, 2021.

[10] S. Reineke, M. Thomschke, B. Lüssem, and K. Leo. White organic light-emitting diodes: Status and perspective. *Rev. Mod. Phys.*, 85:1245, 2013.

[11] A. Sharma and V. Zadoroshnyy. Review of the recent development in metallic glass and its composites. *Metals*, 11:1933, 2021.

[12] K. Binder and A. P. Young. Spin glasses: Experimental facts, theoretical concepts and open questions. *Rev. Mod. Phys.*, 58:801, 1986.

[13] K. Susman, D. L. Price, M. Grimsditch, J. P. Rino, R. K. Kalia, P. Vashishta, G. Gwanmesia, Y. Wang, and R. C. Liebermann. Intermediate-range order in permanently densified vitreous sio_2: A neutron-diffraction and molecular-dynamics study. *Phys.Rev. B*, 43:1194, 1991.

[14] B. Mandelbrot. *The fractal geometry of nature.* Freeman, New York, 1977.

[15] A. Hasmy, S. Ispas, and B. Hehlen. Percolation transitions in compressed sio2 glasses. *Nature*, 599:62, 2021.

[16] A. de St. Exupéry. *Le Petit Prince.* Reynal & Hitchcock, New York, 1943.

[17] P. Flory. Molecular size distribution in three dimensional polymers. *J. Am. Chem. Soc.*, 63:3083, 3091, and 3096, 1941.

[18] W. H. Stockmayer. Theory of molecular size distribution and gel formation in branched polymers ii, general cross-linking. *J. Chem. Phys.*, 12:125, 1944.

[19] J. C. Maxwell. On the dynamical theory of gases. *Phil. Trans. Roy. Soc.*, 157:49, 1867.

[20] T. Hecksher, D. H. Torchinsky, C. Klieber, J. A. Johnson, and J. C. Dyre. Toward broadband mechanical spectroscopy. *Proceedings of the Nat. Acad. of Science of America (PNAS)*, 114:8910, 2017.

[21] C. A. Angell. Formation of glasses from liquids and biopolymers. *Science*, 267:1924, 1995.

[22] U. Bengtzelius, W. Götze, and A. Sjölander. Dynamics of supercooled liquids and the glass transition. *J. Phys. C: Solid State Phys.*, 17:5915, 1984.

[23] W. Götze. *Complex Dynamics of Glass-forming Liquids: A mode-coupling theory.* Oxford University Press, Oxford, 2012.

[24] A. Cavagna. Supercooled liquids for predestrians. *Phys. Reports*, 476:51, 2009.

[25] M. Reiner. The deborah number. *Phys. Today*, 17:62, 1964.

[26] O. Gulbiten, J. C. Mauro, X. Guo, and O. N. Boratav. Viscous flow of medieval cathedral glass. *J Am Ceram Soc.*, 101:5, 2018.

[27] Th. E. Markland, J. A. Morrone, K. Miyazaki, B. J. Berne, D. R. Reichman, and E. Rabani. Theory and simulations of quantum glass forming liquids. *J Chem. Phys.*, 136:074511, 2012.

[28] P. Atkins, J. de Paula, and J. Keeler. *Physical Chemistry, 12th Edition.* Oxford University Press, Oxford, 2023.

[29] W. Kauzmann. he nature of the glassy state and the behavior of liquids at low temperatures. *Chem. Rev.*, 43:219, 1948.

[30] W. Nernst. *Die theoretischen und experimentellen Grundlagen des neuen Wärmesatzes.* Verlag W. Knapp, Halle, 1918.

[31] A. Einstein. Beiträge zur quantentheorie. *Verh. Deutsche Phys. Ges.*, 16:820, 1914.

[32] L. Pauling. The structure and entropy of ice and of other crystals with some randomness of atomic arrangement. *J. Am. Chem. Soc.*, 57:2680, 1935.

[33] J. C. Mauro, P. K. Gupta, and R. J. Loucks. Continuously broken ergodicity. *J. Chem. Phys.*, 126:184511, 2007.

[34] P. K. Gupta and J. C. Mauro. The laboratory glass transition. *J. Chem. Phys.*, 126:224504, 2007.

[35] J. C. Mauro and M. M. Smetskaer. Statistical mechanics of glass. *J. Noncryst. Sol.*, 396-397:41, 2014.

[36] M. Goldstein. On the reality of residual entropies of glasses and disordered crystals. *J. Chem. Phys.*, 128:154510, 2008.

[37] A. Takada, R. Conradt, and P. Richet. Residual entropy and structural disorder of glass: a two-level model and a review of spatial and ensemble vs. temporal sampling. *J. Noncryst. Sol.*, 360:13, 2013.

[38] A. Takada, R. Conradt, and P. Richet. Residual entropy and structural disorder of glass: a review of history and an attempt to resolve two apparently conflicting views. *J. Noncryst. Sol.*, 429:33, 2015.

[39] I. Gutzow, B. Petroff, J. Möller, and J. P. Schmelzer. Glass transition and the third principle of thermodynamics: reconsideration of a classical problem. *Phys. Chem. Glasses: Eur J. Glass Sci. Technol. B*, 48:168, 2007.

[40] I. Gutzow and J. P. Schmelzer. The third principle of thermodynamics and the the zero-point entropy of glasses: History and new developments. *J. Noncryst. Sol.*, 355:581, 2009.

[41] K. Shirai. Residual entropy and the third law expression. *preprint arXiv:2207.11421v4*, 2021.

[42] L. D. Landau and E. M. Lifshitz. *Statistical Physics.* Pergamon Press, Oxford, 1958.

[43] M. Goldstein. Viscous liquids and the glass transition: a potential energy barrier picture. *J. Chem. Phys.*, 51:3728, 1969.

[44] P. G. Debenedetti and F. H. Stillinger. Supercooled liquids and the glass transition. *Nature*, 410:259, 2001.

[45] E. Leutheusser. Dynamical model of the liquid-glass transition. *Phys. Rev. A*, 29:2765, 1984.

[46] G. Adam and J. H. Gibbs. On the temperature dependence of cooperative relaxation properties in glass-forming liquids. *J. Chem. Phys.*, 43:139, 1965.

[47] L.-M. Martinez and C. A. Angell. A thermodynamic connection to the fragility of glass-forming liquids. *Nature*, 410:663, 2001.

[48] S. Capaccioli, G. Ruocco, and F. Zamponi. Dynamically correlated regions and configurational entropy in supercooled liquids. *J. Phys. Chem B*, 112:10652, 2008.

[49] J. Wuttke, W. Petry, and S. Pouget. Structural relaxation in viscous glycerol: Coherent neutron scattering. *J. Chem. Phys.*, 105:5177, 1996.

[50] R. Kubo. Statistical-mechanical theory of irreversible processes i. *J. Phys. Soc. Japan*, 12:570, 1957.

[51] J.-P. Hansen and I. R. McDonald. *Theory of simple liquids.* Academic Press, New York, 2013.

[52] B. J. Berne and R. Pecora. *Dynamic Light scattering with applications to chemistry, biology and physics.* Wiley, New York, USA, 1985.

[53] H. Mori. A continued-fraction representation of the time correlation functions. *Prog. Theor. Phys.*, 33:423, 1965.

[54] W. Götze and M. R. Mayr. Evolution of vibrational excitations in glassy systems. *Phys. Rev. E*, 61:587, 1999.

[55] H. Mori. Transport, collective motion, and brownian motion. *Prog. Theor. Phys.*, 34:399, 1965.

[56] R. Zwanzig. Memory effects in irreversible thermodynamics. *Phys. Rev.*, 124:983, 1961.

[57] R. Zwanzig. *Nonequilibrium statistical Mechanics.* Oxford University Press, Oxford, 1978.

[58] W. Götze. The essentials of the mode-coupling theory for glassy dynamics. *Condensed Matter Phys.*, 12:873, 1998.

[59] R. Thom. *Structural stability and morphogenesis: An outline of a general theory of models.* Addison-Wesley, Reading, Mass. USA, 1989.

[60] V. Arnol'd. *Catastrophe theory.* Addison-Wesley, Reading, Mass. USA, 1992.

[61] W. Götze. In J.-P. Hansen, D. Levesque, and J. Zinn-Justin, editors, *Liquids, Freezing and the Glass Transition.* Elsevier, Amsterdam, 1991.

[62] W. Petry, E. Bartsch, F. Fujara, M Kiebel, H. Sillcscu, and B. Farago. Dynamic anomaly in the glass transition region of orthoterphenyl. *Z. Physik B*, 83:175, 1991.

[63] L. Comez, D. Fioretto, J. Gapinski, G. Monaco, A. Patkowski, and W. Steffen. Inelastic x-ray scattering reveals the ergodic to nonergodic transition of salol, a liquid with local order. *Condensed Matter Phys.*, 22:43603, 2019.

[64] M. Abramowitz and I. A. Stegun. *Handbook of mathematical formulas.* Dover Publications, New York, USA, 1964.

[65] L. N. Petzold and E. A. Rössler. Light scattering study on the glass former o-terphenyl. *J. chem. Phys.*, 133:124512, 2010.

[66] Y. S. Elmatad, D. Chandler, and J. P. Garrahan. Corresponding states of structural glass formers. *J. Phys. Chem. B*, 113:5563, 2009.

[67] J. P. Garrahan and D. Chandler. Coarse-grained microscopic model of glass formers. *Proc. Nat. Acad. Soc. America (PNAS)*, 100:9710, 2003.

[68] T. Castellani and A. Cavagna. Spin-glass theory for predestrians. *J. statist. Mech.: Theory and Experiment*, 5:P05012, 2005.

[69] A. Altieri and M. Baity-Jesi. An introduction to the theory of spin glasses. In *Encyclopedia of condensed matter physics (second edition)*, volume 2, page 361. Elsevier, Amsterdam, 2024.

[70] S. F. Edwards and P. W. Anderson. Theory of spin glasses. *J. Phys. F*, 5:965, 1975.

[71] S. F. Edwards and R. C. Jones. The eigenvalue spectrum of a large symmetric random matrix. *J. Phys. A: Math. Gen.*, 9:1595, 1976.

[72] D. Sherrington and S. Kirkpatrick. Solvable model of a spin-glass. *Phys. Rev. Lett.*, 35:1792, 1975.

[73] T. Kirkpatrick, D. Thirumalai, and P. G. Wolynes. Scaling concepts for the dynamics of viscous liquids near an ideal glassy state. *Phys. Rev. A*, 40:1045, 1989.

[74] A. K. Jonscher. Frequecy dependence of conductivity in hopping systems. *J. Non-cryst. sol.*, 8-10:293, 1972.

[75] J. Wong and C. A. Angell. *Glass: structure by spectroscopy.* M. Dekker, 1976.

[76] S. Alexander and R. Orbach. Density of states of fractals, "fractons". *J. Phys. (France), Lett.*, 43:L625, 1982.

[77] T. Nakayama, K. Yakubo, and R. L. Orbach. l3ynamical properties of fractal networks: Scaling, numerical simulations, and physical realizations. *Rev. Mod. Phys.*, 66:381, 1994.

[78] R. Rammal. Spectrum of harmonic excitations on fractals. *J. Phys. (France)*, 45:191, 1984.

[79] R. J. Elliott, J. A. Krumhansl, and P. L. Leath. The theory and properties of randomly disordered crystals and related physical systems. *Rev. Mod. Phys.*, 46:465, 1974.

[80] D. Vollhardt. Dynamical mean-field theory of electronic correlations in models and materials. *AIP Conf. Proc.*, 1297:339, 2010.

[81] I. Webman. Effective-medium approximation for diffusion on a random lattice. *Phys. Rev. Lett.*, 47:1493, 1981.

[82] S. Summerfield. Effective-medium theory of a. c. hopping conductivity for random-bond lattice models. *Sol. State Comm.*, 39:401, 1981.

[83] T. Odagaki and M. Lax. Coherent-medium approximation in the stochastic transport theory of random media. *Phys. Rev. B*, 24:5284, 1981.

[84] S. Köhler, G. Ruocco, and W. Schirmacher. Coherent potential approximation for diffusion and wave propagation in disordered systems. *Phys. Rev. B*, 88:064203, 2013.

[85] J. E. Shelby and S. C. Keeton. Temperature dependence of gas diffusion in glass. *J. Appl. Phys.*, 45:1458, 1973.

[86] H. Jain. Temperature dependence of electrical conductivity of glasses. *J. Non-Cryst. Sol.*, 66:517, 1984.

[87] S. Kirkpatrick. Percolation and conduction. *Rev. Mod. Phys.*, 45:574, 1973.

[88] V. Ambegaokar, S. Cochran, and J. Kurkijärvi. Conduction in random systems. *Phys. Rev. B*, 8:3682, 1973.

[89] B. I. Shklovskii and A. L. Efros. *Electronic properties of doped semiconductors.* Springer Verlag, Berlin, 1979.

[90] H. F. Weber. Die specifische Wärme des Kohlenstoffs. *Ann. Phys. (Leipzig)*, 147:311, 1872.

[91] A. Einstein. Die Plancksche Theorie der Strahlung und die Theorie der spezifischen Wärme. *Ann. Phys. (Leipzig)*, 22:180, 1907.

[92] P. Debye. Zur Theorie der spezifischen Wärme. *Ann. Phys. (Leipzig)*, 39:789, 1912. (in German).

[93] A. Bosak, M. Krisch, D. Chernyshov, B. Winkler, V. Milman, K. Refson, and C. Schulze-Briese. New insights into the lattice dynamics of α-quartz. *Z. Kristallogr.*, 227:84, 2012.

[94] J. Horbach and K. Binder. High frequency sound and the boson peak in amorphous silica. *Eur. Phys. J. B*, 19:531543, 2001.

[95] R. Shuker and R. W. Gammon. Raman-scattering in amorphous materials. In *Proceedings of the Second International Conference on Light Scattering in Solids*, page 334. Flammarion, Paris, 1971.

[96] R. Shuker and R. W. Gammon. Raman-scattering selection-rule breaking and the density of states in amorphous materials. *Phys. Rev. Lett.*, 25:222, 1970.

[97] J. Jäckle. In W. A. Phillips, editor, *Amorphous Solids: Low-Temperature Properties*, page 135. Springer-Verlag, Berlin, 1981.

[98] J. Wuttke, W. Petry, G. Coddens, and F. Fujara. Fast dynamics of glass-forming glycerol. *Phys. Rev. E*, 52:4026, 1995.

[99] T. Uchino and T. Yoko. Low-frequency Raman scattering and the fast relaxation process in glycerol. *Science*, 273:480, 1996.

[100] Z. Pan, O. Benzine, S. Sawamura, R. Limbach, A. Koike, T. D. Bennett, G. Wilde, W. Schirmacher, and L. Wondraczek. Disorder classification of the vibrational spectra of modern glasses. *Phys. Rev. B*, 104:134106, 2021.

[101] B. Schmid and W. Schirmacher. Raman scattering and the low-frequency vibrational spectrum of glasses. *Phys. Rev. Lett.*, 100:137402, 2008.

[102] R. C. Zeller and R. O. Pohl. Thermal conductivity and specific heat of noncrystalline solids. *Phys. Rev. B*, 4:2029, 1971.

[103] C. C. Yu and A. J. Leggett. Low temperature properties of amorphous materials: though a glass darkly. *Comm. Condens. Matter Phys.*, 14:231, 1988.

[104] W. Schirmacher. Thermal conductivity of glassy materials and the boson peak. *Europhys. Lett.*, 73:892, 2006.

[105] J. J. Freeman and A. C. Anderson. Thermal conductivity of amorphous solids. *Phys. Rev. B*, 34:5684, 1986.

[106] W. A. Phillips. Tunneling states and the low-temperature thermal expansion of glasses. *J. Low-Temp. Phys.*, 7:351, 1972.

[107] P W Anderson, BI Halperin, and C M Varma. Anomalous low-temperature thermal properties of glasses and spin glasses. *Philosophical Magazine*, 25:1, 1972.

[108] A. F. Ioffe and A. R. Regel. Non-crystalline, amorphous and liquid electronic semiconductors. *Prog. Semicond.*, 4:237, 1960.

[109] N. W. Ashcroft and D. Mermin. *Solid state physics.* Harcourt College Publishers, Fort Worth, USA, 1976.

[110] N. F. Mott and E. A. Davis. *Electronic processes in non-crystalline materials.* Clarendon-Press, Oxford, 1971.

[111] N. F. Mott. *Metal-insulator transitions.* Taylor & Francis, London, 1990.

[112] P. W. Anderson. Absence of diffusion in certain random lattices. *Phys. Rev.*, 109:1492, 1958.

[113] E. Akkermans and R. Maynard. Weak localization and anharmonicity of phonons. *Phys. Rev. B*, 32:7850, 1985.

[114] J. E. Graebner, B. Golding, and L. C. Allen. Phonon localization in glasses. *Phys. Rev. B*, 34:5696, 1986.

[115] H. Shintani and H. Tanaka. Universal link between the boson peak and transverse phonons in glass. *Nature Materials*, 7:870, 2008.

[116] A. Marruzzo, W. Schirmacher, A. Fratalocchi, and G. Ruocco. Heterogeneous shear elasticity of glasses: the origin of the boson peak. *Sci. Rep.*, 3:1, 2013.

[117] P. Sheng, M. Zhou, and Z.-Q. Zhang. Phonon transport in strong-scattering media. *Phys. Rev. Lett.*, 72:234, 1994.

[118] W. Schirmacher, G. Diezemann, and C. Ganter. Harmonic vibrational excitations in disordered solids and the boson peak. *Phys. Rev. Lett.*, 81:136, 1998.

[119] G. Müller. Theory of elastic waves. In M. Weber, G. Rümpker, and D. Gajewski, editors, *Seismic waves.* GFZ Potsdam, https://doi.org/10.2312/GFZ.b103-07037, Potsdam, 2007.

[120] G. Monaco and V. M. Giordano. Breakdown of the debye approximation for the acoustic modes with nanometric wavelengths in glasses. *Proc. Nat. Acad. Sci.*, 106:3659, 2009.

[121] G. Baldi, V. M. Giordano, and G. Monaco. Elastic anomalies at terahertz frequencies and excess density of vibrational states in silica glass. *Phys. Rev. B*, 83:174203, 2011.

[122] C. Talón, Q. W. Zou, M. A. Ramos, R. Villar, and S. Vieira. Low-temperature specific heat and thermal conductivity of glycerol. *Phys. Rev. B*, 65:012203, 2001.

[123] E. Duval, A. Boukenter, and T. Achibat. Vibrational dynamics and the structure of glasses. *Journal of Physics: Condensed Matter*, 2:10227, 1990.

[124] S. R. Elliott. A unified model for the low-energy vibrational behaviour of amorphous solids. *Europhys. Lett.*, 19:201, 1992.

[125] V. Janiš. Free-energy functional in the generalized coherent-potential approximation. *Phys. Rev. B*, 40:11331, 1989.

[126] W. Schirmacher, T. Scopigno, and G. Ruocco. Theory of vibrational anomalies in glasses. *J. Noncryst. Sol.*, 407:133, 2014.

[127] W. Schirmacher, G.Ruocco, and T. Scopigno. Acoustic attenuation in glasses and its relation with the Boson Peak. *Phys. Rev. Lett.*, 98:025501, 2007.

[128] S. F. Edwards. A new method for the evaluation of electric conductivity in metals. *Philos. Mag.*, 3:1020, 1958.

[129] E. Rat, M. Foret, G. Massiera, R. Vialla, M. Arai, R. Vacher, and E. Courtens. Anharmonic versus relaxational sound damping in glasses. i. brillouin scattering from densified silica. *Phys. Rev. B*, 72:214203, 2005.

[130] R. Vacher, E. Courtens, and M. Foret. Anharmonic versus relaxational sound damping in glasses. ii. vitreous silica. *Phys. Rev. B*, 72:214205, 2005.

[131] C. Ferrante, E. Pontecorvo, G. Cerullo, A. Chiasera, G. Ruocco, W. Schirmacher, and T. Scopigno. Acoustic dynamics of network-forming glasses at mesoscopic wavelengths. *Nature Comm.*, 4:1793, 2013.

[132] C. Tomaras, B. Schmid, and W. Schirmacher. Anharmonic elasticity theory for sound attenuation in disordered solids with fluctuating elastic constants. *Phys. Rev. B*, 81:104206, 2010.

[133] G. Monaco and S. Mossa. Anomalous properties of the acoustic excitations in glasses on the mesoscopic length scale. *Proc. Nat. Acad. Sci.*, 106:16907, 2009.

[134] B. Rufflé, G. Guimbretière, E. Courtens, R. Vacher, and G. Monaco. Glass-specific behavior in the damping of acousticlike vibrations. *Phys. Rev. Lett.*, 96:045502, 2006.

[135] A. Rahman, M. J. Mandell, and J. P. McTague. Molecular dynamics study of an amorphous lennard-jones system at low temperature. *J. Chem. Phys.*, 64:1564, 1976.

[136] A. J. Martin and W. Brenig. Model for brillouin scattering in amorphous solids. *phys. status solidi (b)*, 64:163, 1974.

[137] A. I. Chumakov, I. Sergueev, U. van Bürck, W. Schirmacher, T. Asthalter, R. Rüffer, O. Leupold, and W. Petry. Collective nature of the boson peak and universal transboson dynamics of glasses. *Phys. Rev. Lett.*, 92:245508, 2004.

[138] J. M. Carpenter and D. L. Price. Correlated motions in glasses studied by coherent inelastic neutron scattering. *Phys. Rev. Lett.*, 54:441, 1985.

[139] S. Ciliberti and T. S. Grigeranz. Localization threshold of instantaneous normal modes from level-spacing statistics. *Phys. Rev. E*, 70:061502, 2003.

[140] C. Ganter and W. Schirmacher. Rayleigh scattering, long-time tails and the harmonic spectrum of topologically disordered systems. *Phys. Rev. B*, 82:094205, 2010.

[141] U. Buchenau, M Prager, N. Nücker, A. J. Dianoux, N. Ahmad, and W. A. Phillips. Low-frequency modes in vitreous silica. *Phys. Rev. B*, 34:5665, 1986.

[142] S. N. Taraskin and S. R. Elliott. Connection between the true vibrational density of states and that derived from inelastic neutron scattering. *Phys. Rev. B*, 55:117, 1997.

[143] E. Fabiani, A. Fontana, and U. Buchenau. Neutron scattering study of the vibrations in vitreous silica and germania. *J. Chem. Phys.*, 128:244507, 2008.

[144] B. Velický. Theory of electronic transport in disordered binary alloys: coherent-potential approximation. *Phys. Rev.*, 184:614, 1969.

[145] A. L. Burin, L. A. Maksimov, and I. Ya. Polishchuk. The phonon transport in crystals with heavy defects. *Physica B*, 210:15, 1995.